Investigations on subunit-specific assembly and structure-function studies of the voltage sensor in KCNQ potassium channels

Dissertation zur Erlangung des Doktorgrades
der Naturwissenschaften

vorgelegt beim Fachbereich Chemische und Pharmazeutische Wissenschaften
der Johann Wolfgang Goethe - Universität
in Frankfurt am Main

von
Despina Athanasiadu
aus Mannheim

Frankfurt am Main 2007

Die Arbeit wurde in der Abteilung Biophysikalische Chemie des Max-Planck-Instituts für Biophysik in Frankfurt am Main durchgeführt und vom Fachbereich Chemische und Pharmazeutische Wissenschaften der Johann Wolfgang Goethe - Universität als Dissertation angenommen

Dekan: Prof. Dr. Harald Schwalbe

Gutachter: Prof. Dr. Ernst Bamberg
              Prof. Dr. Thomas Friedrich
Datum der Disputation: 23 November 2007

Table of Contents

AIM OF THE WORK

A detailed understanding of how potassium channels function is crucial e. g. for the development of drugs, which could lead to novel therapeutic concepts for diseases ranging from diabetes to cardiac abnormalities. An improved understanding of channel structure may allow researchers to design medication that can restore proper function of these channels.

This is particularly important for KCNQ channels, since four out of five family members are involved in human inherited disease. In addition to structure and function relationships the determinants which govern assembly of KCNQ subunits are decisive to understand the physiological role of the KCNQ channel family members.

Many details of KCNQ channel assembly remain incompletely understood. Previous work has shown that the subunit-specific heteromerisation between KCNQ subunits is determined by a ~115 amino acid-long subunit interaction domain (*si*) within the C-terminus (Schwake et al., 2003). Recently, Jenke et al. (2003) proposed that the C-terminal domains in *eag* and *erg* K^+ channels act as sites which drive tetramerization. From their ability to form coiled coils, these domains were referred to as tetramerizing coiled-coil (TCC) sequences. Jenke et al. also pointed out that KCNQ channels contain bipartite TCC motifs within their C-termini, exactly within the *si* domain, which is responsible for the subunit-specific interaction pattern.

The first part of this thesis was dedicated to determine the individual role of these TCC domains on homomeric and heteromeric channel formation in order to further characterize the molecular determinants of KCNQ channel assembly.

In the second part of this thesis cystein-scanning mutagenesis was employed, followed by thiol-specific modification using MTS reagents to screen more than 20 residues in the S3-S4 linker region and in the S4 transmembrane domain of the KCNQ1 channel to gain information about residue accessibility, the functional effects of thiol-modifying reagents (MTSES), and effects of crosslinking selected pairs of Cys residues by Cd^+ ions, which could be used for testing model predictions based upon known Kv channel structures from the literature.

According to homology modelling based on the Kv1.2 structure it was attempted to determine the proximity of individual residues from different transmembrane segments using the metal bridge approach (crosslinking by Cd^+ ions). This led us to derive structural

constraints for interactions between the S4 voltage sensor and adjacent transmembrane segments of KCNQ1. Similar studies have previously been performed on the *Shaker* K^+ channel, which has served as a paradigm for structure-function research of voltage-gated K^+ channels for a long time, but little is known for KCNQ channels concerning their similarity to published K^+ channel structures.

A   INTRODUCTION

A 1   Ion channels

Ion channels form pores that allow the passive diffusion of ions across biological membranes according to concentration gradients. They have several key functions in the physiology of the nervous system, including the generation and propagation of action potentials. The net flow of electric charge carried by ions as they move along their electrochemical gradient through the pores leads to changes in the membrane voltage. The rapid propagation of these voltage changes is the basis for the electrical signalling in the brain and other tissues. Ion channels can also change the concentrations of second messengers such as calcium ions, and are important in the ionic homeostasis of the cytoplasm, of intracellular organelles and of extracellular compartments. The latter function is most obvious in the transport of ions and water across epithelia, but is also important in the homeostasis of the extracellular space between neurons and glia (Jentsch, 2000).

A 2   Potassium channels

The first K^+ channel genes were discovered, because they produced phenotypic changes in *Drosophila* when spontaneously mutated. Examples such as *Shaker* and *ether-à-go-go* (eag) illustrate this point. This led to the discovery of mammalian and human homologues by genetic approaches. Within the last two decades mutations in a variety of K^+ channels have been linked to human inherited diseases. It is intriguing to note that from the recently discovered KCNQ K^+ channel family four out of five members are involved in human pathologies (Jentsch, 2000).

Electrophysiologal studies have revealed a remarkable functional diversity among voltage-gated K^+ channels. It is evident that in terms of voltage dependence, rate constants of activation and inactivation, as well as pharmacology, almost every type of excitable cell has its own unique set or subset of K^+ channels. Furthermore, the same type of cell, but depending on its individual role, can have its K^+ channels "tuned" by splice variants, which is almost literally apparent in the case of auditory hair cells (Ramanathan et al., 1999). More recently, this heterogeneity of channels has been confirmed by molecular biologists.

At least 8 families of K$^+$ channel α-subunit genes have been cloned and identified, and each of these families contains a large number of individual members, numbering in total over 60 different subunits (**Table A.1**).

Table A.1: K$^+$ channel α (pore-forming) subunit families (Robbins, 2001)

Subunit Structure	Gene	Subunit Family	Members	Functional correlates
7TMD-1P	KCNMA1	KvCa (Slo poke)		I_{BK}
6TMD-1P	KCNA	Kv1 (Shaker)	Kv1.1-1.8	I_{Kv}
	KCNB	Kv2 (Shab)	Kv2.1-2.3 (8.1)	I_{KA}
	KCNC	Kv3 (Shaw)	Kv3.1-3.4	I_{Kv}
	KCND	Kv4 (Shal)	Kv4.1-4.3	I_{Kv}
	KCNF	Kv5	Kv5.1	I_{Kv}
	-	Kv6	Kv6.1-6.3	I_{Kv}
	-	Kv7	Kv7.1	I_{Kv}
	KCNS	Kv9	Kv9.1-9.3	-
6TMD-1P	KCNH	eag	eag1 eag2	
		erg	erg1 erg2 erg3	I_{Kr} (HERG1+ KCNE2)
		elk	elk1 elk2 elk3	
6TMD-1P	KCNQ1	KvLQT1		I_{Kr} (KCNQ1+ KCNE1)
				I_{KcAMP} (KCNQ1+ KCNE3)
	KCNQ2			$I_{K(M)}$
	KCNQ3			$I_{K(M)}$
	KCNQ4			I_{Kn}, I_{KL}
	KCNQ5			$I_{K(M)}$?
6TMD-1P	KCNN4	1K		I_{IK}
	KCNN1	SK	SK1	I_{SK}
	KCNN2		SK2	I_{SK}
	KCNN3		SK3	I_{SK}
2TMD-1P	KCNJ1	Kir1	Kir 1.1.1.3	
	KCNJ2	Kir2	Kir 2.1...2.3	
	KCNJ3/6/9/5	Kir3	Kir 3.1...3.4	I_{KACh} (Kir 3.1 + 3.4)
		Kir4	Kir 4.1	
		Kir5	Kir 5.1	
	KCNJ8/11	Kir6	Kir 6.1...6.2	I_{KACh} (Kir 6.2 + SUR1)
		Kir7	Kir 7.1	
4TMD-2P	KCNK1	TWIK	TWIK1	
			TWIK2	
	KCNK2	TREK		S-current
	KCNK3	TASK	TASK1	I_{Kso}, $I_{K(resting)}$
	KCNK5		TASK2	
	KCNK4	TRAAK		
	KCNK6			
	KCNK7			
8Tmd-2P	?	TOK1 (YOK1, DUK1) ?		?

Unlike voltage-gated Na$^+$ or Ca^{2+} channels, a complete K$^+$ channel pore-forming protein is not translated from a single gene, but is made up of four separate subunits, which come together in the membrane to form the functional channel (MacKinnon, 1991a; Papazian, 1999). This has allowed significant diversity of native K$^+$ channels, as a wide range of heterotetramers is possible using different subunits from within the same subfamily.

This introduction concentrates on one specific class of K$^+$ channels in humans, those from the KCNQ gene family. This family has caused considerable excitement among K$^+$ channel researchers, due to the linkage of a large number of mutations to diverse human diseases. Another interesting observation is that at least some recently developed

pharmacological agents specifically act on these channels, and therefore represent potentially important therapeutic drugs (Robbins, 2001).

A 3   KCNQ genes

KCNQ1, previously named KvLQT1, was first identified in a linkage study, which concentrated on the genetic causes of a certain form of sudden death from cardiac arrhythmia, the Long-QT syndrome, LQT (Wang et al., 1996). A number of genomic loci had been mapped for this disease, and one locus, responsible for over 50 % of LQT cases, was shown to code for a K^+ channel, which was subsequently termed KvLQT1. A number of mutations in this channel correlated with families displaying the disease. To date, five genes of this family KCNQ1-5, all encoding K^+ channel subunits with the "*Shaker*-like" topology of 6 transmembrane domains (TMD) and a single pore loop (P) (**Figure A.1**), have been identified. These proteins share between 30 and 65 % amino acid identity (**Table A.1**), with a particularly high homology in the transmembrane regions (Schroeder et al., 1998; Lerche et al., 2000). The P-loop contains the K^+ pore signature sequence TxxTxGYG. All five proteins display a highly homologous region on their intracellular C-terminus termed the "A-domain" (Schroeder et al., 1998a; Schwake et al., 2000). The length of the C-terminus is variable between the subtypes in the following order (longest first): KCNQ5 > KCNQ2 > KCNQ3 > KCNQ4 > KCNQ1.
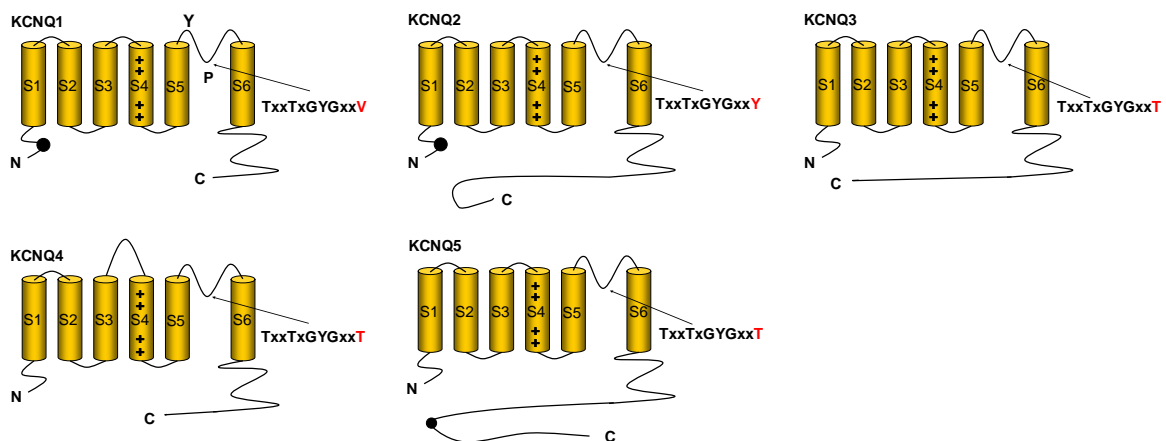
Figure A.1: Structural characteristics of KCNQ K^+ channel subunits with six transmembrane domains (S1-S6) and a single P-loop (P). Glycosylation (Y) and PKA phosphorylation (●). The length of the COOH terminus (C) is representative of the relative size between the different subunits. The numbers of charged residues (+) in the S4 segment are indicated, and the signature amino acid sequence for K^+ channel selectivity is shown (single letter code, x = any amino acid), along with the variation in the residue important in external TEA binding (red).

This variable length of the channels' C-termini may have implications on how these channels are modulated. Conversely, the length of the N-terminus is in the order of 100 amino acids, and is similar between the 5 subtypes. The number of amino acids coded in the gene sequences range from 676 in KCNQ1 to ~900 in KCNQ5. Only KCNQ1 has been suggested to contain a glycosylation site on the extracellular loop between TMDs 5 and 6 (Barhanin et al., 1996). A number of putative phosphorylation sites have been identified. In particular these are protein kinase A (PKA) phosphorylation sites on KCNQ1 and KCNQ2 N-termini.

Table A.2: KCNQ amino acid identity (Robbins, 2001)

KCNQ	1	2	3	4
1	100	-	-	-
2	60	100	-	-
3	31	41	100	-
4	38	44	37	100
5	40	50	50	65

A 4   Potassium channel structure

A 4.1   Selectivity and high throughput (Ion selectivity and ion conductance)

The voltage-gated K^+ channels are composed of tetramers of identical or highly homologous subunits (**Figure A.2A**). Each subunit contains six transmembrane regions, from which S4 forms an essential part of the voltage sensor, and contributes its S5-P-S6 domains to the central pore. Both, amino- and carboxy-termini are oriented towards the intracellular space.

The pore's "inverted tepee" (**Figure A.2B)** arrangement of inner helices, which contains the selectivity filter located at the most constricted part of the pore from the extracellular surface, is also expected to be a conserved feature (Doyle et al., 1998).

A   **B**
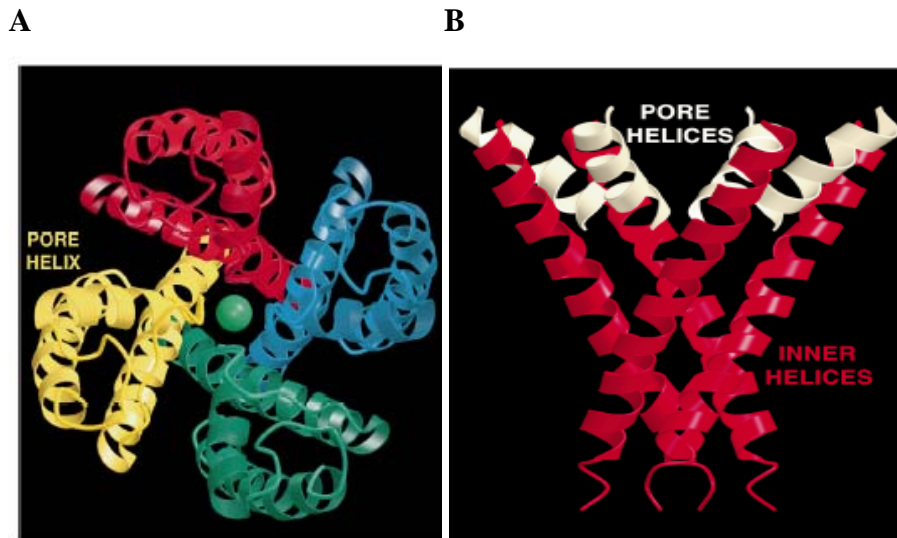
Figure A.2: **A** View of the KcsA tetramer. The four subunits are distinguished by colour. **B**: Inverted tepee architecture of the tetramer, only two opposing subunits are shown for clarity. (From Doyle et al., 1998)

K^+ channels are extremely selective concerning ion species they allow to pass, yet they allow transport rates close to the aqueous diffusion limit. Selectivity and speed are both crucial for the biological function of the channels. In neurons and other cells the ion specificity of a channel determines the direction of current flow. Na^+ and Ca^{2+} ions flow inward and thus carry positive charge into the cell, leading to depolarization. Because most voltage-gated channels are activated by positive potentials, this further activates channels and produces regenerative excitation. Subsequently, K^+ ions flowing through delayed rectifier K^+ channels exit the cell and thereby reduce the positive polarisation inside the cell and in effect terminate excitation.

The reason that ions require assistance to cross lipid membranes is that they have an extremely favourable interaction with water, which is not met in a lipid environment. The K^+ channel proteins have four specific architectural features that keep the ion almost exactly as stable as it is in water.

First, the channels contain a large cavity nearly exactly at the center of the membrane, which enables the stabilization of a hydrated K^+ ion in a place where the energy barrier usually is highest. The intracellular permeation pathway is broad and contains a large amount of water (**Figure A.3**).

Second, the K^+ channels apparently stabilize the ions and achieve cation selectivity by using the electrostatic influence of helix dipoles. Every α-helix has a dipole moment and

the intracellular vestibule of K^+ channels has the negative ends of four helix dipoles pointed towards its central cavity.

A third feature of the K^+ channels' approach to match permeation with ion selectivity is creation of a series of customized polar oxygen cages. As a K^+ ion diffuses through water itself, it is more or less constantly surrounded by a cage of polar oxygen atoms from the water molecules (inner hydration shell). Water is extremely flexible and accommodating and easily adapts the size and configuration of the cage to accommodate ions of different sizes, such as K^+ and Na^+. The selectivity filter of the potassium channel is designed to mimic the water structure around a K^+ ion, but is also designed not to adopt the presumably more compact structure around a Na^+ ion. Each K^+ ion in the selectivity filter is surrounded by two groups of four oxygen atoms, just as in water: these oxygen atoms are held in place by the protein, and are in fact the backbone carbonyl oxygens of the selectivity filter loops from the four subunits.

Finally, a long-known feature of potassium channels is that K^+ ions pass through in single file, with simultaneous occupancy by multiple ions. The mutual electrostatic repulsion between adjacent K^+ ions (spaced about 7 Å apart) destabilizes ions in the pore, permitting the other favourable interactions to produce ion selectivity without producing overly tight binding that would impair rapid permeation.
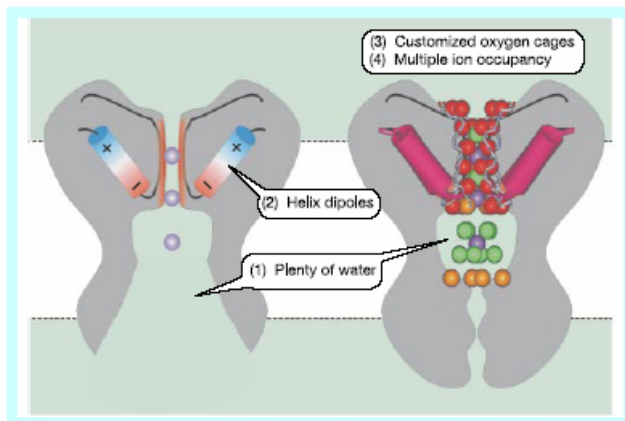
Figure A.3: Architectural features of K^+ channels important for ion permeation. Approximate cross-section of an open K^+ channel, based on the crystal structure of the MthK channel (left). The wide-open intracellular vestibule and pore helix dipoles are highlighted. The diagram on the right is a view derived from the high resolution structure of the KcsA channel, showing a narrower and probably closed access to a water-filled cavity in the middle of the membrane protein. A trapped K^+ ion (purple sphere) and its eight water molecules of hydration (green spheres) are remarkably well resolved; the backbone oxygens of the selectivity filter (red spheres) provide a good match to this hydration environment for the K^+ ions. Occupancy of the pore by multiple K^+ ions has an important role in selectivity and other properties of the channel. This basic architecture can also produce non-selective cation channels or channels selective for Na^+ or Ca^{2+} ions. Orange spheres indicate side chain oxygen atoms. (From Garry Yellen 2002)

A 4.2   Gating

The rapid signalling in neurons requires a fast mechanism for closing and opening the pore. There are three established mechanisms by which the voltage-gated K^+ channels can close.

First the channel can close by pinching shut at the intracellular entrance. The top ends of the four S6 helices form a cradle for the selectivity filter, whereas the bottom ends converge to a right-handed 'bundle crossing' below the cavity.

A second mechanism for closing the pore uses the S6 gate to regulate the binding of an auto-inhibitory peptide that is part of the channel protein (**Figure A.4**).
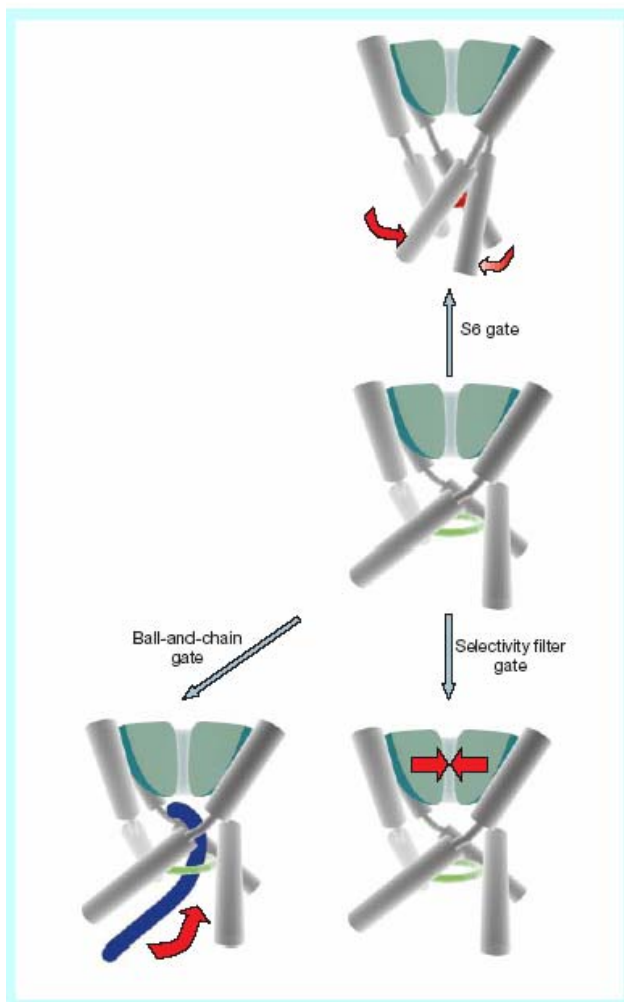
Figure A.4: The conformational changes that gate the K^+-channel pore. The three best understood conformational changes for closing potassium channels are shown here. The centre diagram shows the core structure of an open K^+-channel, on the basis of the MthK structure. The selectivity filter (green) is shown with a cutaway to reveal the narrow pore. The outer helices have been stripped away to show the configuration of the inner helices, corresponding to S6. In the open state these are splayed apart, as in the MthK structure, using the conserved glycine hinge near the selectivity filter. The top diagram structure shows a closed K+-channel, on the basis of the KcsA structure. The four S6 transmembrane segments swing together to produce a secure closure at the bundle crossing. This shuts off ion flow and can trap organic channel blockers in the enclosed cavity. The green and red rings in the diagrams illustrate the open and closed states, respectively, of the S6 gates. Alternatively, the channel may be closed at the selectivity filter (lower right diagram), or by binding of an auto-inhibitory peptide (lower left diagram) when a binding site in the pore is revealed by opening of the S6 gate. (From Garry Yellen 2002)

The N-terminus of *Shaker* K^+ channels can act as a channel blocker, probably by binding directly to the cavity. Because this interaction occurs only after the S6 gate has opened, some voltage-gated K^+ channels conduct only transiently, during the brief period after the

S6 gate opens and before the N-terminal peptide blocks the channels: this behaviour is known as 'N-type inactivation'.

A third type of inactivation is the C-type inactivation. C-type inactivation persists in *Shaker* channels when the inactivation ball is deleted. This inactivation process (normally slower than N-type inactivation) probably has a function in regulating repetitive electrical activity; its sensitivity to $[K^+]$ may also determine a physiological response to accumulation of extracellular K^+ ions.

A 4.3   S4 structure and movement

All KCNQ subunits contain a regular arrangement of six positively charged amino acids in the S4 region (Schroeder et al., 1998a), except KCNQ1, whose S4 segment carries only four positive charges.

The voltage sensor is a specialized structure with intricate geometry that includes S4, but also the S1-S3 transmembrane segments contribute charged side chains involved in the voltage sensing process. The whole module made up by S1, S2, S3, and S4 is referred to as the voltage-sensing module (Hille, 2001).

When a *Shaker* channel opens, a net equivalent of 12 to 14 positive elementary charges is moved across the membrane electric field from inside to outside, and most of this charge is carried by four Arg residues on each S4 segment of the four identical channel subunits (Schoppa et al., 1992).

Translocation of these S4 charges from one side of the membrane to the other can be confirmed biochemically, by replacing a charged residue with cysteine and applying cystein modifying agents to one or the other side of the membrane in voltage- or patch-clamp experiments.

Francisco Bezanilla and coworkers substituted a histidine residue for the arginine at R2 (second arginine position in S4) or R3 of the *Shaker*-IR channel construct ("IR" denotes "inactivation removed" by cutting off the N-terminal inactivation ball). In order to increase the resolution of gating-current measurements, they started with an engineered channel that passes no K^+ current because of a mutation in the pore helix near the selectivity filter. The channels with histidine mutations passed a steady ionic current at some intermediate voltages, which could be shown to be carried by protons. This current flows outward when the proton gradient is outward and inward when the proton gradient is oppositely directed, and exhibits unusual voltage dependence. Amplitudes of the proton currents are small at very hyperpolarized or depolarized voltages, where the voltage sensors remain in their extreme "closed" or "open" positions. The maximum H^+ current is reached at intermediate potentials, where the voltage sensor is expected to be shuttling most frequently between the two extreme positions. Apparently, the histidine in S4 picks up a proton on the low-pH side and releases a proton on the high-pH side each time a voltage sensor makes a transition back and forth across the membrane, so it acts as a proton carrier shuttling back and forth.

Isacoff and coworkers investigated the state-dependent intracellular and extracellular solvent exposure of the *Shaker* S4 segment by substituting cysteins at various positions and assayed their accessibility to a membrane-impermeant thiol-reactive compound.

Figure 4 shows a model of S4 movement that is consistent with the observations of Isacoff. The five S4 residues that are buried in the closed state are depicted. They span approximately half the thickness of the hydrocarbon core of the bilayer, a distance intermediate between that which would be spanned as an α-helix (8 Å) or β-sheet (18 Å). Upon depolarization, S4 moves as a unit between 9 and 15 amino acids outwards (**Figure A.5**).
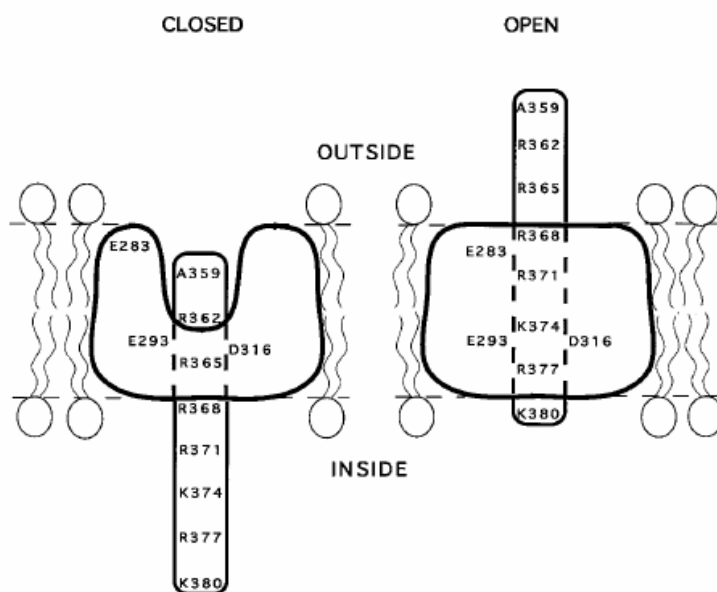
Figure A.5: The diagrams depict a region of protein around the S4 region of a single subunit of the *Shaker* channel in the conformations associated with the channel's closed and open states. Five residues (363–367) span the distance between the intracellular and extracellular solutions in closed channels, leaving only one basic residue buried (R365). This distance is shown as 50% of the thickness of the bilayer hydrocarbon core (~25–30 Å), or intermediate between the distance which can be spanned by an a helix (8 Å) and a b sheet (18 Å). A crevice permits but restricts access to 359 and 362 from the external solution in the closed state. When channels open, S4 moves outward as a unit. This movement of S4, or a subsequent conformational change, closes the crevice, leaving a total of 12 residues buried (experiments show that the number is between 9 and 15). The basic residues buried in the open state form salt bridges with acidic residues in S2 and S3 (R368 and R371 are shown interacting with E283, and K374 and R377 interacting with E293 and D316) (From Larsson et al., 1996).

Recently, MacKinnon and colleagues investigated the mechanism by which voltage-dependent cation channels sense the membrane voltage by determining the X-ray crystal structure of a mammalian *Shaker*-related K$^+$ channel Kv1.2 (**Figure A.6A**). From analysis of the three-dimensional structure, the following conclusions were derived:

First, the voltage sensors are independent membrane-embedded domains.

Second, the voltage sensors have to perform mechanical work on the pore through the S4-S5 linker helices, which are positioned to constrict or dilate the S6 inner helices of the pore (**Figure A.6B, C**).

The third conclusion was that in the open conformation two of the four conserved Arg residues on S4 are on a lipid-facing surface and two are buried in the voltage sensor.

Figure A.4: The conformational changes that gate the K$^+$-channel pore. The three best understood conformational changes for closing potassium channels are shown here. The centre diagram shows the core structure of an open K$^+$-channel, on the basis the MthK structure. The selectivity filter (green) is shown with a cutaway to reveal the narrow pore. The outer helices have been stripped away to show the configuration of the inner helices, corresponding to S6. In the open state these are splayed apart, as in the MthK structure, using the conserved glycine hinge near the selectivity filter. The top diagram structure shows a closed K+-channel, on the basis of the KcsA structure. The four S6 transmembrane segments swing together to

Two aspects of the Kv1.2 crystal structure suggest that the determined channel conformation was an open conformation in contrast to the closed conformation of the

KvAP. First, the inner helix bundle (activation gate) of the pore is opened to ~12 Å in diameter (see **Figure A.7**) and, second, the voltage sensor appears to be in an open ("activated") position.

A   **B**   **C**
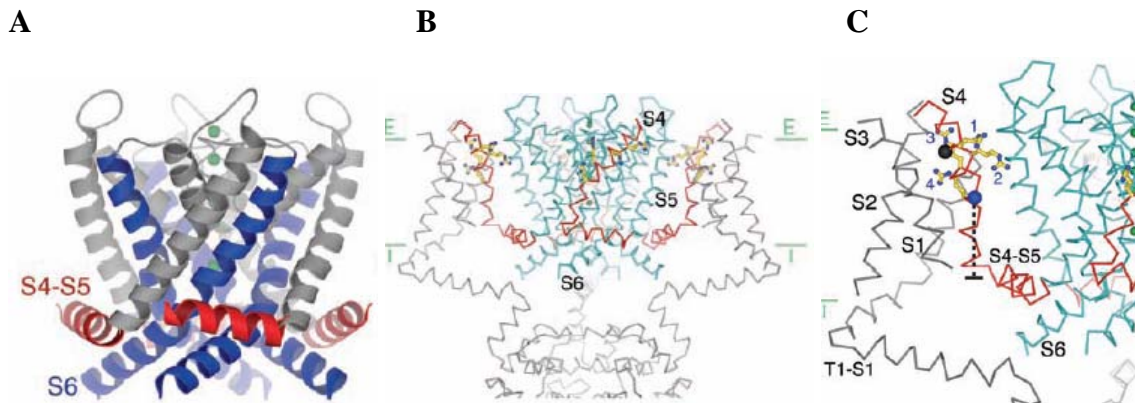
Figure A.7: A) A view of the Kv1.2 channel tetramer showing the S4-S5 (red), S5 (gray), and S6 (blue) helices as ribbons. The perspective is from the side of the channel with the extracellular side above and the intracellular side below. **B)** The protein main chain is represented as a C$_a$ trace. The pore is shown in cyan; the S4 helix and the S4-S5 linker in red; and voltage-sensor helices S1 to S3, the T1-S1 linker, and the T1 domain (bottom) is represented in gray. Side chains of Arg 1 to 4 on the S4 helix are shown. The α helices S1 to S3, the T1-S1 linker, and the T1 domain are removed from the subunit nearest the viewer. Green lines labeled E (extracellular) and I (intracellular) mark the approximate boundaries of a membrane 30 Å thick. **C)** An enlarged view of one voltage sensor is shown with the same orientation and coloring as in B). A black sphere at position 295 highlights that the α carbon of the equivalent amino acid in KvAP approaches within a few angstroms of the extracellular solution (top) when the channel is opened at depolarized membrane voltages (positive inside), as assessed through avidin capture of tethered biotin. A blue sphere at position 302 shows that the equivalent position in KvAP approaches within a few Angstroms of the intracellular solution (approximate distance shown as dashed line) when the channel is closed at negative membrane voltages (negative inside). (From Long et al., 2005)

The comparison of Kv1.2 and KvAP serves many useful purposes. First, their fundamental similarity reinforces the confidence in the accuracy of the Kv1.2 voltage-sensor model and shows that S4 and S3 form a voltage sensor paddle as in KvAP. Second, because Kv1.2 and KvAP are similar, KvAP functional data can be used, in order to predict possible motions of the Kv1.2 voltage sensor. Third, certain differences between their structures may provide useful information about movements of the voltage sensor. For example, the voltage-sensor paddles in Kv1.2 are in a slightly different position with respect to the S1 and S2 helices (**Figure A.8**). This is understandable, if the paddles are mobile, allowing them to move in the gating process. Fourth, S4 (and S3) is nearly two helical turns longer at its extracellular end in Kv1.2 than in KvAP (the Kv1.2 S4 contains two extra helical turns preceding the Arg residues) (compare Fig. 2, A and C). This means that the paddle in Kv1.2 will project further into the extracellular solution and therefore may exhibit differences (relative to KvAP) in accessibility to spider toxins and small molecules that interact with the voltage sensor from outside the cell (Long et al., 2005)
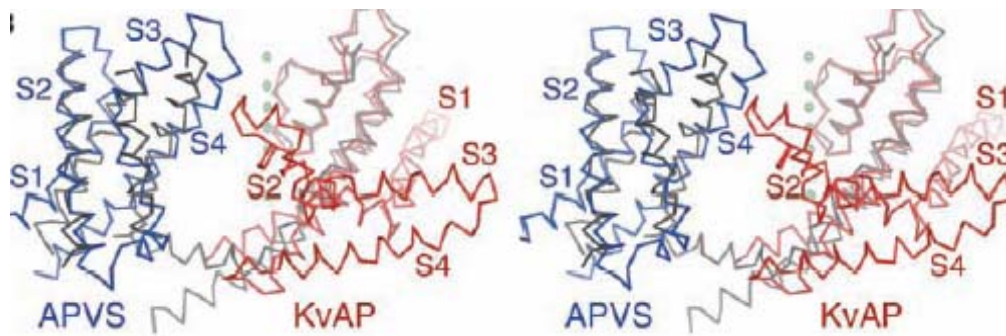
Figure A.8: The Kv1.2 structure (gray) viewed with a full-length crystal structure of KvAP (red trace) superimposed by alignment of main-chain atoms of the pore helices and selectivity filter, and with an isolated voltage-sensor structure of KvAP (*Aeropyrum pernix* voltage sensor, or APVS) (blue trace) superimposed by alignment of main-chain atoms of a helices S1 and S2. (From Long et al., 2005)

A 5   Properties of currents mediated by KCNQ channels

To determine the biophysical characteristics of KCNQ channel currents these proteins have been heterologously expressed in *Xenopus* oocytes (Wang et al., 1996; Biervert et al., 1998; Schroeder et al., 1998a), Chinese hamster ovary (CHO) cells (Hadley et al., 2000a), human embryonic kidney (HEK) 293 cells (Shapiro et al., 2000), and Sf9 cells (Barhanin et al., 1996). Subtle differences have been reported, possibly arising from the different expression systems. However, in general, expression of these channels induces outwardly rectifying voltage-dependent K^+ currents that activate at voltages more positive than −60 mV, with little or no inactivation. However, there are particular characteristics associated with each current, depending of whether the subunits are expressed alone (homomultimers) or together with other subunits (heteromultimers) (Robbins, 2001).

A 5.1   Homomultimers

KCNQ1 homomultimeric channels exhibit outwardly rectifying currents with a half-activation voltage ($V_{0.5}$) of −10 to −20 mV, with a slope *(k)* of ~12 mV per e-fold increase in conductance. Activation kinetics is sigmoidal, with typical time constants in the order of 100–200 ms to achieve 90 % activity level. When expressed in oocytes, the current does not seem to reach maximum within a 2- or 3-sec step (Schroeder et al., 1998a). In contrast, when expressed in mammalian cell lines, the current activates more rapidly and seems to reach full activation within 1 sec (Sanguinetti et al., 1996). Very little inactivation is

apparently seen until the tail currents are carefully inspected, where a characteristic "hook" can be observed (Sanguinetti et al., 1996). This characteristic has been studied in detail and has been explained by a fast removal of inactivation and a relatively slow deactivation, allowing the channels to open again before they are deactivated on repolarisation (Tristani-Firouzi and Sanguinetti, 1998).

KCNQ2 can be successfully expressed in a range of cells, including oocytes, CHO cells, HEK cells, and COS cells. The biophysical parameters of the current seem to depend on the expression system and/or voltage protocol, with values of $V_{0.5}$ of −14 mV, −21 mV, −37 mV, and −38 mV for CHO, HEK, oocytes, and COS cells, respectively. Slope values (k) range between 7 mV and 14 mV per e-fold increase in conductance.

Expression of KCNQ3 homomultimers in oocytes and CHO cells seems to be rather variable. In some studies especially in oocytes, the expression was very weak (Schroeder et al., 1998a). In the studies where expression has been successful (Hadley et al., 2000a), KCNQ3 currents activate at voltages more positive than −60 mV, again with sigmoidal activation characteristics. A particular property of KCNQ3 currents is an apparent inward rectification at membrane potentials more positive than 0 mV that leads to a "crossover" phenomenon. This is where successive steady-state currents evoked by incremental voltage steps to values above 0 mV get smaller, even though the driving force for K^+ ions is still increasing. Whether this is a gating behaviour of the channel comparable to an inactivation mechanism or a voltage-dependent block brought about by a particular ion species has not yet been investigated.

KCNQ4, when expressed alone in CHO cells, displays a $V_{0.5}$ of −19 mV and a k value of +10 mV. The activation onset is exponential, except at very positive voltages, and little or no inactivation can be seen (Hadley et al., 2000a). In oocytes, the $V_{0.5}$ is −10 mV with a k value of 18 mV, and the activation is slow, with a time constant of 600 msec at +40 mV (Kubisch et al., 1999).

KCNQ5 homomultimers activate very slowly and bi-exponentially, with time constants between ~0.1 and 1.0 sec, and do not fully activate during 3-sec test pulses (Lerche et al., 2000b). Similar to KCNQ3, KCNQ5 currents display an apparent inward rectification of steady-state currents at very positive potentials.

A 5.2   Heteromultimers

It has been well established that KCNQ1 can functionally co-assemble with members of the KCNE gene family, in particular KCNE1 (Sanguinetti et al., 1996) and KCNE3 (Schroeder et al., 2000a). In the presence of KCNE1, KCNQ1 currents increase very slowly in amplitude, activate at even more positive potentials than KCNQ1 expressed alone. Activation occurs more slowly, and little or no inactivation seems to persist. In contrast, co-assembly of KCNQ1 and KCNE3 produces a current with nearly instantaneous activation, some time-dependent activation at very positive potentials, and a linear current voltage relationship. KCNQ1 does not seem to functionally co-assemble with any other members of the KCNQ family (Schwake et al., 2000).

Upon heterologous expression of KCNQ2 together with KCNQ3 the currents measured are more than 10 times higher in amplitude than expected from the simple summation of the currents produced by expression of KCNQ2 or KCNQ3 channels alone. This strongly indicated that upon KCNQ2+KCNQ3 coexpression, heteromeric channels with novel characteristics are formed. Further analysis of the nature of this interaction between KCNQ2 and KCNQ3 suggested that the increase in current was not due to changes in single-channel conductance or mean open time (open probability), but to an increase in the number of functional channels at the plasma membrane (Schwake et al., 2000). This improved membrane expression was dependent on an intact carboxy-terminus. The so-called "A-domain", which is highly conserved between KCNQ channels, has been implicated in this subunit interaction, since the current stimulation was absent upon truncation of the KCNQ2 C-terminus.

KCNQ2 has also been reported to functionally interact with KCNE1, however, the physiological significance of this observation is unclear yet. KCNQ3 is by far the most promiscuous KCNQ subunit, since it can functionally interact with all other KCNQ subunits except KCNQ1 (Schroeder et al., 1998a). KCNQ3 can also interact with KCNE1. Interestingly KCNE2, a related protein associated with the HERG K^+ channel in the heart (Abbott et al., 1999) is much more widely distributed (including brain), and interacts with both KCNQ2 homomultimers and KCNQ2+KCNQ3 heteromultimers in a functional manner (Tinel et al., 2000).

KCNQ4 does not functionally co-assemble with KCNQ1 or KCNQ2, and dominant negative mutants of KCNQ1 or KCNQ2 do not affect the KCNQ4 current amplitude (Schroeder et al., 2000a)

KCNQ3, on the other hand, apparently co-assembles with KCNQ4, as co-expression leads to current amplitude greater than the homomultimeric sum and KCNQ4 currents are significantly reduced by the KCNQ3 dominant negative mutant (Kubisch et al 1999). KCNQ5, as with KCNQ4, seems to functionally interact with KCNQ3 and KCNQ2, but not KCNQ1, or any of the four members of the KCNE family (Lerche et al., 2000b). It is interesting that of the five KCNQ subtypes, KCNQ3 seems to be the most promiscuous in terms of interactions with the other subtypes, but the least able to form homomultimers.

The principles determining whether channel subunits assemble predominantly with themselves (homotetramerization) or with other members of the protein family (heterotetramerization) are thus of great importance, but the processes which govern this interaction pattern have not been completely defined. One possibility could be that different but related mRNAs are bound in a translational unit via RNA binding proteins and are coordinately translated at the ER (Deutsch, 2003).

A 6   KCNQ channel pharmacology

A 6.1   Channel blockers

Ba^{2+} ions produce at least a 50 % inhibition of currents at a concentration of 1 mM. The channel-blocking activity of tetraethylammonium (TEA) has been more systematically studied (Hadley et al., 2000b), showing that the sensitivity of the homomultimeric channels is KCNQ2>KCNQ4= KCNQ1>KCNQ5>KCNQ3).

KCNQ2 contains a tyrosine (Y) residue at 284 and KCNQ1 a valine (V), the rest of the subtypes have a threonine (T) in the equivalent position (see **Figure A.1**), which is similar to the situation in *Shaker* channels, where the presence of a tyrosine residue confers high external TEA sensitivity (MacKinnon, 1991b). Some studies have tried to test this directly by expressing the KCNQ3 (T323Y) mutants, but have been unsuccessful in generating sufficient functionally active homomultimers in both CHO cells (Hadley et al., 2000b) and *Xenopus* oocytes.

The putative cognitive enhancer linopirdine and its more potent analogue 10,10-bis(4-pyridinylmethyl)-9(10H)-anthracenone (XE991) have been used as specific pharmacological markers of the KCNQ currents (Hadley et al., 2000a).

From a clinical point of view, the Class-III antiarrhythmic drug clofilium can also block the cardiac KCNQ1-containing channels generating a cardiac-delayed rectifier-like K^+ current (I_{Ks}), as well as having significant effects on the noncardiac currents containing KCNQ3, KCNQ5, and KCNQ2/3 heteromultimers. In light of increasing knowledge of KCNQ channels and their heteromultimeric nature, there are no highly specific and selective channel blocking compounds available yet.

A 6.2   KCNQ channel activators

It had been reported that Cl^--channel blockers, such as 4,4′-diisothiocyanatostilbene-2,2′-disulfonic acid (DIDS) and mefenamic acid, can activate KCNQ1 channels and oocyte I_{Ks} currents (Busch et al., 1994). In a more detailed study, it was demonstrated that DIDS can shift the voltage dependence of activation of monomultimeric KCNQ1 currents in the negative direction by ~17 mV and significantly slow deactivation kinetics (Abitbol et al., 1999).

Of more clinical significance are the recent reports (Rundfeld and Netzer, 2000; Rundfeldt and Netzer, 2000) that the novel anticonvulsant drug retigabine can shift the activation of KCNQ2/3 currents to more negative potentials by more than 20 mV at 10 μM, increasing the rate of activation and decreasing the rate of deactivation. Therefore, KCNQ channels in the brain may represent a novel target for antiepileptic drugs.

A 7   KCNQ physiological correlates

A 7.1   KCNQ1 forms part of the cardiac I_{Ks} current

During a cardiac action potential, a number of K^+ channel currents come into play (Nerbonne, 2000). Many of these currents have different relative importance, both in time during the electrical cycle of the heart beat and in different areas of the cardiac tissue. The I_{Ks} current, which would be described as a slow delayed rectifier, has a significant role in the repolarising phase of the cardiac action potential.

In two simultaneous publications, two groups defined the I_{Ks} current as a KCNQ1 + KCNE1 heteromultimer (Barhanin et al., 1996). Evidence was based on the similar kinetics of the I_{Ks} current and that seen for heterologously expressed KCNQ1 and KCNE1 heteromultimers. The mRNA expression patterns of KCNQ1 and KCNE1 include cardiac muscle as well as other tissues. As mentioned above, co-expression of both KCNQ1 and KCNE1 produced a current with kinetics and pharmacology similar to the I_{Ks} current. Pharmacological evidence shows that the Type-III antiarrhythmic drug clofilium blocks I_{Ks} with an IC_{50} of ~0.1 mM, and this is similar to the sensitivity of KCNQ1+KCNE1 heteromultimers. Conversely, blockers such as E-4031 and dofetilide, which are effective on I_{Kr} currents (HERG+KCNE2), are ineffective on KCNQ1+KCNE1 (Yang et al., 1997).

A 7.2   KCNQ1 forms part of the K$^+$ current of colonic crypt cells

KCNQ1 mRNA is also found in the intestine, particularly in the crypt cells of the small intestine and colon (Schroeder et al., 2000b). Here it is thought to assemble with another member of the KCNE family, KCNE3, which shows an overlapping mRNA distribution in intestinal tissue. Upon expression with KCNE3 an instantaneously activating current is seen with a nearly linear current–voltage relationship. It is thought that this particular current has an important role in intestinal Cl$^-$ homeostasis, which is altered in conditions such as cystic fibrosis and cholera.

A 7.3   KCNQ1 plays a role in K$^+$ recycling in the inner ear

Two lines of evidence have implicated KCNQ1 in the functioning of the inner ear. First, mRNA for KCNQ1 and KCNE1 has been shown in the apical surface of marginal cells of the stria vascularis of the cochlea (Neyroud et al., 1999) (**Figure A.9**). Second, in the homozygous form of Jervell-and-Lange-Nielsen syndrome (JLNS), mutant KCNQ1 channels cause a bilateral deafness. As in the heart, it is thought that KCNQ1 co-assembles with KCNE1 to form functional channels. However, in this case, the channels are thought to be tonically active. Unlike the action of KCNQ1 in the heart where the channels underlie a repolarising current, in the cochlea it has a different role, as KCNQ1 subunits contribute to the recycling circuit for K$^+$ ions. The endolymph contained in the scala media is more

akin to intracellular media in terms of its ionic composition. The endolymph has a high K^+ and low Na^+ concentration, setting a positive endolymph potential of ~ +80 mV. During auditory stimulation, K^+ moves from the endolymph into the hair cells. K^+ ions then move out of the basal portion of hair cells (most likely utilizing KCNQ4 channels in the outer hair cells) into what is thought to be a cellular syncytium of supporting cells, which recycle the K^+ ions back into the endolymph via the stria vascularis. The K^+ channels on the marginal cells regulating the flux are thought to contain KCNQ1+KCNE1 proteins. Any reduction in the concentration gradient for K^+ leads to a reduction of the endolymph potential, and this can eventually reduce sensitivity to auditory stimuli. A similar mechanism is also thought to occur in the marginal cells of the vestibular epithelium. Mutations in both KCNQ1 (JLNS1) and KCNE1 (JLNS2) can lead to hearing loss *and* vestibular disturbance. However, the latter is phenotypically less obvious, due to the ability of humans to adapt well to loss of vestibular function.
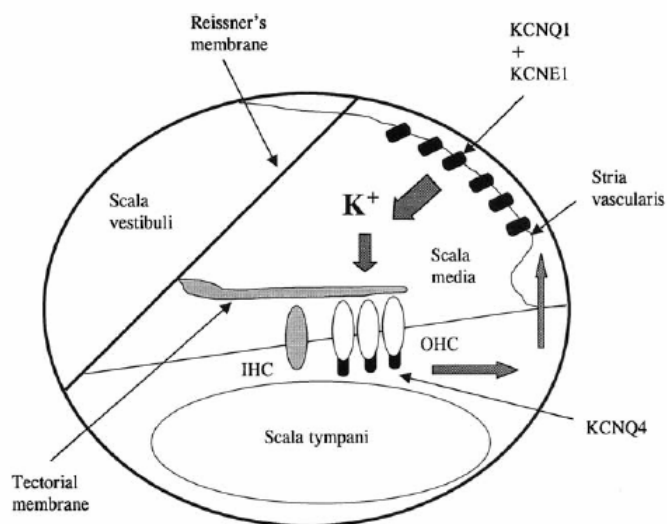
Figure A.9: K^+ homeostasis in the cochlea. Cross-section of one turn of the organ of Corti. The fluid in the scala media (endolymph) is more akin to intracellular media, in that it has a high K^+/low Na^+ composition. During auditory stimulation, the Outer Hair Cells (OHCs), which are thought to be important for amplification rather than sound transduction, take up K^+, which is returned to the endolymph via KCNQ4-containing channels on the basal portion of the OHCs. K^+ is then moved into the stria vascularis, where it is returned by KCNQ1+ KCNE1-containing channels IHC (Inner Hair Cells). (From J.Robbins 2001)

A 7.4   KCNQ2 and KCNQ3 heteromultimers may form the M-current

The M-current ($I_{K(M)}$) was first described in bullfrog sympathetic ganglia (Brown and Adams, 1980) as a slowly activating and slowly deactivating K^+ current that showed no

inactivation. It was inhibited by activation of a number of G-protein-coupled receptors, including muscarinic receptors and, hence, was given the name "M-current". The mammalian equivalent was soon described in rat superior cervical ganglion (SCG) cells, which became the "benchmark" current against which other M-like currents were compared.

Identification of the molecular correlate for $I_{K(M)}$ has been hampered in the past due to a lack of selective pharmacological agents to block M channels. With the discovery of linopirdine and the related compound XE991, both reasonably selective M-current blockers, the screening of known K^+ channel genes became possible. Using linopirdine and XE991 sensitivity mapping, as well as a comparison of biophysical parameters and mRNA expression, it was concluded that KCNQ2 and KCNQ3 heteromultimers could be the molecular correlates of IK(M) in rat SCG;(Wang et al., 1998; Cooper et al., 2000)

KCNQ1, KCNQ2, KCNQ3, and KCNQ4 homomultimers, as well as KCNQ2/3 heteromultimers and KCNQ5, can all produce functional currents that display M-like characteristics. Indeed, all combinations of current can be inhibited by M_1 muscarinic activation (Selyanko et al., 2000) and blocked (albeit with different efficiency) by linopirdine (Wang et al., 1998).

A 7.5   KCNQ4 is the molecular correlate of $I_{K,n}$ and $I_{K,L}$

As with almost all other sensory transduction systems, hearing and balance involve the modulation of K^+ channels at an early stage of the process of turning sensory stimuli such as sound into electrical signals. The "holy grail" of auditory physiology is to identify the channel responsible for mechanoelectrical coupling in hair cells. Although this has not been unequivocally discovered, a number of K^+ currents in hair cells have been identified. In outer hair cells (OHCs), the dominating K^+ current is termed $I_{K,n}$ (Housley and Ashmore, 1992). The vestibular apparatus, just like the cochlea, contains two types of hair cells, Type I and Type II. The Type I hair cells display a large voltage-gated K^+ current ($I_{K,L}$) not seen in the Type II cells (Chen and Eatock, 2000), with a very negative potential of half-maximal activation (-73 mV). On the other hand, KCNQ4, like $I_{K,L}$, is found only in Type I cells in the vestibular apparatus.

A 7.6   KCNQ4 and KCNQ5 may underlie M-current heterogeneity

As discussed, the M-current may be mediated by KCNQ2/3 heteromultimers. However, a number of issues is still unresolved. First, homomultimers and KCNQ2/3 heteromultimers display a noticeable sigmoidal activation (Wang et al., 1998; Selyanko et al., 2000). The native $I_{K(M)}$ shows an exponential activation and deactivation. Interestingly, KCNQ4 (Selyanko et al., 2000) and KCNQ5 homomultimers (Lerche et al., 2000a) show more of an exponential activation, and so do KCNQ3/5 heteromultimers, which may suggest a role for at least one of these subunits in native M-currents. The rather restricted distribution in the brain of KCNQ4 (Kharkovets et al., 2000) probably rules this out as a major contribution to M-current in many neurons.

A 8   KCNQ pathophysiology

A 8.1   Long QT syndromes

The cardiac action potential is an extraordinarily complex phenomenon, depending on the coordination of the activity of many channels, of which a number are K^+ channel types. It is thus not surprising that any perturbation in this event could have serious and life-threatening consequences. One particular set of perturbations are the LQT syndromes. The QT time within the ECG refers to the interval between the beginning of the QRS complex (ventricular contraction) and the T wave (cardiac repolarization), and an increased QT duration in the absence of drugs that delay cardiac repolarisation can be diagnostic of the syndrome. LQT syndromes can be both acquired and congenital (Viskin, 1999).

The congenital forms are of particular interest, as they are all the result of mutations in ion channel proteins, with the singular exception of LQT4, which is due to mutations in ankyrin B, a cellular matrix protein involved in proper targeting of certain membrane proteins.

From the patient's point of view, there may be very little in the way of symptoms until some event (strenuous exercise, stress, drugs, etc.) leads to a form of distinctive re-entrant arrhythmia, known as "torsades de pointes". Torsades de pointes („twisting of the peaks") refer to a type of ventricular tachycardia in which the amplitude of the QRS complex of the ECG varies around the isoelectric line. Torsades de pointes can self-terminate or

degenerate into lethal ventricular fibrillation. Acquired LQT syndrome can occur in young asymptomatic patients, and may explain a substantial part of undiagnosed sudden death cases associated e. g. with an event such as near-drowning (Ackerman et al., 1999).

An autosomal dominant form of LQT1, known as Romano-Ward syndrome, is the result of the dominant negative effect, where mutant channels are not only dysfunctional themselves, but also inhibit the function of apparently healthy wild-type subunits present in the assembled channel (Wollnik et al., 1997). Conversely, the autosomal recessive forms of LQT1, also known as JLNS (Jervell-and Lange-Nielsen Syndrome), in its heterozygous form, displays a weak form of cardiac dysfunction, but in its homozygous form both a severe cardiac dysfunction and a bilateral deafness are apparent.

The mutations in KCNQ1 that cause dominant Romano-Ward syndrome, in the main, seem to result in dominant-negative effects, where the mutant protein is not functional. It can also inhibit the function of any wild-type protein upon co-assembly (Wollnik et al., 1997). On the other hand, the recessive JLNS-type mutants do not display a dominant negative effect; however, the mutations may result in defective subunit assembly (Schmitt et al., 2000).

A 8.2   Epilepsy

A certain form of epilepsy, benign familial neonatal convulsions (BFNC), was first mapped to loci on chromosomes 20 and 8 (Leppert et al., 1989). The resultant genes were identified as K^+ channels KCNQ2 and KCNQ3, respectively (Schroeder et al., 1998). BFNC is rare, with an incidence of 1 in 100,000. It is characterised by generalised seizures in early life, which disappear within weeks or months after birth. However, some 16% of the patients do display seizures in later life.

It is thought that the total current in BFNC is reduced by only ~20–30 % (Schroeder et al., 1998b), which is critical during postnatal brain development and results in seizures, but later in life compensatory mechanisms (complementation by other K^+ channels?) do allow normal functioning. This type of mutation has been termed haploinsufficiency (Rogawski, 2000). To date, the majority of the mutants associated with BFNC are in KCNQ2 (Jentsch, 2000). However, a recent report has highlighted mutations in KCNQ3 that are linked to BFNC. A note of caution has to be stated here, as inhibition of KCNQ channels in hippocampal slices by linopirdine (Dup996) does not alone lead to seizure activity. The

seizure-like behaviour is seen only when there is already some other disruption of neuronal activity and KCNQ channel activity is blocked in addition (Zhu et al., 2000). These results may suggest that a mutation in KCNQ2 and/or KCNQ3 alone may not be sufficient to trigger BFNC, but in combination with some other impairment, a mutation may increase susceptibility.

A 8.3   Deafness

As mentioned above, a homozygous recessive form of LQT1, JLNS, is also associated with a form of congenital deafness. It is thus not surprising that mutations which disrupt the channels involved in this K^+ homeostasis may have significant effects on hearing. Both, frameshift and missense mutations have been described, resulting in nonfunctional channels, either by dominant negative effects, or by impaired assembly of channels.

KCNQ4 could almost be considered as a "hearing K^+ channel", as it is almost exclusively expressed in the inner ear, vestibular apparatus, and a number of nuclei in the central auditory pathway (Kharkovets et al., 2000).

However, the pathophysiological link between the resultant deafness, termed nonsyndromic autosomal dominant deafness type 2 (DFNA2), and impaired channel function in the OHCs of the inner ear, in the central auditory pathway (or both) is as yet unclear.

B   MATERIALS AND METHODS

B 1   Molecular biology

B 1.1   cDNA constructs and cRNA synthesis

KCNQ cDNAs were subcloned into the expression vector pTLN. The KCNQ1/KCNQ3 chimeras, as well as the KCNQ2 and KCNQ3 mutants and deletion constructs and the pore mutant KCNQ1-(G314S) were generated by recombinant PCR. The HA epitope with the amino acid sequence (YPYDVPDYA) stems from the hemaglutinin A protein of the human influenza virus. The HA-tagged KCNQ1 construct contains the amino acid sequence SEH**YPYDVPDYA**VTF after the amino acid Ala-149 within the extracellular loop between transmembrane segments S1 and S2. The HA-tagged KCNQ2- and KCNQ3-channels contained an HA epitope with extended flexibility by carrying further amino acids of the extracellular loop between transmembrane segments D1 and D2 of the chloride channel ClC-5 (Schwake et al., 2000). The single cystein substitutions were introduced in to the KCNQ1 wild-type sequence by recombinant PCR. Within the KCNQ1 S3-S4 loop following substitutions were generated: G216C, S217C K218C, G219C and within the S4 segment Q220C, V221C, F222C, A223C, T224C, S225C, A226C, I227C, R228C, G229C, I230C R231C, F232C, L233, Q234C, and I235C. The double cystein constructs tested were M159C(S2 loop)/I230C, T224C/F279(S5 loop)and L282C(S5-S6 loop)/R228C. All PCR-derived cDNA streches were verified by sequencing (MWG Biotech AG, Ebersberg).

After linearization of plasmids with HpaI, cRNA synthesis was carried out with the SP6 mMessage mMachine Kit (Ambion, Austin, TX).

B 2   Heterologous expression in *Xenopus* laevis oocytes

Female *Xenopus* laevis frogs were operated in order to obtain parts of the ovarial tissue. The extracted tissue was subjected to collagenase treatment to isolate individual stage V to VI oocytes. Collagenase is a mixture of several enzymes, which are purified from the mushroom *Clostridium histolyticum*. The proteolytic ability helps to digest the follicular

matrix. KCNQ cRNA (10 ng) was injected into oocytes, also for coinjection experiments, which contained a 1:1 cRNA mixture. After injection, oocytes were kept at 17 °C in MBS solution (88 mM NaCl, 2.4 mM NaHCO$_3$, 1 mM KCl, 0.41 mM CaCl$_2$, 0.33 mM Ca(NO$_3$)$_2$, 0,82 mM MgSO$_4$, 10 mM HEPES, pH 7.6).

A)   **B)**   **C)**
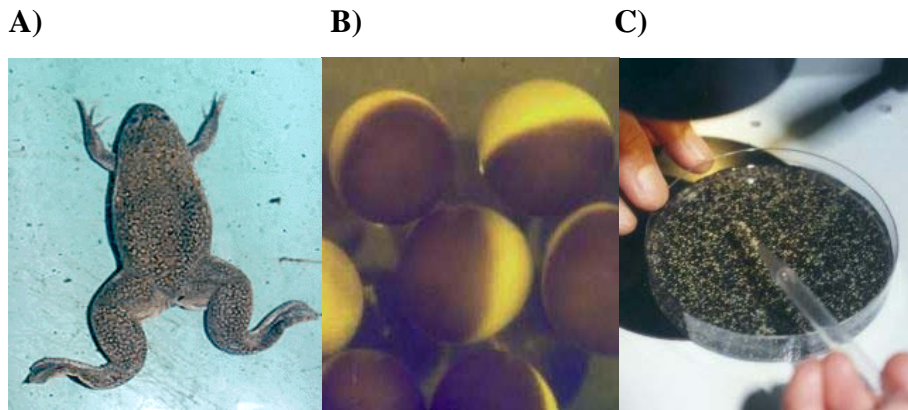
Figure B.1: **A)** *Xenopus* leavis female frog. **B)** Oocytes from *Xenopus leavis* frogs **C)** Oocytes prepared for injection.

B 3   Chemiluminescence surface detection assay

The surface expression of HA-tagged KCNQ constructs was carried out as described previously (Schwake et al., 2000; Zerangue et al., 2000). Briefly, oocytes were placed for 30 min in blocking solution (BS = ND 96 plus 1% BSA). After that oocytes were incubated for 1 h with rat monoclonal anti-HA antibody 3F10 (Roche Diagnostics, Mannheim, Germany) diluted in BS (1 µg/ml), washed three times (BS) and incubated with HRP-conjugated goat anti-rat F$_{AB}$ fragments as secondary antibody (Jackson Immuno Research, West Grove, PA) in BS, followed by three washes each, first in BS and then in ND96. All incubation and washing steps were performed on ice. Surface expression was quantified by placing individual oocytes in 50 µl of SuperSignal ELISA Femto Sensitivity Substrate solution (Pierce, Rockford, IL), and luminescence was measured in a TD 20/20 luminometer (Turner Designs, Sunnyvale, CA).
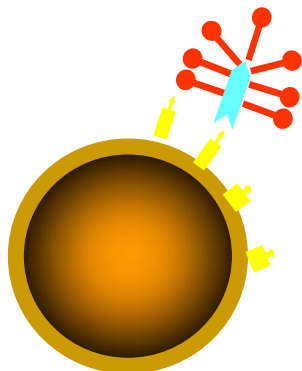
Figure B.2: Surface detection of epitope-tagged channel subunits in *Xenopus* leavis oocytes. The tagged protein at the oocyte surface is marked yellow, the primary antibody is marked blue, and the secondary antibody with the HRP-moiety is depicted in red.

B 4   Coimmuneprecipitation

For coimmuneprecipitation experiments, Cos7 cells were used that exhibited sufficiently high transfection efficiency for KCNQ channel cDNAs. Cells were cultured in DMEM with 4.5 g/L glucose (PAA Laboratories, Cölbe, Germany) containing 10 % fetal bovine serum, penicillin, and streptomycin at 37 °C in 5 % CO_2. The cells were transiently transfected using FuGENE 6 (Roche Products). When KCNQ2-FLAG was contransfected with KCNQ1, KCNQ3, and various KCNQ1/KCNQ3 chimeras, four times more KCNQ2-FLAG cDNA was used. Forty-eight hours after transfection, homogenization buffer [ice-cold PBS (137mMNaCl, 2.7mMKCl, 7.4mMNa2HPO4, 1.5mMKH2PO4, pH 7.4) containing 1 X Complete (Roche Products)] was added to the plates, and cells were gathered with a scraper. Cells were lysed and homogenized by sonication. Cell lysates were centrifugated at 1000 g for 10 min to remove cellular debris, and supernatants were collected. Membranes were pelleted at 100,000 g (0.5 h; 4 °C) and resuspended in lysis buffer (120 mM NaCl, 5 mM DTT, 1 mM EGTA, 0.5 % NP-40, 10 % glycerol, 1 x Complete$^{®}$, 50 mM Tris-HCl, pH 8.0). Protein concentration was determined using the BCA protein assay system (Pierce). The samples were adjusted with lysis buffer to obtain equal protein concentrations. Proteins were immunoprecipitated with the 3F10 anti-HA monoclonal antibody (Roche Molecular Biochemicals) for 4.5 h and protein-G Sepharose (Roche Molecular Biochemicals) for an additional 0.5 h at 4°C. After five washes with

lysis buffer, immunoprecipitates were released at 55 °C in SDS sample buffer for 12 min and separated on 10 % SDS polyacrylamide gels. Immunodetection used primary mouse anti-FLAG monoclonal M2 (Sigma, St. Louis, MO) and secondary HRP-conjugated goat anti-mouse (Jackson ImmunoResearch) antibodies. Reacting proteins were detected using the ECL detection system (Amersham Biosciences, Arlington Heights, IL). Signals were recorded by a luminescent image analyzer (Fujifilm image reader, LAS1000; Fujifilm, Tokyo, Japan).

B 5   Western blot analysis

The oocytes used for TEA-sensitivity measurements were subsequently pooled and stored at 20 °C. After homogenization of the pooled oocytes in an ice-cold lysis solution containing 250 mM sucrose, 0.5 mM EDTA, 5 mM Tris-HCl, pH 7.4, and a protease inhibitor mix (Complete®; Roche Molecular Biochemicals), the yolk platelets were removed by three low-speed centrifugations. The resulting supernatant was mixed with SDS-Laemmli sample buffer, and the protein equivalent to one oocyte was analyzed by SDS-PAGE (10 % polyacrylamide). The separated proteins were transferred to polyvinylidene difluoride membrane. Blots were blocked with TBS (150 mM NaCl, 25 mM Tris, pH 7.4) containing 5 % milk powder and 0.1 % Nonidet P-40. Primary [KCNQ2(N-19); 1:500; Santa Cruz Biotechnology, Santa Cruz, CA] and secondary (horseradish peroxidase-conjugated rabbit ant-goat IgG; 1:5000) antibodies were diluted in TBS blocking solution. Blot membranes were washed with TBS with 0.1% Nonidet P-40. Reacting proteins were detected by using the ECL detection system (Amersham Biosciences). Signals were recorded by a luminescent image analyzer (Fujifilm image reader, LAS1000).

B 6   Electrophysiology: two-electrode voltage-clamp

The voltage clamp technique is a fundamental electrophysiological method, which allows at a given membrane potential the measurement and analysis of currents across the cell membrane, that are mediated by specialized ion channels or carrier/transporter proteins (**Figure B.3**). Three to five days after injection, currents were measured in ND96 (96 mM NaCl, 2 mM KCl, 0.2mM $CaCl_2$, 2 mM $MgCl_2$, 5 mM HEPES, pH 7.4) at room

temperature in two-electrode voltage-clamp recordings using a Turbotec 10C amplifier (NPI Electronics, Tamm, Germany) and pClamp8 software (Axon Instruments/Molecular Devices, Union City, CA). The voltage protocol for current recordings, unless stated differently, was as follows: from a holding potential of -70 mV cells were pulsed for 2.5 s to voltages between -80 and +40 mV in steps of 20 mV.
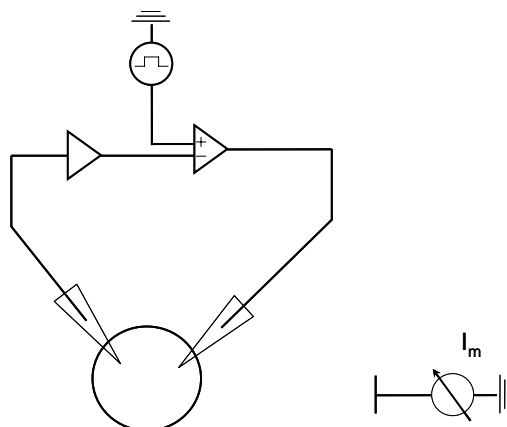
Figure B.3: Simple diagram of voltage clamping ball-shaped cells (Schwarz / Rettinger 2003)

B 7   Data analysis and statistics

All data were obtained from at least three different batches of oocytes with at least six oocytes per batch and cRNA injection scheme. The total numbers of oocytes for the respective constructs are given in the figures. The current values from each oocyte were normalized to a batch average and thus combined from oocytes of different batches. Data are given as means $\pm$ SE. To probe for significance, Student's t tests on pairs of data sets were performed. All data presented are significant at least on the $p < 0.05$ level, unless stated differently.

B 8   Quantitative analysis of I/I_{max} curves and tetraethylammonium dose–response curves

To determine the parameters for the voltage dependence of activation, I/I_{max} curves were fitted by a Boltzmann function as follows:

$$B(V) = \frac{B_{max} - B_{min}}{1 + \exp\left(\frac{R \times T}{z_q \times F} \times (V - V_{1/2})\right)} + B_{min}$$

in which B_{min} and B_{max} are the minimal or maximal I/I_{max} values, respectively, R is the molar gas constant, z_q is the slope factor (equivalent charge), F is the Faraday constant, T is the absolute temperature in K, V is he transmembrane potential, and $V_{1/2}$ is the potential of half-maximal activation.

For probing tetraethylammonium (TEA) sensitivity, 2 s-long voltage pulses were applied from -80 to -40 mV in the presence of different TEA concentrations, and the total activation amplitude at the end of the test pulse was measured. Amplitudes were normalized for each oocyte to the value measured in the absence of TEA. Data are means ± SE of normalized amplitudes. The resulting dose–response curves were fitted with the following equation:

$$I = I_{max} \times \frac{1}{\left(1 + \left(\frac{c}{IC_{50}}\right)^{n_H}\right)}$$

in which I_{max} is the maximal activation amplitude, c is the TEA concentration, IC_{50} is the concentration for the half-maximal inhibition, and n_H is the Hill coefficient.

B 9   Chemical modification by cystein-specific MTS reagents and Cd^{2+}

MTS (Methanethiosulfonate) reagents were first developed by Arthur Karlin and colleagues as powerful tools to probe structure and function of membrane proteins, and ion channels in particular. The reagents selectively and rapidly react with thiols (sulfhydryls) to form a disulfide bond (**Figure B.4**) and as a result are highly efficient modifying agents for cystein residues in proteins. The so-called SCAM method (substituted-cystein accessibility method) employs a combination of chemical and genetic approaches. First, cystein residues are systematically introduced at various positions in a protein via site-

directed mutagenesis. Then the introduced cysteines are assessed for their reactivity and accessibility toward various MTS reagents. Reactivity is determined by measuring the effects of cystein labelling on protein function. By using a series of MTS compounds differing in charge or size of the reagents, SCAM can yield information on the physical size and electrostatic potential of an ion channel and on the orientation of the labelled residue with reference to the membrane and accessibility (buried or exposed) of a residue.

The negatively charged MTSES⁻ (sodium (2-sulfonatoethyl) methanethiosulfonate) was purchased from Toronto Research Chemicals. About 25 mg aliquots MTSES were prepared in Eppendorf tubes, and the compound was dissolved in an appropriate volume of ND96 high buffer solution (ND96 with 20mM HEPES, pH 7.4) to obtain a final concentration of 10 mM, which was rapidly frozen in liquid N2. 1 ml samples were stored at -20 °C to be warmed up immediately before an experiment. The MTS modification and the Cd^{2+} modification of the cysteines was monitored by a change in the current amplitude of a specific channel construct at a specific test voltage in the two-electrode voltage-clamp configuration. A comparison of current-voltage curves before and after MTS (Cd^{2+}) application allowed determining the optimal test voltage for each residue, that is, the voltage at which the difference in current amplitude before and after MTSES application is maximal.
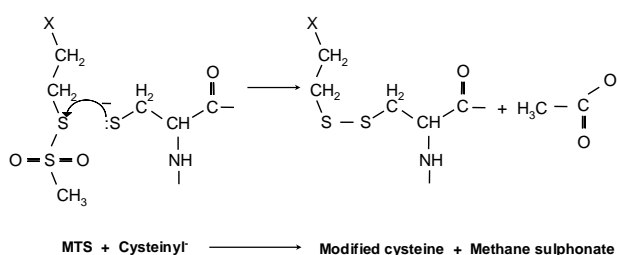
A Reaction   **B** MTS Reagents
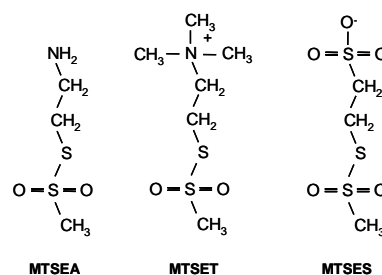
Figure B.4: **A** The cysteinyl group, in the sulfar anion form, makes a nucleophilic attack on the alkylthio group of the MTS reagent and forms a disulfide bridge to the thioalkyl moietyas the membrane sulphonate moiety leaves. **B** Three commonly used MTS reagents: MTSEA, MTSES, MTSET

C   RESULTS

The description of the results is arranged in two parts. The first part describes the structural determinants of the M-type KCNQ (Kv7) K$^+$ channel assembly. In the second part cystein-scanning mutagenesis was used in order to probe the influence of single amino acid side chains within the S4 segment and the preceding S3-S4 loop on KCNQ1 channel properties. The results of the latter part were used for testing three-dimensional structural models of KCNQ channels.

RESULTS 1

C 1.1   Role of TCC domains in KCNQ channel assembly

Schwake and co-workers showed that the broad heterooligomerization properties from KCNQ3 can be transferred to KCNQ1 by replacing a C-terminal segment of KCNQ1 (amino acids 530–620) by the corresponding stretch of KCNQ3 (amino acids 535–650). This strategy resulted in a construct termed KCNQ1-sidQ3, in which the *si*-domain was swapped between KCNQ3 and KCNQ1. To determine the role of the two TCC domains (Jenke et al., 2003) within the KCNQ *si*-domain (**Figure C1.1A**) on channel assembly, both TCC domains were replaced within the *si*-domain of KCNQ1 by the corresponding segments from KCNQ3 (**Figure C1.1B**). It could be demonstrated that the construct KCNQ1(TCC1-TCC2)Q3 was able to interact with KCNQ2 by performing two-electrode voltage-clamp experiments on *Xenopus* oocytes. The currents measured after coexpression of KCNQ1-sidQ3 with KCNQ2 (**Figure C1.2A**) or KCNQ1(TCC1-TCC2)Q3 with KCNQ2 (**Figure C1.2B**) were very similar in time course and voltage dependence. Both KCNQ1(TCC1-TCC2)Q3 and KCNQ1-sidQ3 increased currents by a factor of 8–10 compared with KCNQ2 expressed alone (**Figure C1.2C**). Only KCNQ2/KCNQ3 had a stronger current increase of about 1/3 more than KCNQ1(TCC1-TCC2)Q3 and KCNQ1-sidQ3.

A

```
                                          |------------------si-domain--
                                          |-------------TCC1--------
KCNQ1-415   HRATIKVIRRMQYFVAKKKFQQARKPYDVRDVIEQYSLGHLNLMVRIKELQ        465
KCNQ2-536   LKVSIRAVCVMRFLVSKRKFKESLRPYDVMDVIEQYSAGHLDMLSRIKELQ        586
KCNQ3-515   LKAAIRAVRILQFRLYKKKFETLRPYDVKDVIEQYSAGHLDMLSRIKVLQ        565

                  ------------------si-domain----------------------
                  ---|
            ARIDQSIGKPSLFISVSEKSKDRG                          S        490
            ARIDQIVGRGPAITDKDR    TKG              PAEAELPED            616
            TRIDMIFTPGPPSTPKHKKSQKGSAFTFPSQQSPRNEPYVARPSTSEI ED        615

                  --------------si-domain-----------|
                  |---------------TCC2--------------
            NTEGARLNRVEDKVTQLDQRLALYTDMLRQLLSLHGGSTPGSGGPPREGGA        541
            PSMMGRLGKVEKQVLSMEKKLDFLVNIYMQRMGIPPTETEAYFGAKEPEPA        667
            QSMMGKFVKVERQVQDMGKKLDFLVDMHMQHMERIQVQVTEYYPTKGTSSP        666

            HITQPCGSGGSVDPELFLPSNTLPTYEQLTVPRRGPDEGS.             581-KCNQ1
            PPYHSPEDSREHVDRHGCIVKIVRSSSSTGQKNFSAPPAAPPVQCPPST...  716-KCNQ2
            AEAEKKEDNRYSDLKTIICNYSETGPPEPPYSFHQVTIDKVSPYGFFAH...  715-KCNQ3
```

B

Figure C1.1: A) Alignment of the C-terminal sequences of KCNQ1, KCNQ2 and KCNQ3. The green box indicates the *si*-domain. The TCC1 and TCC2 domains are shown in blue. Amino acids different within the three subtypes are marked in pink. **B)** Schematic illustration of the KCNQ1-*sid*Q3 and KCNQ1(TCC1+TCC2)Q3.

The results indicate that the construct KCNQ1(TCC1-TCC2)Q3 was able to interact with KCNQ2.
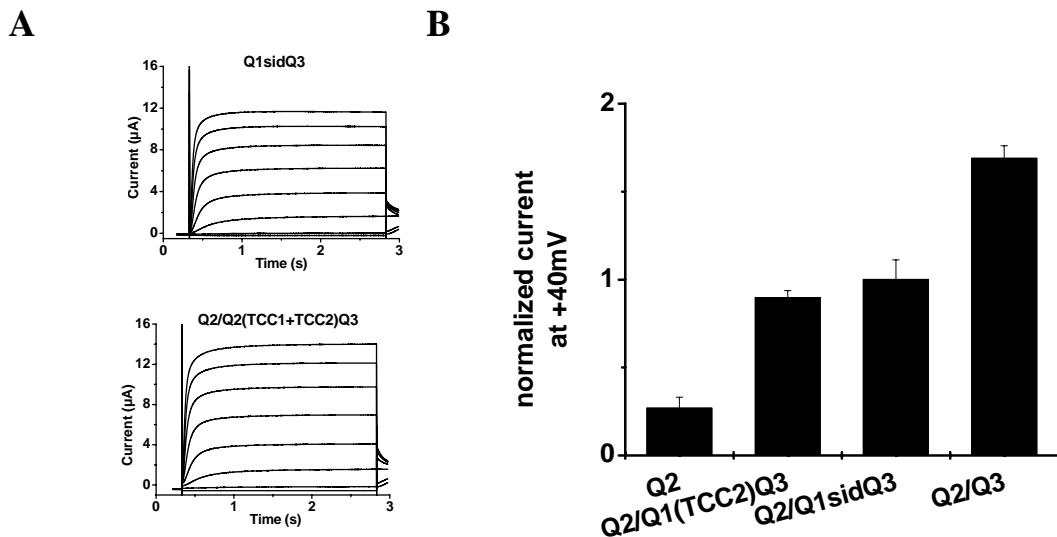
Figure C1.2: A) Representative currents from KCNQ2 expressed with KCNQ1-*sid*Q3 in *Xenopus* oocytes. (upper left) and representative currents from KCNQ2 coinjected with KCNQ1(TCC1+TCC2) in *Xenopus* oocytes (lower left). **B)** Bar graphs represent currents from KCNQ2 ($n= 22$), KCNQ2 plus KCNQ3 ($n=26$), KCNQ2 plus KCNQ1*sid*Q3 ($n=12$) and KCNQ2 plus KCNQ1(TCC1-TCC2) ($n=20$) measured at the end of a 2.5 s voltage pulse at +40mV. Currents from different oocyte batches were normalized to the mean current of KCNQ2 plus KCNQ1*sid*Q3 at +40mV.

C 1.2   The second TCC domain of KCNQ3 is sufficient to determine the subunit specificity of KCNQ channel assembly

Subsequently, chimeras were constructed in which only the first or the second TCC domain were exchanged, resulting in constructs KCNQ1(TCC1)Q3 and KCNQ1(TCC2)Q3, respectively (**Figure C1.3A, B**). When KCNQ1(TCC1)Q3 was coexpressed with KCNQ2, currents were not significantly enhanced compared with KCNQ2 alone (**Figure C1.3C**), whereas KCNQ1(TCC2)Q3/KCNQ2 coexpression led to an approximately eightfold increase, similar to a KCNQ1-sidQ3/KCNQ2 expression scheme (**Figure C1.3D**).
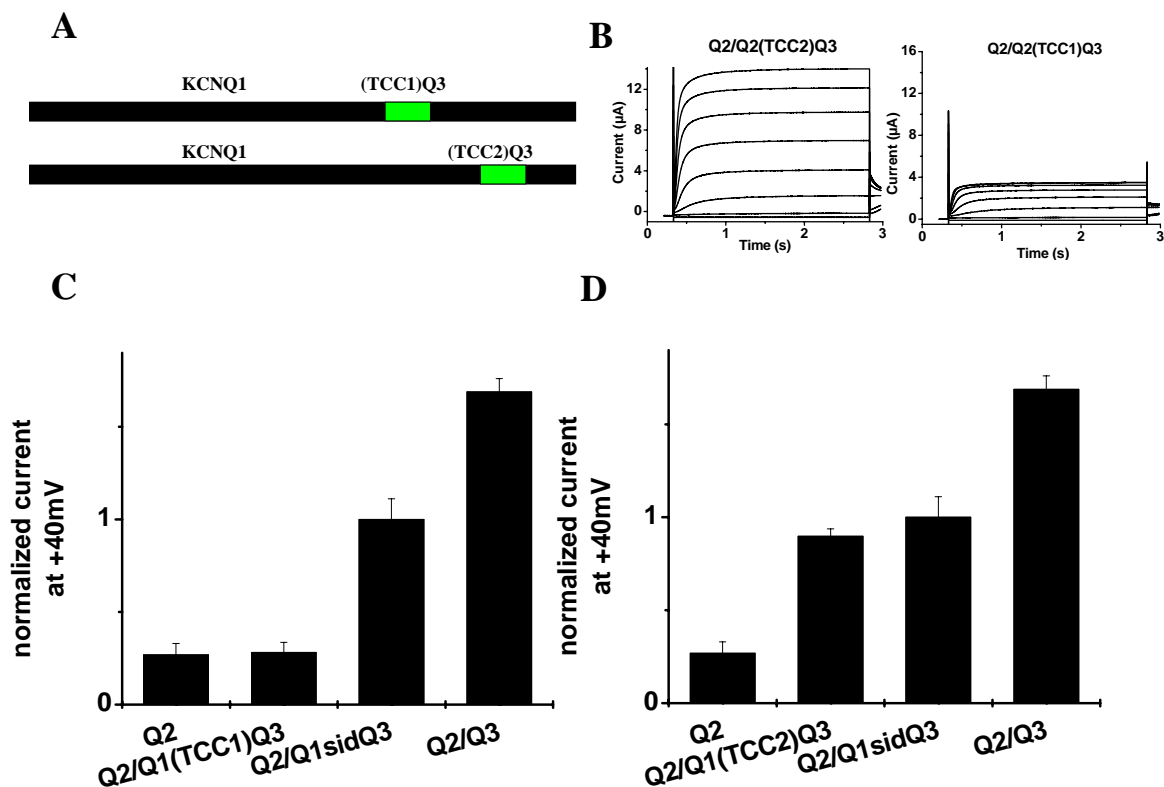
Figure C1.3: A) Schematic illustration of the KCNQ1(TCC1)Q3 and KCNQ1(TCC2)Q3. **B)** Representative currents from KCNQ2 coinjected with KCNQ1(TCC2)Q3 (left) and from KCNQ2 coinjected with KCNQ1(TCC1)Q3 (right) in *Xenopus* oocytes. **C)** Bar graphs obtained from normalized current amplitudes at the end of a 2.5 s voltage pulse at +40mV. Currents from different oocyte batches expressing KCNQ2 (n=20), KCNQ2 plus KCNQ3 (n=24), KCNQ2 plus KCNQ1*sid*Q3 (n=16) and KCNQ2 plus KCNQ1(TCC1)Q3 (n=28) were normalized to the mean of KCNQ2 plus KCNQ1-*sid*Q3 (n=24) at +40mV. **D)** Bar graphs obtained from mean currents measured at the end of 2.5 s voltage pulse at +40mV. Currents from different oocyte batches of KCNQ2 (n=18), KCNQ2 plus KCNQ3 (n=22), KCNQ2 plus KCNQ1-*sid*Q3 (n=20) and KCNQ2 plus KCNQ1(TCC2)Q3 (n=24) were normalized to the mean of KCNQ2 plus KCNQ1-*sid*Q3 at +40mV

C 1.3   Dominant negative pore mutant G314S

To further analyze this interaction, we constructed KCNQ1(TCC1)Q3 and KCNQ1(TCC2)Q3 mutants, that contained the dominant-negative pore mutation KCNQ1-G314S (Wollnik et al., 1997) and coexpressed these mutants with KCNQ2. Whereas KCNQ1-G314S-(TCC1)Q3 had no effect on KCNQ2 currents (**Figure C1.4),** the pore mutant KCNQ1-G314S-(TCC2)Q3 reduced KCNQ2 currents by 70%.
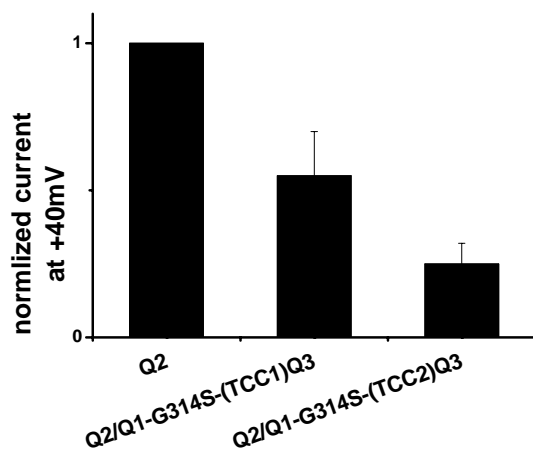
Figure C1.4: Bar graph of KCNQ2 (*n*=18) currents and effects of coexpression of pore mutants KCNQ1-G314S-(TCC1) Q3 (*n*=14) and KCNQ1-G314S-(TCC2)Q3 with KCNQ2 (*n*=12). The current amplitudes were normalized to KCNQ2 currents measured at the end of a test pulse to +40mV.

C 1.4   Surface expression

The strong current increase after KCNQ2/KCNQ3 and KCNQ2/KCNQ1-sidQ3 coexpression primarily results from an increased surface expression (Schwake et al., 2000, 2003). At the University of Kiel Schwake and co-workers have tested whether such an effect also explains the current enhancement measured with KCNQ1(TCC2)Q3/KCNQ2 channels. **Figure C1.5** shows that the KCNQ1(TCC2)Q3 chimera was as efficient as KCNQ3 in stimulating the surface expression of epitope-tagged KCNQ2. In contrast, coexpression of the KCNQ1(TCC1)Q3 chimera resulted in a surface expression of epitope-tagged KCNQ2 of about the same magnitude as in a 1:1 coinjection scheme with WT KCNQ2.
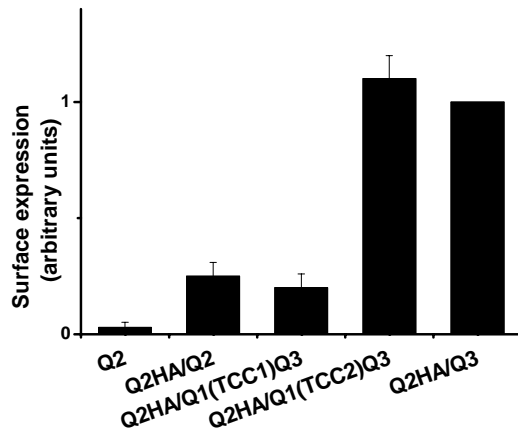
Figure C1.5: Surface expression determined from luminescence measurements of oocytes coinjected with HA-tagged KCNQ2 and non-tagged KCNQ2 (n=35), KCNQ1(TCC1)Q3 (n=39), KCNQ1(TCC2)Q3 (n=39), KCNQ3 (n=42). Data were normalized to the value of KCNQ2(HA) plus KCNQ3.

.

C 1.5   Coimmuneprecipitation experiments

Coimmuneprecipitation experiments were performed at the University of Kiel by Schwake and co-workers in order to confirm the role of the TCC domains in channel assembly on the protein level. **Figure C1.6** shows results obtained after coexpressing HA-tagged KCNQ1, KCNQ1(TCC1)Q3, KCNQ1(TCC2)Q3, or KCNQ3 with FLAG-tagged KCNQ2. In contrast, there was only a very faint signal when coimmuneprecipitation was attempted with HA-tagged KCNQ1, which was also observed in controls, in which HA-tagged KCNQ1 was not included. These results suggested that both TCC domains from KCNQ3 can mediate interactions between KCNQ3 and KCNQ2. The transfer of the TCC1 domain from KCNQ3 to KCNQ1 already facilitates subunit interaction, which, however, does not lead to current enhancement. In addition, the transfer of the TCC2 domain is responsible for the efficient forward transport of heteromeric KCNQ2/KCNQ3 channels to the plasma membrane.
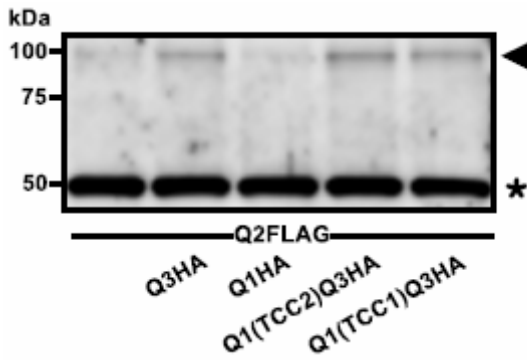
Figure C1.6: Coassembly of the HA-tagged KCNQ1(TCC1), KCNQ1(TCC2), KCNQ3 and KCNQ1 constructs with FLAG-tagged KCNQ2. Protein complexes obtained from Cos-7 cells expressing various KCNQ subunits were immunprecipitated with anti-HA antibody, separated by SDS-PAGE, and detected by Western blot analysis using an anti-FLAG antibody. The arrowhead denotes the molecular weight of FLAG-tagged KCNQ2 proteins, and the asterisk represents the weight of the heavy chain of the anti-HA antibody. The molecular weight marker is shown on the left.

C 1.6 TCC2 of KCNQ2 is needed for heteromeric KCNQ2/KCNQ3 formation but not for homomeric KCNQ2 channel assembly

Since the TCC2 domain from KCNQ3 is very important for an efficient plasma membrane expression of heteromeric KCNQ2/KCNQ3 channels, we also investigated a possible involvement of the TCC2 domain of KCNQ2 in this process. Therefore, we replaced TCC2 of KCNQ2 by the corresponding TCC2 of KCNQ1 and tested the resulting chimera KCNQ2(TCC2)Q1 for its effect on KCNQ3 currents. KCNQ2(TCC2)Q1 yielded functional K^+-channels (**Figure C1.7A**).

Coexpression of KCNQ2(TCC2)Q1 with KCNQ3 did not lead to current enhancement. This result is in contrast to the strong augmentation of KCNQ2 currents by KCNQ1(TCC2)Q3 (**Figure C1.3B**) or KCNQ3, suggesting that the interaction between KCNQ2(TCC2)Q1 and KCNQ3 is impaired, resulting in inefficient plasma membrane expression of KCNQ2(TCC2)Q1/KCNQ3 heteromers (**Figure C1.7B**).
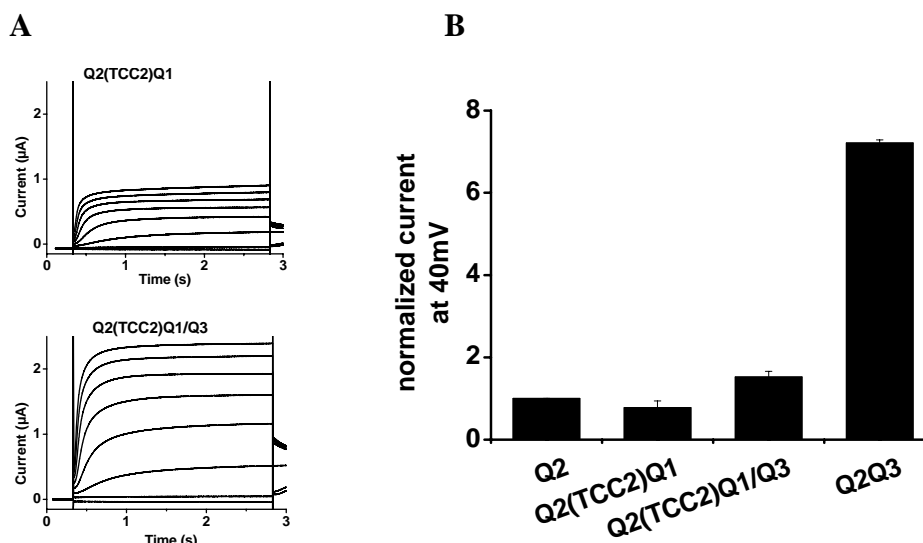
Figure C1.7: A) Representative current recordings from oocytes (co-)injected with cRNA(s) of KCNQ2(TCC2)Q1 (top left) and KCNQ2(TCC2)Q1 plus KCNQ3 (bottom left). **B)** Bar diagram of current levels recorded at the end of a 2.5 s long test pulse to +40mV from oocytes expressing KCNQ2 (n=25), KCNQ(TCC2)Q1 (n=21), KCNQ(TCC2)Q1 plus KCNQ3 (n=20), KCNQ2 plus KCNQ3 (n=26). Currents were normalized to the value obtained from KCNQ2 plus KCNQ3 at +40mV.

C 1.7   Investigation of the second TCC domain of KCNQ2

The important role of TCC2 from KCNQ2 in heteromerisation was the reason to investigate further the individual roles of TCC1 and TCC2 within the *si*-domain in channel assembly and trafficking. Therefore, KCNQ2 deletion constructs were analyzed at the University of Kiel by Schwake and co-workers, in which either the complete *si*-domain (KCNQ2-Δ*sid*), or TCC1 (KCNQ2-ΔTCC1) and TCC2 (KCNQ2-ΔTCC2) were removed, respectively. Expression of KCNQ2-Δ*sid* and KCNQ2-ΔTCC1 did not yield K$^+$-currents (data not shown), suggesting that TCC1 of KCNQ2 is also essential for forming functional homomeric channels.

In contrast, currents obtained from the deletion construct KCNQ2-ΔTCC2 (**Figure C1.8A**) were very similar to those of wild-type KCNQ2 channels. The formation of KCNQ2 homomers obviously does not depend on TCC2. Coexpression of either the KCNQ2-Δ*sid* or the KCNQ2-ΔTCC1 with KCNQ3 again did not yield K$^+$-currents (data not shown). Additionally, no significant increase in currents was observed after coexpression of KCNQ2-ΔTCC2 with KCNQ3 (**Figure C1.8B**).

In summary, we conclude that TCC1 is necessary for assembly of both homomeric and heteromeric channels, whereas TCC2 determines the formation of heteromers, but is dispensable for homomeric channel assembly.
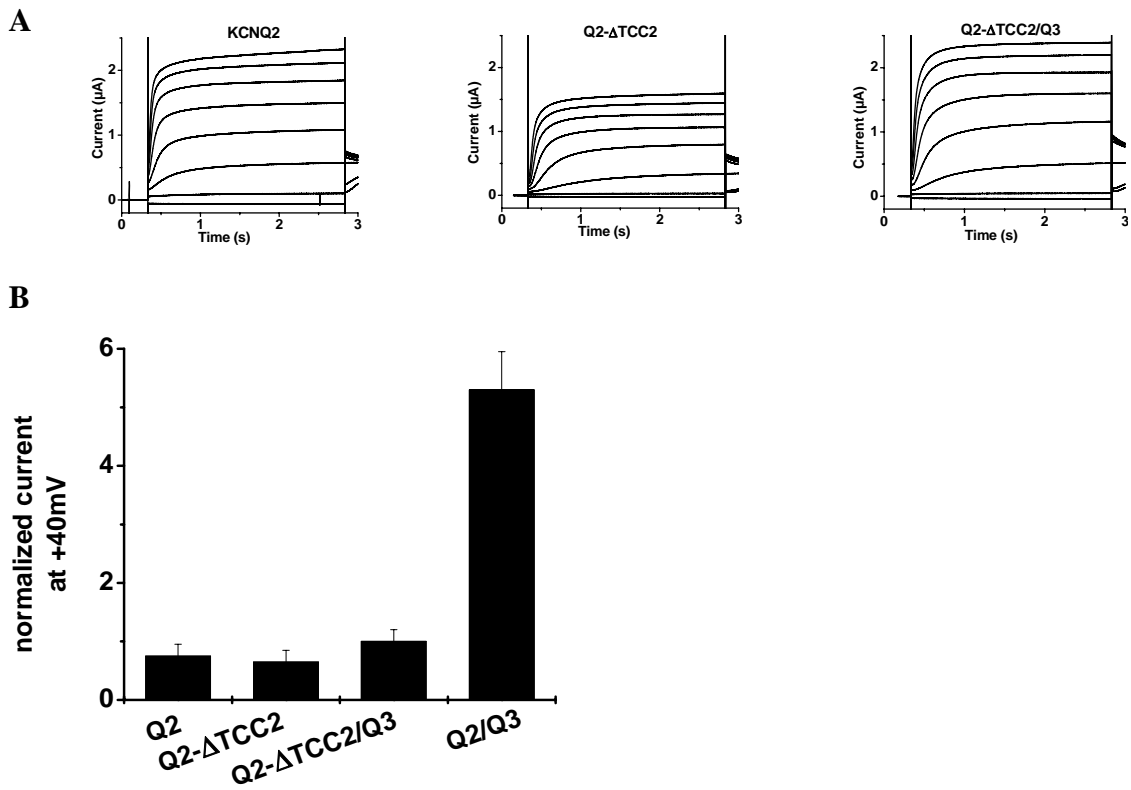

Figure C1.8: **A)** Representative current recordings from oocytes (co-)injected with cRNA(s) of KCNQ2 (top left), KCNQ2-ΔTCC2 (top centre) and KCNQ2-ΔTCC2 plus KCNQ3 (top right). **B)** Bar diagram of current levels recorded at the end of a 2.5 s long test pulse to +40mV from oocytes expressing KCNQ2 (n=19), KCNQ2-ΔTCC2 (n=18), KCNQ2-ΔTCC2 plus KCNQ3 (n=25) or KCNQ2 plus KCNQ3 (n=22). Currents were normalized to the value obtained from KCNQ2 plus KCNQ3 at +40mV.

C 1.8   Investigation of the second TCC domain of KCNQ3

Next the question was addressed, whether or not the TCC2 domain from KCNQ3 is also important for heteromer formation. For this reason truncation constructs were generated as indicated in **Figure C1.9.**

```
KCNQ1-511   RATIKVIRRMQYFVAKKKFQQARKPYDVRDVIEQYSQGHLNLMVRIKELQ        560
KCNQ3-516   KAAIRAVRILQFRLYKKKFKETLRPYDVKDVIEQYSAGHLDMLSRIKYLQ        565

            --------------sid-domain------------------------
            .
            RRLDQSIGKPSLFISVSEKS                          KDRGS        585
            TRIDMIFTPGPPSTPKHKKSQKGSAFTFPSQQSPRNEPYVARPSTSEIED        615

            -------------sid-domain-----------|
            NTIGARLNRVEDKVTQLDQRLALITDMLHQLLSLHGGSTPGSGGPPREGG        635
            QSMMGKFVKVERQVQDMGKKLDFLVDMHMQHMERLQVQVTEYYPTKGTSS        665

            AHITQPCGSGGSVDPELFLPSNTLPTYEQLTVPRRGPDEGS*        676-KCNQ1
            PAEAEKKEDNRYSDLKTIICNYSETGPPEPPYSFHQVTIDKVSPYGFFAH...    715-KCNQ3
```

Figure C1.9: Alignment of the C-terminal sequences of KCNQ1 and KCNQ3. The *si* domain is indicated in grey and the TCC domains are indicated in light grey. The positions of prolines which were mutated to STOP codons are shown in bold.

A stop codon was inserted instead of the proline in position 574 resulting in construct KCNQ3-P574X (truncation after TCC1) and in another construct the stop codon was inserted in the position 659 proline (KCNQ3-P659X, truncation after TCC2). These truncation constructs were coexpressed together with KCNQ2 in *Xenopus* oocytes. It is important to note, that not only the TCC's, but the complete further C-terminus is missing.

Figure C1.10 shows that the KCNQ3-P574X construct, which is lacking the TCC2 domain and the further C-terminus, still induced current enhancement upon coexpression with KCNQ2. This is in contrast to the results obtained with KCNQ2-ΔTCC2 constructs, indicating that in KCNQ3 the TCC2 domain does not play the same role in heteromeric interaction as TCC2 of KCNQ2.
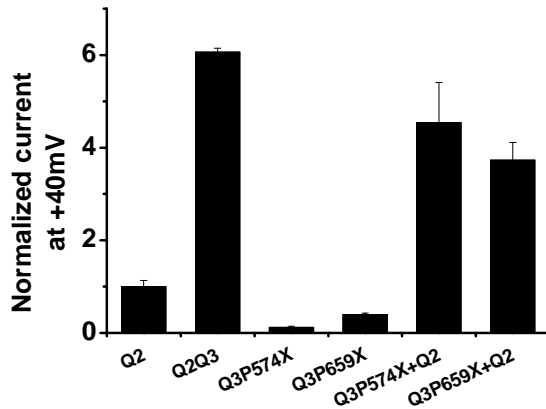
Figure:C1.10: Bar diagram of current levels recorded at the end of a 2.5 s long test pulse to +40mV from oocytes (co-)injected with cRNA(s) of KCNQ2 (*n*=12), KCNQ2 plus KCNQ3 (*n*=10), KCNQ3-P574X (*n*=8), KCNQ3-P659X (*n*=9), KCNQ3-P574X plus KCNQ2 (*n*=8) and KCNQ3-P659X plus KCNQ2 (*n*=7). Currents were normalized to the value obtained from KCNQ2 at +40mV.

Schwake and coworkers analyzed KCNQ3-L564P (**Figure C1.11**) and KCNQ3-L636P constructs and finds out that, complete disruption of the TCC1 coiled-coil probability by mutation L564P abolished currents and no functional interaction of the KCNQ3-L564X mutant with KCNQ2 was seen.

When the coiled-coil probability of TCC2 from KCNQ3 was mostly disrupted by mutation L636P, again functional K$^+$-channel currents were obtained. As judged from prediction algorithms, the coiled coil probabilities for TCC2 were high for KCNQ2 (0.75) and for KCNQ3 (0.6) and ~0.4 for TCC1 of KCNQ2 and even lower for TCC1 of KCNQ3 (<0.1). Coexpression of KCNQ3-L636P mutant with KCNQ2 still led to a robust enhancement of currents, which were comparable in amplitude with KCNQ2 plus KCNQ3. This also indicates that in contrast to the TCC2 domain of KCNQ2, less rigorous structural requirements are needed for the KCNQ3 TCC2 domain during KCNQ2/KCNQ3 heteromeric interaction.

Figure C1.11: Bar diagram of current levels recorded at the end of a 2.5 s long test pulse to +40mV from oocytes (co-)injected with cRNA(s) of KCNQ2 (*n*=36), KCNQ3 (*n*=42), KCNQ2 plus KCNQ3 (*n*=45), KCNQ3-L564P(*n*=24), KCNQ3-L564P plus KCNQ2 (*n*=28), KCNQ3-L636P (*n*=31) and KCNQ3L636P plus KCNQ2 (*n*=47). Currents were normalized to the value obtained from KCNQ2 plus KCNQ3 at +40mV.
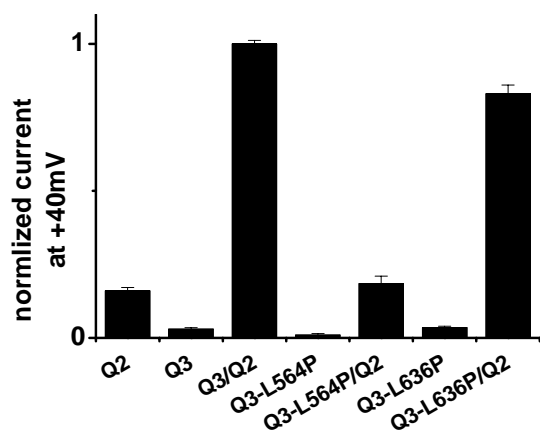
C1.9   Insertion of "artificial" TCC sequences

To test the hypothesis that tetramerization of cytoplasmic domains stimulates transmembrane domain assembly, the TCC1 and TCC2 domain were replaced one after the other with a 33-amino acid long coiled-coil domain from an unrelated protein (GCN4-LI) (Zerangue et al., 2000)(**Figure C1.12C**). The GCN4-LI peptide can act as a tetramerization domain, since it forms extremely stable parallel tetrameric, but not dimeric or trimeric, coiled-coil structures.(Zerangue et al., 2000) The constructs generated were named KCNQ1-(GCN4-LI)TCC1 and KCNQ1-(GCN4-LI)TCC2 (**Figure C1.12A,B**). The exchanged TCC1 and TCC2 domains had the same length (both 33 amino acids long) and the hydrophobicity of the amino acids in positions a and d was unchanged.

Unfortunately, the insertion of the artificial tetramerization domain (GCN4-LI) into the KCNQ1 backbone did not lead to efficient channel formation suggesting that not only the structure but also the individual amino acid composition of the domains is important to drive assembly of functional KCNQ1 channels.

A

```
GCN4-LI
  MKQIEDKLEEILSKLYHIENELARIKKLLGERT


>TCC1-Q1
  VRDVIEQYSQGHLNLMVRIKELQRRLDQSIGKP
>TCC2-Q1
  IGARLNRVEDKVTQLDQRLALITDMLHQLLSLH
```

C

Coiled-Coil

B
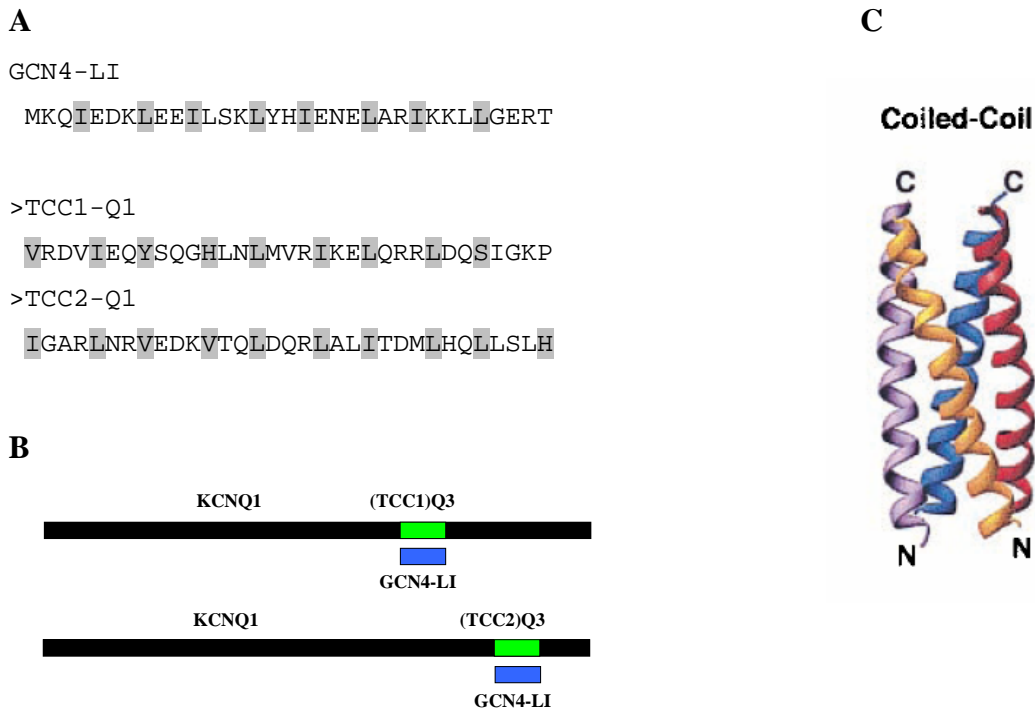
Figure C1.12: A) Amino acid sequence from the GCN4-LI peptide and the replaced TCC1, TCC2 domains from KCNQ1. Hydrophobic amino acids are boxed grey. **B)** Schematic illustration of the KCNQ1(GCN4-LI)TCC1 and KCNQ1(GCN4-LI)TCC2 constructs. **C)** Crystal structure of GCN4-LI. (From Zerangue et al., 2000)

C 1.10   Analysis of the interaction of the two TCC domains within one KCNQ subunit

To address the question whether the two adjacent TCC domains within the KCNQ2 *si*-domain could interact with each other, as might be expected for tetramerizing coiled-coil sequences the KCNQ2 channel was split between the TCC domains (**Figure C1.13A**), resulting in constructs KCNQ2-TCC1-X (comprising the KCNQ2 transmembrane domains including TCC1) and TCC2-CT-KCNQ2 (a soluble C-terminal fragment including TCC2), which were tested for functional channel formation after coexpression in oocytes. KCNQ2 was chosen for these experiments because of its robust expression. Neither the expression of truncated polypeptides KCNQ2-TCC1-X or TCC2-CT-KCNQ2 alone nor coexpression of KCNQ2-TCC1-X with TCC2-CT-KCNQ2 yielded measurable K^+-currents (data not shown).

However, it was also tested whether the fragments KCNQ2-TCC1-X and TCC2-CT-KCNQ2 exerted some effect in coexpression with KCNQ3. Currents measured after KCNQ2-TCC1-X plus KCNQ3 coexpression could be differentiated from those of KCNQ3, but no enhancement compared with KCNQ3 current levels was detected (**Figure C1.13B**).

In contrast, functional channels were obtained in a KCNQ2-TCC1-X plus TCC2-CT-KCNQ2 plus KCNQ3 coexpression scheme, reaching 50 % of the KCNQ2/KCNQ3 current level. Strikingly, coexpression of KCNQ3 with only the cytosolic fragment TCC2-CT-KCNQ2 led to an approximately fourfold increase in currents compared with KCNQ3 alone.

To test whether this effect depends on the presence of TCC2, an additional C-terminal fragment termed dCT-KCNQ2 was generated, which comprises only the distal KCNQ2 C-terminus following TCC2. Coexpression of this construct did not enhance KCNQ3 currents (**Figure C1.13B**), suggesting that the TCC2 domain of KCNQ2 augments KCNQ3 currents even when present as a soluble protein fragment.
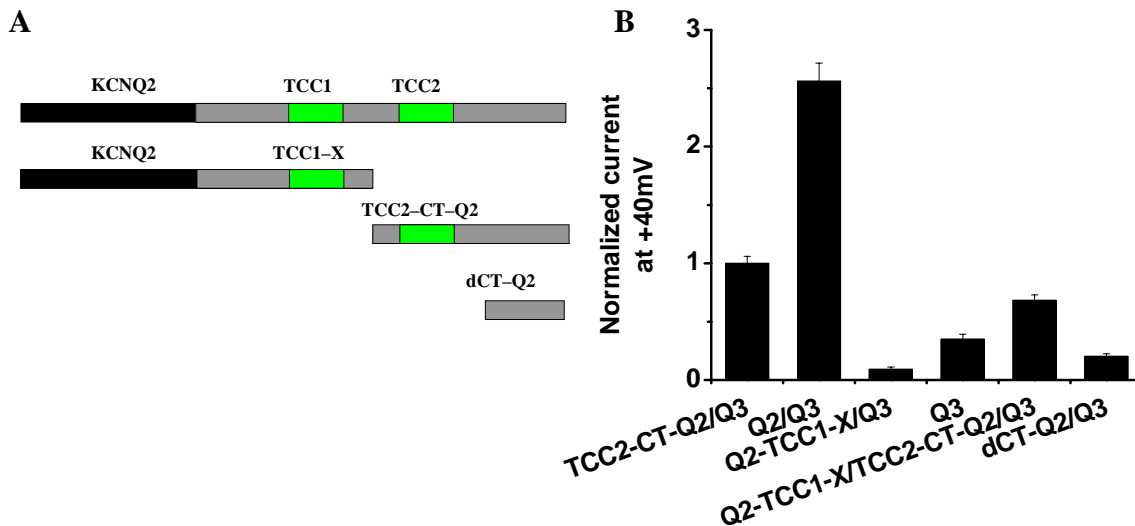
Figure C1.13: **A**) Schematic illustration of the KCNQ2 split channels. The *si* domain is shown as light grey box and the TCC domains are indicated as green boxes. **B**) Comparison of current levels recorded at the end of a 2.5 s long test pulse to +40mV from oocytes (co-)injected with cRNA(s) of TCC2-CT-KCNQ2 plus KCNQ3 ($n=20$), KCNQ2 plus KCNQ3 ($n=22$), KCNQ2-TCC1-X plus KCNQ3 ($n=14$), KCNQ3 ($n=26$), KCNQ2-TCC1-X plus TCC2-CT-KCNQ2 plus KCNQ3 ($n=22$), and dCT-KCNQ2 plus KCNQ3 ($n=12$). Currents were normalized to the value obtained from KCNQ3 plus TCC2-CT-KCNQ2 at +40mV.

C 1.11 Properties of channels formed upon co-expression of KCNQ3 with C-terminal fragments of KCNQ2

Because the C-terminal fragment of KCNQ2, TCC2-CT-KCNQ2, was able to enhance the current in coexpression with KCNQ3, it was important to test the exact nature of channel pores being created by this coexpression. The differential sensitivity of KCNQ channels for TEA should aid identification. The voltage protocol used is indicated in **Figure C1.14A**. In accordance with Hadley et al. (2000), it was found, that the TEA sensitivity of KCNQ2 is high (IC_{50} = 0.3mM), that of KCNQ3 is low (IC_{50} > 30 mM) and that of KCNQ2/ KCNQ3 is intermediate (IC_{50} = 3.8 mM) (**Figure C1.14B**).
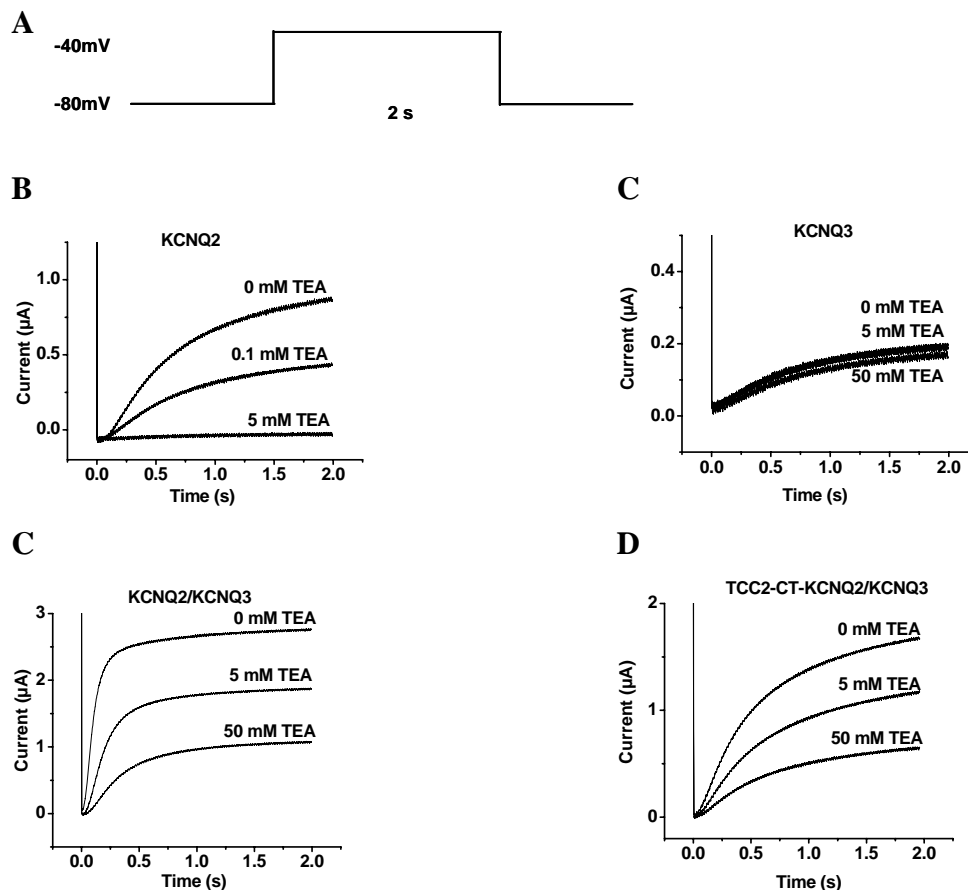
Figure C1.14: A) Voltage protocol for testing inhibition by TEA. Starting from a holding potential of -80mV 2 s-long voltage pulses to -40mV were applied in the presence of different TEA concentrations, and the total activation amplitude at the end of the test pulse was measured. **B, C, D)** Differential TEA sensitivities of KCNQ2, KCNQ3, KCNQ2+KCNQ3 and KCNQ3 + TCC2-CT-KCNQ2 currents expressed in *Xenopus* oocytes are shown. Current traces were recorded in response to the voltage protocol described above in the absence and presence of different concentrations of TEA as indicated on top of each trace.

Remarkably, the TEA sensitivity of channels formed by KCNQ3 and the cytoplasmatic KCNQ2 fragment (TCC2-CT-KCNQ2) (**Figure C1.15A**) was comparable with that of KCNQ2 plus KCNQ3 heteromers. In contrast, the dCT-KCNQ2 construct did not influence the TEA sensitivity of KCNQ3 (**Figure C1.15A**).

In an inverted situation, when KCNQ2 was co-expressed with a CT-TCC2-KCNQ3 fragment the TEA sensitivity of KCNQ2 was not changed (**Figure C1.15B**).

A
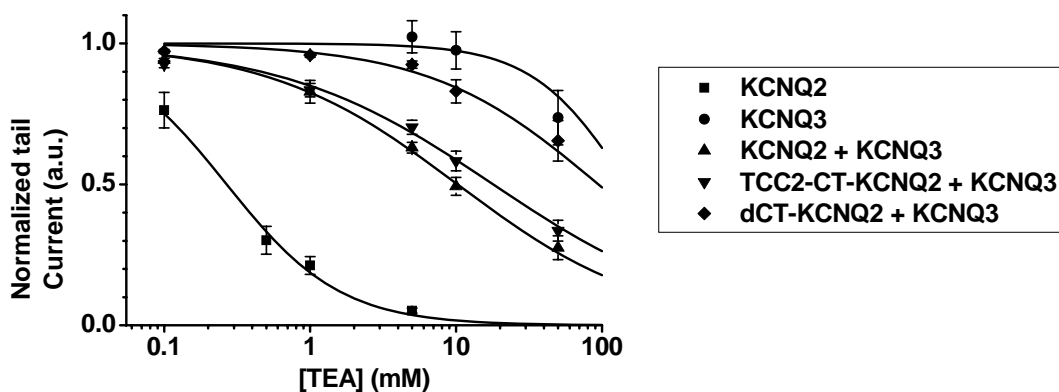
B
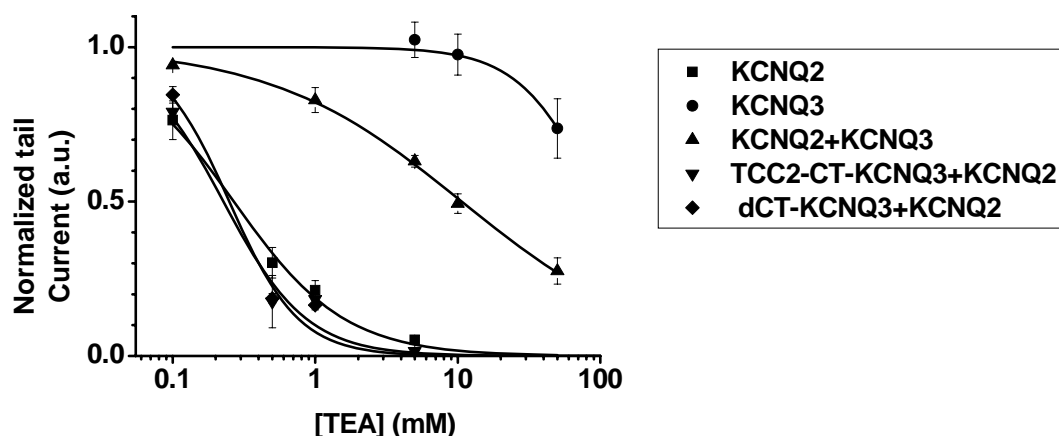
Figure C1.15: **A)** Differential TEA sensitivities of KCNQ2, KCNQ3, KCNQ2+KCNQ3, TCC2-CT-KCNQ2+KCNQ3, dCT-KCNQ2+KCNQ3 **B)** TEA sensitivities resulting from an inverted situation for KCNQ2, KCNQ3, KCNQ2+KCNQ3,dCT-KCNQ3+KCNQ2, TCC2-CT-KCNQ3+KCNQ2 (*n*=10 for each data set). Currents in the absence of TEA were taken as reference.

Complementary to experiments with TEA, which acts as a differentially effective blocker on KCNQ channels, we wanted to make use of the anticonvulsant retigabine, which differentially enhances KCNQ channel activity, for identification of the channels' pore properties. Also in these experiments, an influence of the cytoplasmatic KCNQ2 fragment (TCC2-CT-KCNQ2) on the KCNQ3 was seen.

Retigabine is known to exert its effect by shifting the voltage dependence of activation and increasing the maximal open probability. Since KCNQ3 is very sensitive to retigabine (**Figure C1.16A**) whereas KCNQ2 is not, retigabine sensitivity can be used as a tool to examine the nature of the underlying channels.

In addition, retigabine accelerates the activation and slows the deactivation of these currents. Retigabine-treated KCNQ2/KCNQ3 channels had a more negative potential of half-maximal activation and a higher maximal open probability, which both give rise to the increase of the macroscopic current amplitudes.

A
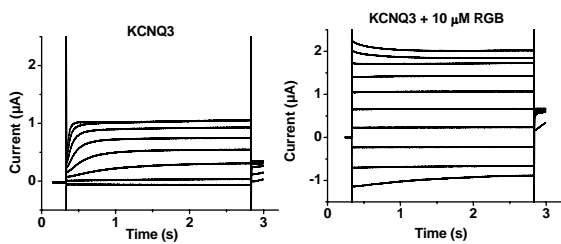
Figure C1.16: A) Representative current recording from KCNQ3 without retigabine (left) and KCNQ3 in presence of 10 μM retigabine. (right). **B)** Voltage dependence of I/I_{max} curves of KCNQ2 (n=12), KCNQ3 (n=10), KCNQ2+KCNQ3 (n=14) and TCC2-CT-KCNQ2+KCNQ3 (n=12) measured in the absence or presence of 10 μM retigabine, obtained from tail current analysis.

B
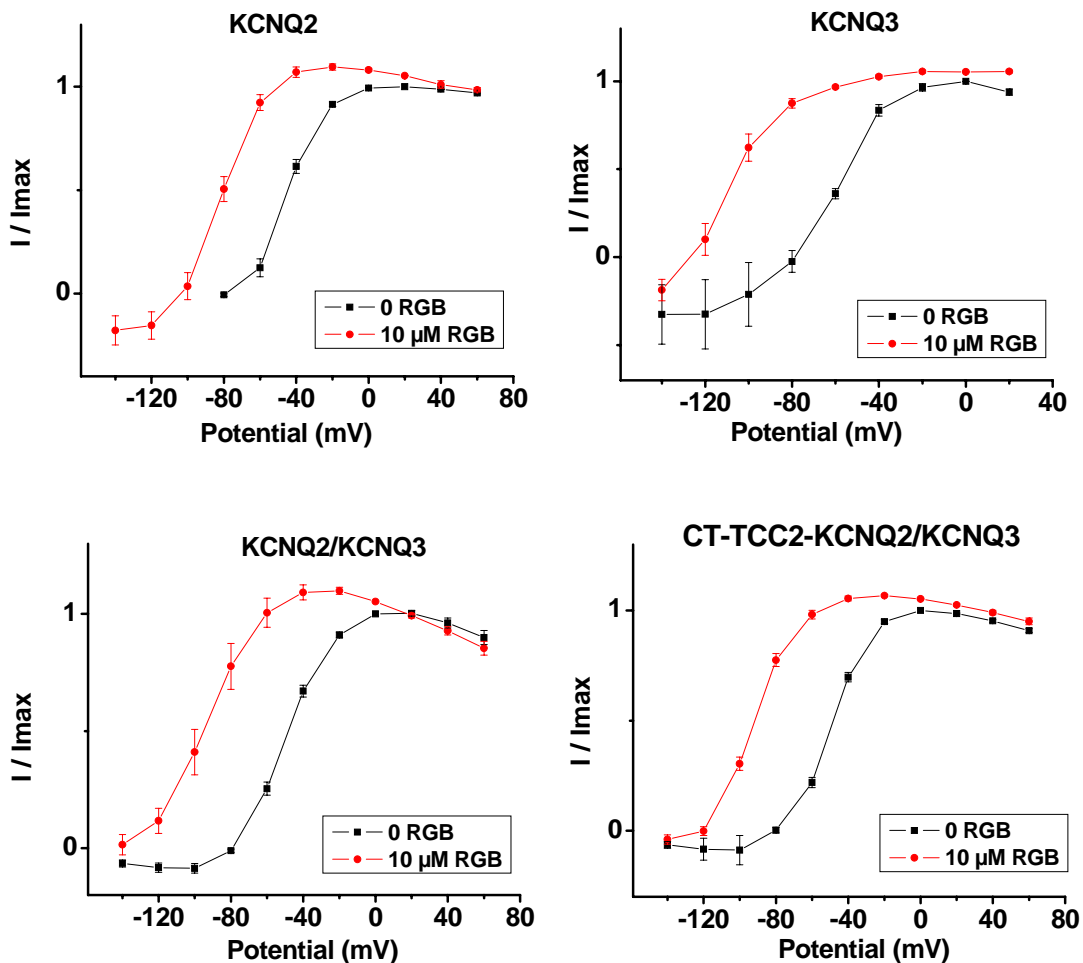
The values for the voltages of half-maximal activation as determined from fitting a Boltzmann function to the I/I_{max} curves (**Table C1.1**) were as follows:

Table C1.1: Apparent voltage of half-maximal activation with and without retigabine

Construct	$V_{1/2}$ [mV] before retigabine	$V_{1/2}$ [mV] after 10μM retigabine
KCNQ2	-44 ± 0.6	-82.2 ± 0.7
KCNQ3	-62.5 ± 1.7	-110.6 ± 2.1
KCNQ2/KCNQ3	-50.4 ± 0.9	-93.4 ± 1.4
KCNQ3/TCC2-CT-KCNQ2	-49.9 ± 0.7	-92.1 ± 0.8

The shift of the I/I_{max} curve in response to 10 µM retigabine is strongest for KCNQ3 (**Figure C1.16B**) and intermediate for KCNQ2/KCNQ3 (**Figure C1.16B**). From the I/I_{max} curves it is evident that the TCC2-CT-KCNQ2 fragment (**Figure C1.16B**) lowered the sensitivity of KCNQ3 towards retigabine, as judged from the less pronounced shift in $V_{0.5.}$

C 1.12 Position-independent effect of the TCC2 domain

Since the current-enhancing effect of the KCNQ2 TCC2 domain on KCNQ3 could essentially be observed with split KCNQ2 channels or the cytosolic TCC2-CT-KCNQ2 fragment alone, we asked whether TCC2 could exert a current-stimulating effect on KCNQ3 when placed in a different position within the KCNQ2 backbone. Therefore KCNQ2 TCC2 fragment was fused to the N-terminus of a KCNQ2 channel, which was truncated after TCC1. This resulted in a construct termed KCNQ2(NT-TCC2) (**Figure C1.17A**).

Although the latter channel did not yield measurable K^+-currents when expressed alone, it increased KCNQ3 currents in coexpression experiments nearly as efficiently as KCNQ2 wild-type. Next, we deleted the TCC1 domain within the KCNQ2 (NT-TCC2) construct and expressed the resultant construct KCNQ2(NT-TCC2;delTCC1) in oocytes.

No functional K^+ channels were observed when KCNQ2(NT-TCC2;delTCC1) was expressed alone, and the current-stimulating effect on KCNQ3 was absent (**Figure C1.17B**). In line with the results obtained from the coexpression of KCNQ3 with the C-

terminal fragment TCC2-CT-KCNQ2, these experiments indicate that the current-stimulating effect of the KCNQ2 TCC2 domain does not depend on its location behind TCC1 in the primary sequence.

A

B
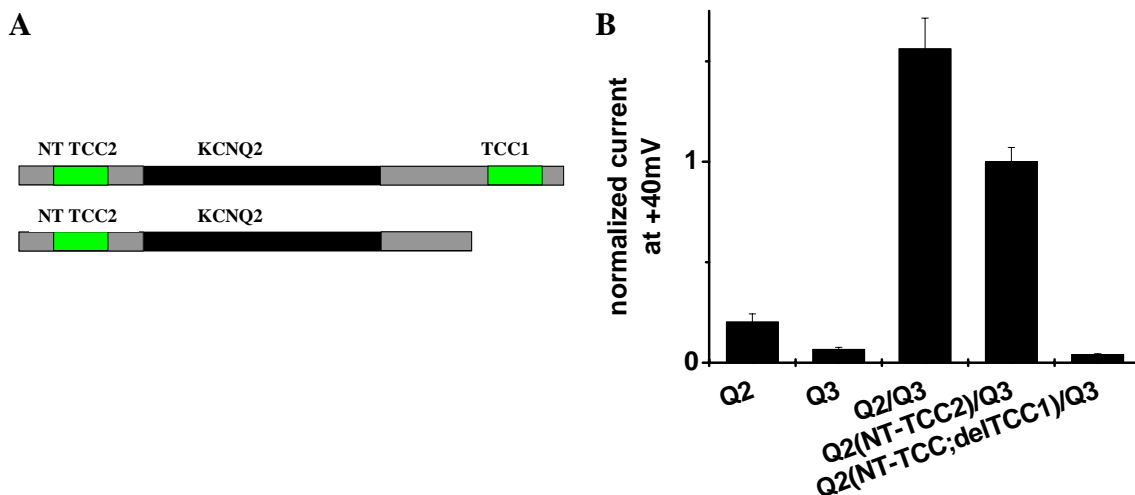
Figure C1.17: **A)** Schematic illustration of the KCNQ2 constructs with TCC2 swapped to the N-terminus. The *si* domain is shown as light grey box and the TCC domains are indicated as green boxes. **B)** Comparison of current levels recorded at the end of a 2.5 s long test pulse to +40mV from oocytes (co-)injected with cRNA(s) of KCNQ2 (*n*= 12), KCNQ3 (*n*=9), KCNQ2 plus KCNQ3 (*n*=14), KCNQ3 plus KCNQ2(NT-TCC2) (*n*=11) and KCNQ3 plus KCNQ2(NT-TCC2;del TCC1) (*n*=8). Currents were normalized to the value obtained from KCNQ3 plus KCNQ2(NT-TCC2) at +40mV.

C 1.13 Single helix turn mutants within TCC2 of KCNQ1

The fact that the KCNQ1-(TCC2)Q3 chimera was able to form heteromeric channels with KCNQ2, whereas KCNQ1 was not, raised the possibility that specific residues within the TCC2 domain might control the subunit-specific assembly pattern. We therefore generated further chimeras in which either only single helix turns within TCC2 were exchanged or the hydrophobic residues along the coiled-coil positions a and d alone or together with the residues at positions b, c, e, f, and g (**Table C1.2**) were exchanged between KCNQ1 and KCNQ3. None of the resultant subchimeras of KCNQ1-(TCC2)Q3 led to a robust enhancement of currents in coexpression with KCNQ2 as seen for the KCNQ2/KCNQ1(TCC2)Q3 coexpression. Thus, we were unable to identify individual or a series of residues that are absolutely required for the formation of KCNQ2/KCNQ3 heteromers.

Table C1.2: KCNQ1 and KCNQ3 mutants with helix turn and amino-acid position exchanges in the TCC2 domain

heptad repeat	<u>d</u>efg<u>a</u>bc<u>d</u>efg<u>a</u>bc<u>d</u>efg<u>a</u>bc<u>d</u>efg<u>a</u>bc<u>d</u>efg<u>a</u>
KCNQ1(TCC2)	*IGARLNRVEDKVTQLDQRLALITDMLHQLLSLH*
KCNQ3(TCC2)	**MMGKFVKVERQVQDMGKKLDFLVDMHMQHMERL**
KCNQ1**(a,d)Q3**	*MGAR* **FNR** *VEDK* **VTQ** *MDQR* **LAL** *LTDM* **HHQ** *HLSL* **L**
KCNQ1**(a,b,d)Q3**	*MGAR* **FVR** *VEDK* **VQQ** *MDQR* **LDL** *LTDM* **HMQ** *HLSL* **L**
KCNQ1**(a,c,d)Q3**	*MGAR* **FN KV** *EDK* **VT** *DM* *DQR* **LA FL** *TDM* **HH** *QHLSL* **L**
KCNQ1**(a,d,e)Q3**	**MM** *AR* **FNR** *VEDK* **VTQ** **MG** *QR* **LAL** **LVDM** **HHQ** **HMSL** **L**
KCNQ1**(a,d,f)Q3**	**MGGRFNRVERKVTQMDKRLALLTDMHHQHLELL**
KCNQ1**(a,d,g)Q3**	**MGAKFNRVEDQVTQMDQKLALLTDMHHQHLSRL**
KCNQ1**(TCC24)Q3**	*IGAR* **FVKVERQVQDMGKKLDFLVDMHMQHMERL**
KCNQ1**(TCC23)Q3**	*IGARLNRVEDK* **VQDMGKKLDFLVDMHMQHMERL**
KCNQ1**(TCC22)Q3**	*IGARLNRVEDKVTQLDQR* **LDFLVDMHMQHMERL**
KCNQ1**(TCC21)Q3**	*IGARLNRVEDKVTQLDQRLALITDM* **HMQHMERL**

C 1.14 Single helix turns mutants within TCC2 of KCNQ2

The observation that the TCC2 domain of KCNQ2 plays an important role in heteromeric assembly of KCNQ2 and KCNQ3, prompted us to further analyse the TCC2 domain of KCNQ2. The aim was to successively shorten the TCC domain of KCNQ2 by individual helix turns, to see, how many segments would be required for an efficient heteromeric interaction. KCNQ2 was chosen for this set of experiments because of its robust expression.

Figure C1.18 C demonstrates, that KCNQ2 with a TCC2 domain shortened to 7 residues, still leads to a rather high current enhancement in coexpression with KCNQ3 (50 % of Q2/Q3 level). This drop to 50 % already occurs upon deletion of the third helix turn which might indicate a decisive role of the last three helix turns. However, a substantial effect remains even with only one TCC2 helix turn remaining.

A

Q2-TCC2-4turn

*EAELPEDPS***LGKVEKQVLSMEKKLDFLVNIYMQRMGIP***PTETEAYFGAKEPE*

Q2-TCC2-3turn

*EAELPEDPS***VLSMEKKLDFLVNIYMQRMGIP***PTETEAYFGAKEPE*

Q2-TCC2-2turn

*EAELPEDPS***LDFLVNIYMQRMGIP***PTETEAYFGAKEPE*

Q2-TCC2-1turn

*EAELPEDPS***YMQRMGIP***PTETEAYFGAKEPE*

B
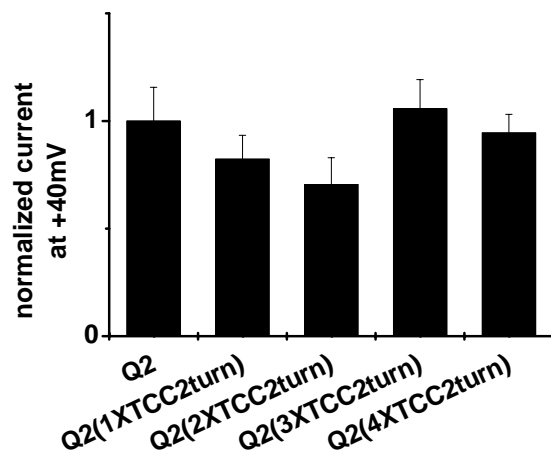
C
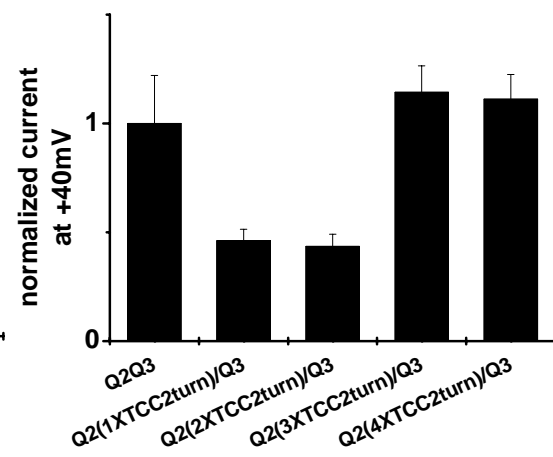
Figure C1.18: **A)** KCNQ2 deletion constructs with helix turn exchanges in the TCC2 domain. Residues of the TCC2 domain are indicated in bold. **B)** Bar graphs obtained from current levels at +40 mV recorded from oocytes injected with KCNQ2 (n=12), KCNQ2 (1X TCC2turn) (n=8), KCNQ2 (2X TCC2turn) (n=10), KCNQ2 (3X TCC2turn) (n=8) and KCNQ2 (4X TCC2turn) (n=7). **C)** Bar graphs obtained from current levels at +40mV recorded from oocytes (co-)injected with KCNQ2/KCNQ3 (n=12), KCNQ2 (1X TCC2turn)/KCNQ3 (n=9), KCNQ2 (2X TCC2turn)/KCNQ3 (n=7), KCNQ2(3XTCC2turn)/KCNQ3 (n=7) and KCNQ2 (4X TCC2turn)/ KCNQ3 (n=8). Currents were normalized to the value obtained from KCNQ2 (in **B**) and from KCNQ2 plus KCNQ3 (in **C**) at +40mV.

RESULTS 2

KCNQ channels share the characteristic 6TM-1P topology of all voltage-gated K^+ channels. However, amongst all Kv channels there are substantial differences in the primary sequence and a large variety of functional characteristics has been realized by evolution based upon this common modular construction principle. Whereas the degree of sequence identity of all KCNQ channels is roughly 40 %, with an even higher amount of sequence conservation within the transmembrane domains (B. C. Schroeder, personal communication), sequence conservation is quite poor with members of other Kv channel families (see **Figure C2.1**). KCNQ channels display a variety of characteristics, which make them functionally distinct from, e. g., the *Shaker* K^+ channel from *Drosophila*, which can by far be considered to be the most thoroughly studied Kv channel.
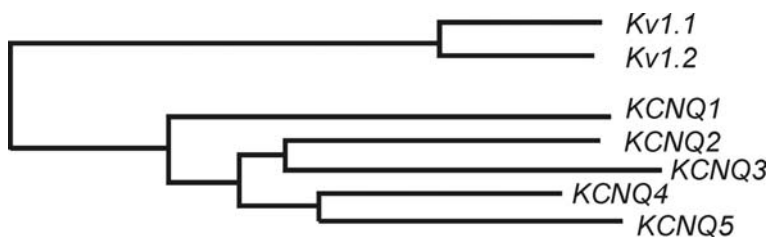
Figure C2.1: Dendrogram showing the relationship between KCNQ channels and with examples of distantly related Kv channels. The length of the horizontal branches is proportional to the mean differences per amino acid number along the branches.

Whereas *Shaker* completely inactivates after a depolarizing voltage pulse through a so-called "ball-and-chain" mechanism, which involves occlusion of the channel pore by an N-terminal inactivation particle, complete inactivation is not observed in KCNQ channels. Under certain circumstances a partial inactivation can be inferred for KCNQ1 and KCNQ3 from the decrease of I/I_{max} curves (apparent p_{open}) at strongly depolarizing potentials. This behaviour sometimes shows up as an overshoot in the current traces measured upon jumps to positive potentials (see e.g. **Figure C2.4** original traces KCNQ1). Also in contrast to the *Shaker* channel KCNQ1 carries only 4 (instead of 8) positively charged amino acid side chains within its S4 segment, therefore the voltage dependence of channel activation (I/I_{max} or apparent p_{open} curve) of KCNQ1 channels in general is more shallow than for *Shaker*. Serving as a paradigm in Kv channel research for long, the *Shaker* channel has been heavily investigated by mutagenesis studies to correlate structure with function, with

special focus on the pore and voltage-sensing segments like S4 concerning the role of individual amino acids in channel activation and other biophysical characteristics.

Since not many systematic studies concerning the role of individual amino acids in KCNQ channel activation are available yet, we wanted to probe the influence of single amino acid side chains within the S4 segment and the preceding S3-S4 loop on channel properties. To address this issue a Cys-scanning mutagenesis study of the S3-S4 linker region and the S4 voltage-sensing segment of the cardiac KCNQ1 channel was carried out. The reason for this strategy was two-fold:

(1) The replacement of individual amino acids with a cysteine offers the possibility to perform accessibility studies with thiol-modifying substances like MTSES. MTS compounds covalently react with SH-groups of cysteines, leading to the formation of a relatively large charged cystein conjugate. This change in the molecular structure is expected to alter the microenviroment surrounding the cysteine residue in terms of volume as well as electrostatic interactions, which frequently leads to functional alterations of the underlying Cys-mutant channel. Thus, MTS accessibility studies bear the advantage of having a clear functional readout for the identification of solvent-exposed amino acid positions, which are critically involved in the channel's activation process.

(2) The identification of individual amino acids, which can be functionally modified by thiol-reactive compounds, can serve as a starting point for testing three-dimensional structural models of KCNQ channels, which can be constructed based upon known crystal structures of voltage-gated K^+ channels. With the aid of these structural models one can propose amino acid positions in different transmembrane segments which might be in proximity to the solvent-accessible positions in S4, as identified by MTS effects. Proximity can be addressed by trying to crosslink cysteines using Cd^{2+} metal ion cross-bridges, which due to their comparatively small size have successfully been used for probing small intramolecular distances. Therefore, these studies can not only yield valuable data about structure-function relationships in general, but they can also serve to test the validity of structural models of KCNQ channels.

A)

B)
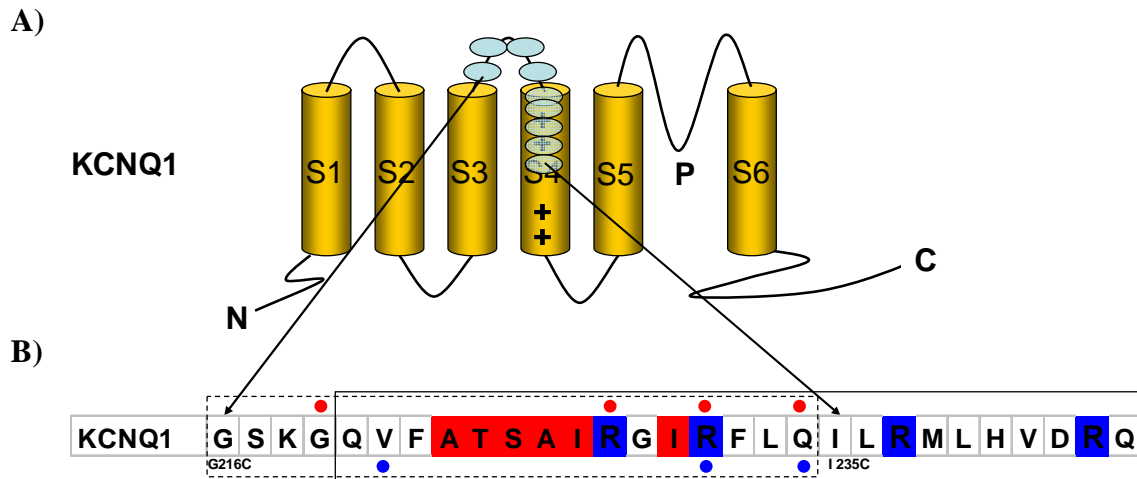
Figure C2.2: **A)** Membrane topology model of voltage-sensitive potassium channels. Six transmembrane domains (S1-S6) and the pore-forming region P are shown. Positions of cystein substitution within the S3-S4 loop and the S4 segment are schematically indicated as circles. Basic residues in S4 are also marked (+). **B)** Amino acid sequence of KCNQ1 in the S3-S4 loop and the S4 segment with the region in which mutations were generated boxed by a dashed line. Residues belonging to the S4 segment according to topology models are boxed with a solid line.

Underlayed in red are amino acid positions at which upon mutation to a cysteine a large increase in conductance after MTSES treatment is observed, resembling an (at least partially) open phenotype. In most cases this behaviour correlated with a large shift in their I/I_{max} curves (if I/I_{max} analysis could be performed). The positively charged amino acids of the voltage sensor are underlayed in blue. Red dots indicate effects of different nature observed upon MTSES application (for description: see text). Blue dots indicate mutants which show a (partially) open phenotype already before MTSES treatment.
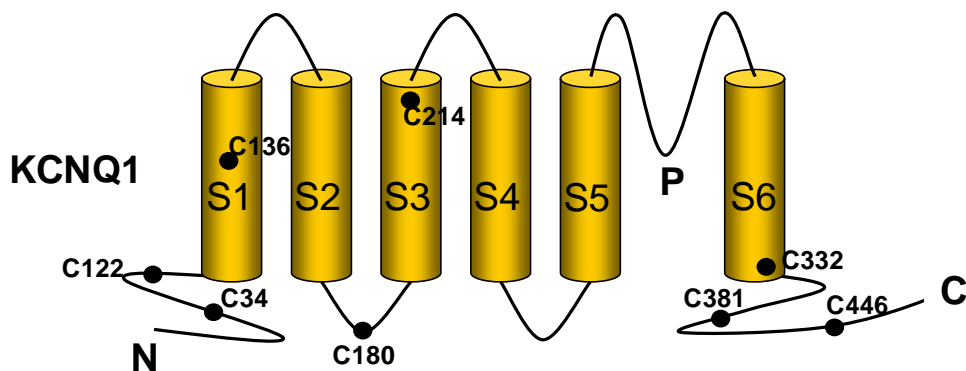
Figure C2.3: Membrane topology model of KCNQ1 with positions of endogenous cysteines indicated as black circles.

To probe the accessibility of individual amino acids for extracellularly applied MTSES, we generated 20 mutants, in which positions of a continuous stretch of amino acids within the S3-S4 loop and the S4 segment of KCNQ1 were individually mutated for cysteines (range of mutations: G216C to I235C, see **Table C2.1** and **Figure C2.2**). Since KCNQ1 carries 3 endogenous cysteines in its transmembrane domains (C136 in S1, C214 in S3 and C332 in S6, see **Figure C2.3**) it was first tested whether KCNQ1 wild-type exhibited some MTSES reactivity. Under standard conditions (10 mM MTSES applied for 2 min) no change in the amplitudes, voltage dependence or kinetics of KCNQ1 currents could be found (**Figure C2.4,** KCNQ1 control measurements). Thus, the endogenous cysteines in KCNQ1 do not produce adverse effects for these labeling studies.

A)   **B)**
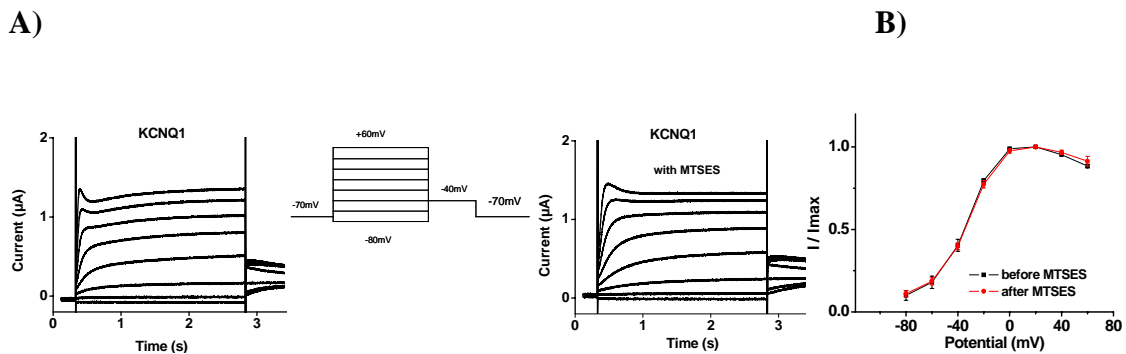
Figure C2.4: **A)**Current traces of the same oocyte expressing KCNQ1 wild-type before (left) and after (right) the application of 10 mM MTSES. The voltage protocol is shown in the inset. **B)** I/I_{max} curves of KCNQ1 as a function of voltage obtained from tail current analysis

C 2.1   Properties of KCNQ1 cysteine mutants in the S3-S4 loop and S4 segment

All mutants generated were first tested for functional expression, and the properties of the mutant's currents were compared to wild-type currents. As can be seen from Table C2.1 only mutant L233C did not show functional expression and most of the mutants exhibited KCNQ1-like current-voltage characteristics (mutants G216C to A226C, G229C, I230C, F232C, I235C), although deviations in the $V_{0.5}$ value (voltage of half-maximal activation) compared to KCNQ1 wild-type were frequently observed (**Figure. C2.5** and **Table C2.1**). Mutants with significant hyperpolarizing shifts in $V_{0.5}$ compared to KCNQ1 wild-type

clustered between G219C and F222C (but also included Q234C and G216C), those with positive $V_{0.5}$ shifts were S217C, A223C, T224C, S225C, A226C, G229C, I230C, F232C and I235C (**Figure. C2.5** and **Table C2.1**). A negative shift in $V_{0.5}$ can be considered as stabilisation of the open state/destabilization of the closed state of the mutant channel, since smaller depolarizations are needed to activate the channel, whereas positive $V_{0.5}$ shifts indicate stabilisation of the closed state/destabilisation of the open state, since larger depolarizations are needed for channel activation.

The Cys-mutants of the two voltage-sensing arginines, R228C and R231C, were especially interesting, since removal of a gating charge is expected to change channel properties dramatically. Indeed, mutant R228C exhibited a very slow activation and deactivation, and currents resembled those, which can be measured for a coexpression of KCNQ1 with KCNE1 (I_{Ks} currents). The slow kinetics possibly implies, that structural changes preceding opening or closure of the channel, or the gating event itself, might be drastically delayed in this mutant. In contrast, mutant R231C behaved like an open channel, mediating a large, virtually voltage-independent K^{+}-selective conductance upon expression in oocytes (as judged from the current's reversal potentials, see **Figure C2.10**) and only very weak residual gating could be observed at strongly hyperpolarizing potentials (see **Figure C2.10**). Such a behaviour indicates that the voltage sensor of this mutant channel is locked in a position which stabilizes the open state. A behaviour resembling an at least partially open phenotype was also displayed by mutants V221C and Q234C (see **Figure C2.9 and C2.6**), these channels had a comparatively large background conductance, but still showed some additional KCNQ1-like activation behavior, and their activation curves (as determined from I/I_{max} analysis of tail current amplitudes) were shifted towards hyperpolarizing potentials (see **Figure C2.5**).
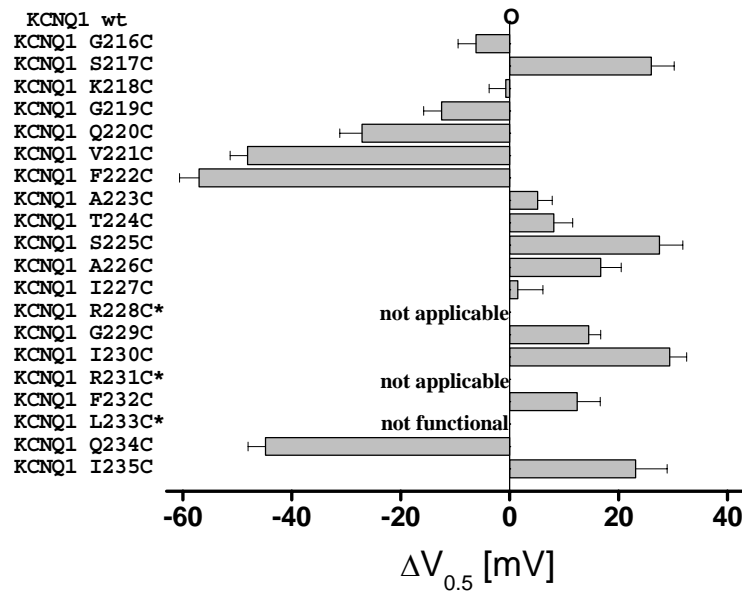
Figure C2.5: Values for the potential at half-maximal activation ($V_{0.5}$) determined from tail current analyses for various KCNQ1 cysteine mutants compared to KCNQ1 wild-type. Indicated are $V_{0.5}$ shifts compared to the wild-type value, which was set to zero.

C 2.2   Residue accessibility probed by MTSES application

In order to detect solvent accessibility of the cysteines introduced at various positions we searched for functional effects of extracellular MTSES application by comparing current characteristics before/after MTSES treatment. MTSES aliquots were prepared in ice-cold ND96 solution with high buffer content (20 mM HEPES, pH 7.4) and immediately stored in liquid nitrogen to be thawed up freshly before each experiment. To achieve robust labeling conditions, 10 mM MTSES was applied for 2 min, as reported to be optimal in the literature (Stauffer and Karlin, 1994) at -70 mV holding potential. These precautions had to be taken, since at pH 7.5 and room temperature MTSES hydrolyzes with a half-lifetime of 20 minutes. It has to be noted, that such a functional read-out scheme can only detect labeling effects, if (1) the respective cysteine is solvent-accessible and (2) the attachment of the bulky side chain leads to functional impairment or other alterations. Thus, from the absence of functional consequences upon MTSES treatment one can not distinguish between a site, which is not accessible, and a site, which may be labeled but does not produce a functional alteration. From the mutants investigated, G216C, S217C, K218C, Q220C, V221C, F222C, G229C, F232C, and I235C did not show any changes in current

characteristics after MTSES application (data not shown, see characteristic current recordings for these mutants in absence of MTSES in **Figure C2.6**). Whereas the residues within the S3-S4 loop might be solvent-accessible but without any functional consequence brought about by attachment of the bulky MTS side chain, the lack of effect in case of residues far downstream the S4 segment might indeed indicate limited or strongly restricted accessibility. Table C2.1 gives an overview about the observed MTSES effects for all cysteine mutants investigated.

Table C2.1: Current characteristics of KCNQ1 cysteine mutants and effects observed upon application of extracellular MTSES

Construct	Characteristics (no MTSES)	$V_{0.5}$ compared to KCNQ1-WT (no MTSES)	MTSES effect	classification of effect: **X** = strong X = weak
G216C	KCNQ1-like	-6 mV	no change	
S217C	KCNQ1-like	+26 mV	no change	
K218C	KCNQ1-like	$\pm$ 0 mV	no change	
G219C	KCNQ1-like	-12 mV	increase in I/I_{max}, pos. shift in $V_{0.5}$	X
Q220C	KCNQ1-like	-27 mV	no change	
V221C	large initial conductance, additional KCNQ1-like activation phase	-48 mV	no change	
F222C	KCNQ1-like	-57 mV	no change	
A223C	KCNQ1-like	+5 mV	open phenotype, residual gating at strong hyperpolariz.	**X**
T224C	KCNQ1-like	+8 mV	open phenotype, residual gating at strong hyperpolariz.	**X**
S225C	KCNQ1-like	+ 28 mV	conductance increase, reduced activating phase, inactivation slowed	**X**

A226C	KCNQ1-like	+ 17 mV	open phenotype, residual gating at strong hyperpolariz.	**X**
I227C	comparatively large background conductance, slow residual gating	± 0 mV	open phenotype without gating	**X**
R228C	very slow activation/deactivation ≈ KCNQ1/KCNE1-like currents	not applicable	gating speeded up, deactivation very slow	**X**
G229C	KCNQ1-like, large currents	+15 mV	no change	
I230C	KCNQ1-like, pronounced inactivation at positive potentials, slower activation/deactivation	+29 mV	part. open phenotype, residual gating only at strong hyperpolariz., inactivation removed	**X**
R231C	open phenotype, some residual gating at strong hyperpolarization	not applicable	completely open phenotype without gating	X
F232C	KCNQ1-like	+12 mV	no change	
L233C	not functional			
Q234C	partially open phenotype, only residual, slow activation/deactivation	-45 mV	even slowed deactivation, apparent negative shift in V0.5	X
I235C	KCNQ1-like	+23 mV	no change	
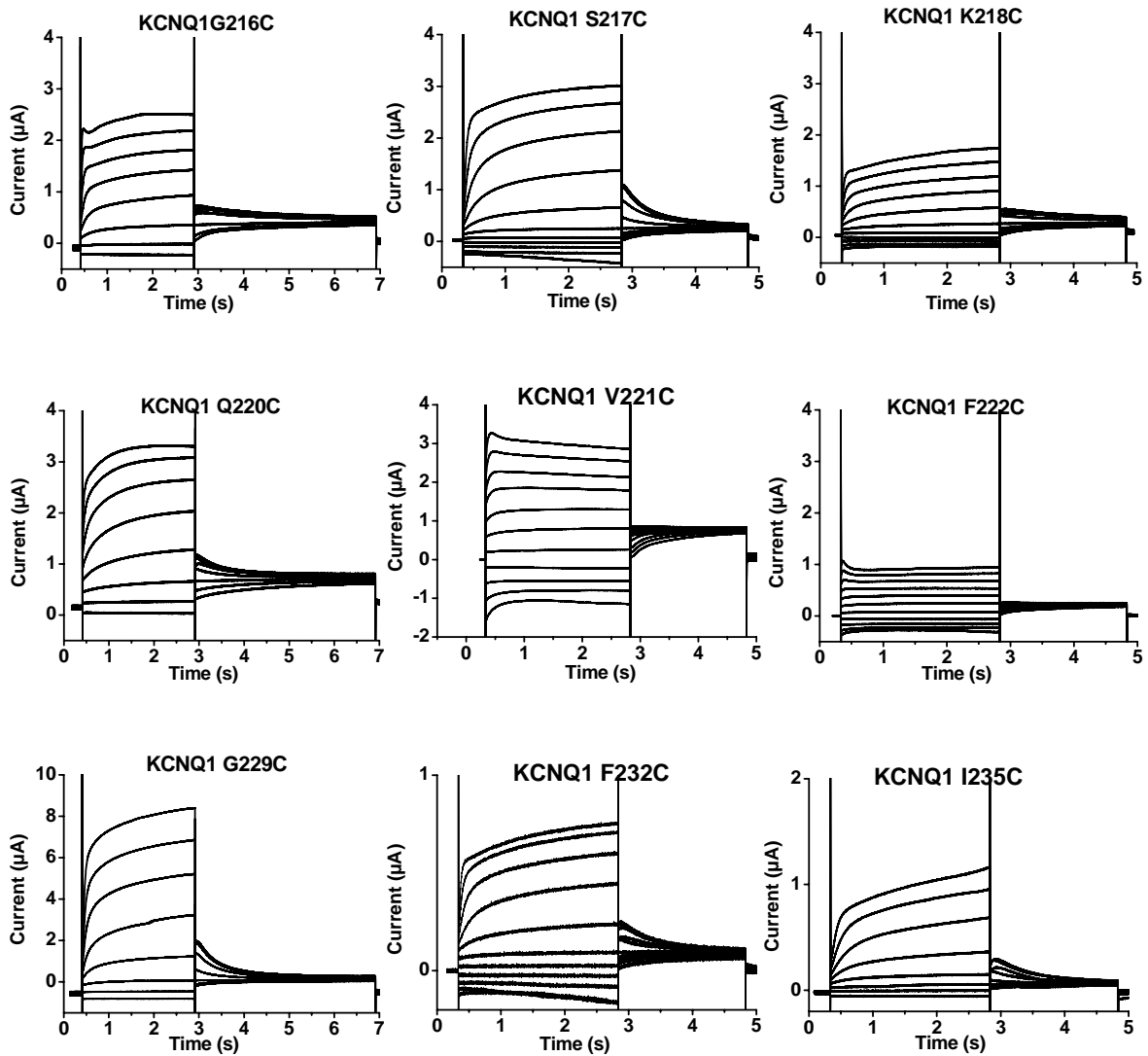
Figure C2.6: Characteristic currents of KCNQ1 cysteine mutants, as indicated above each set of data traces. These mutants did not exhibit functional alterations after MTSES treatment (data not shown). The voltage protocol corresponds basically to that shown in the inset of Figure 2.4., but test pulse potentials from -140 to +60mV were applied.

Notably, a series of mutants from A223C to I227C and mutant I230C exhibited drastical changes in current characteristics after MTSES treatment. These mutants in general showed activation behaviour comparable to KCNQ1 wild-type, but resembled constitutively open channels after MTSES modification (see **Figure C2.7**). In some cases (T224C and S225C) residual activation behaviour could be observed upon depolarizing voltage pulses (see **Figure C2.7** panels **B** and **C**). Currents measured for mutants A223C, A226C, I227C and I230C showed, that these MTSES-modified channels could be driven into deactivation at strongly hyperpolarizing potentials (see **Figure C2.7**, panels **A,D,E,F**).

The observed changes in current characteristics were correlated with a hyperpolarizing shift of the activation curves, as inferred from I/I_{max} analysis of tail currents. Such a behavior indicates that the introduction of the bulky side chain by MTSES treatment prevents the voltage-sensing S4 segment from returning to a conformational position which would lead to channel closure, thus stabilizing the open state. The hyperpolarizing shift of the I/I_{max} curves indicates that strongly hyperpolarizing potentials are needed to induce a movement of the S4 segment into a position which leads to deactivation of the channel. Mutant I230C in addition showed an increase in the saturation values of the I/I_{max} curve upon MTSES treatment, which can be interpreted as an increase in the maximal open probability (**Figure C2.7 F**). Again, such behaviour is consistent with the notion that MTSES modification of the respective mutant leads to a stabilization of the open state.
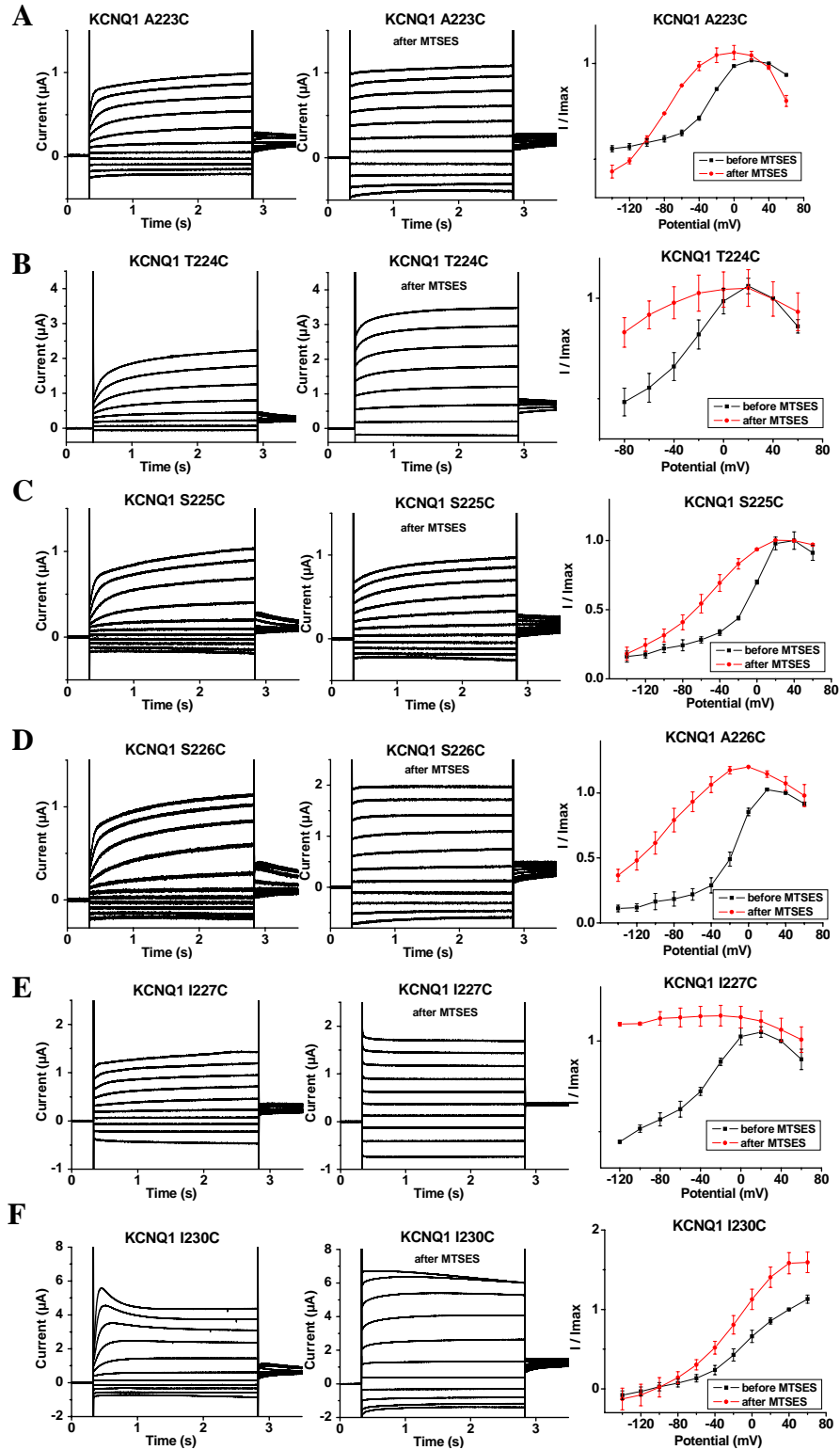
Figure C2.7: Characteristic currents of KCNQ1 cysteine mutants (indicated above each data set) before and after MTSES trreatment, together with I/I$_{max}$ curves as determined from tail current analysis. These mutants exhibited significant functional alterations after MTSES treatment, resembling channels with a stabilization of the open state, which was paralleled by a hyperpolarizing shift of the activation curves. The applied voltage protocol was the same as in Figure 2.4, but test pulse potentials from -140 to +60mV were applied.

Two other cysteine mutants also exhibited significant functional alterations upon MTSES modification, albeit with a somewhat different appearance. In addition to a slight increase in background conductance, mutant G219C displayed a general up-scaling of current amplitudes in the MTSES-modified state, which was paralleled by a 40 % increase in the saturation value of the respective I/I_{max} curve (see **Figure. C2.8**). Again, this can be interpreted as an increase in open probability. From the progression of the I/I_{max} curve also a slight depolarizing shift in the $V_{0.5}$ value for half-maximal activation (~ +15 mV) could be inferred.

Figure C2.8: Typical current traces of oocytes expressing KCNQ1 G219C before (left) and after (middle) 10 mM MTSES application. The voltage protocol used for these current traces is shown in the inset of the Figure 2.4., but test pulse potentials from -140 to +60mV were applied. Left, corresponding I/I_{max} curves as obtained from tail current analysis. The voltage protocol corresponds basically to that showing in the inset of Figure 2.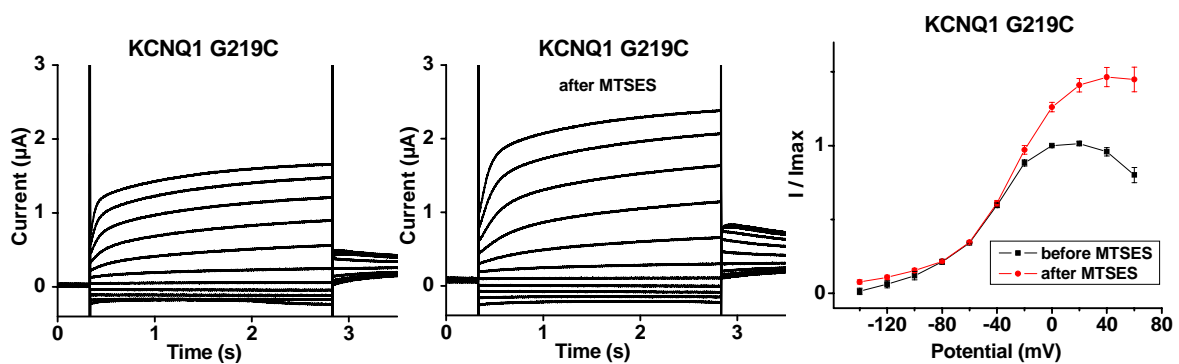4 but test pulse potentials from -140 to +60mV were applied. The activation parameters as determined from fits of a Boltzmann function to I/I_{max} curves were $V_{0.5}$= -44.7 ±1.9 mV (without MTSES) and -30.4 ± 2.7 mV (with 10 mM MTSES) (n=5).

In case of mutant Q234C changes induced by MTSES were more subtle. Currents measured with this mutant already resembled an at least partially open channel before MTSES treatment, with a hyperpolarizingly shifted I/I_{max} curve compared to KCNQ1 wild-type, but still some residual KCNQ1-like activation behaviour could be observed. Upon MTSES modification the residual activating phases of the currents were reduced, the activation/deactivation kinetics slowed down, and a decrease of the slope of the I/I_{max} curves was observed, indicating a weaker voltage dependence of channel activation (see **Figure C2.9**).
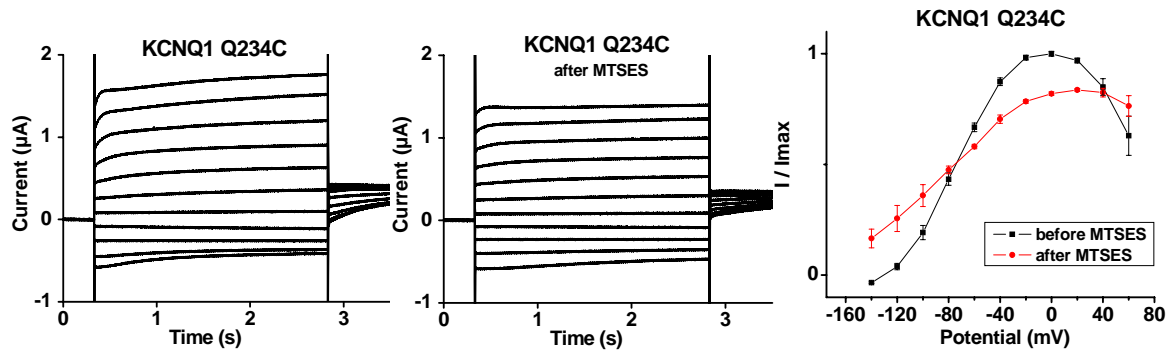
Figure C2.9: Current traces of oocytes expressing mutant KCNQ1 G234C in the absence (left) or the presence (middle) of 10mM MTSES. The voltage protocol used for these current traces is shown in the inset of Figure 2.4., but test pulse potentials from -140 to +60mV were applied. Right, corresponding I/I_{max} curves as obtained from tail current analysis. The activation parameters as determined from fits of a Boltzmann function to I/I_{max} curves were $V_{0.5}$= -77.0 ± 1.8 mV (without MTSES) and -81.4 ± 3.9 mV (with 10 mM MTSES) (n=3).

Also in case of the cysteine insertion at the voltage-sensing arginine position R228 characteristic changes upon MTSES treatment were observed. Mutant R228C, which exhibited very slow activation or deactivation without MTSES, exhibited accelerated activation kinetics after MTSES application, and deactivation was even slower than in the non-modified channel. Therefore R228C also resembled a channel, in which the open conformation was stabilized by reaction with the thiol-reactive compound. In case of mutant R231C effects observed upon MTSES treatment were not conclusive. This channel displayed a locked-open phenotype already before MTSES application. The only changes, which could be observed in some experiments concerned a residual activation, that was present in tail currents upon voltage steps from -140 mV to +40 mV. These activating currents completely disappeared upon MTSES treatment.
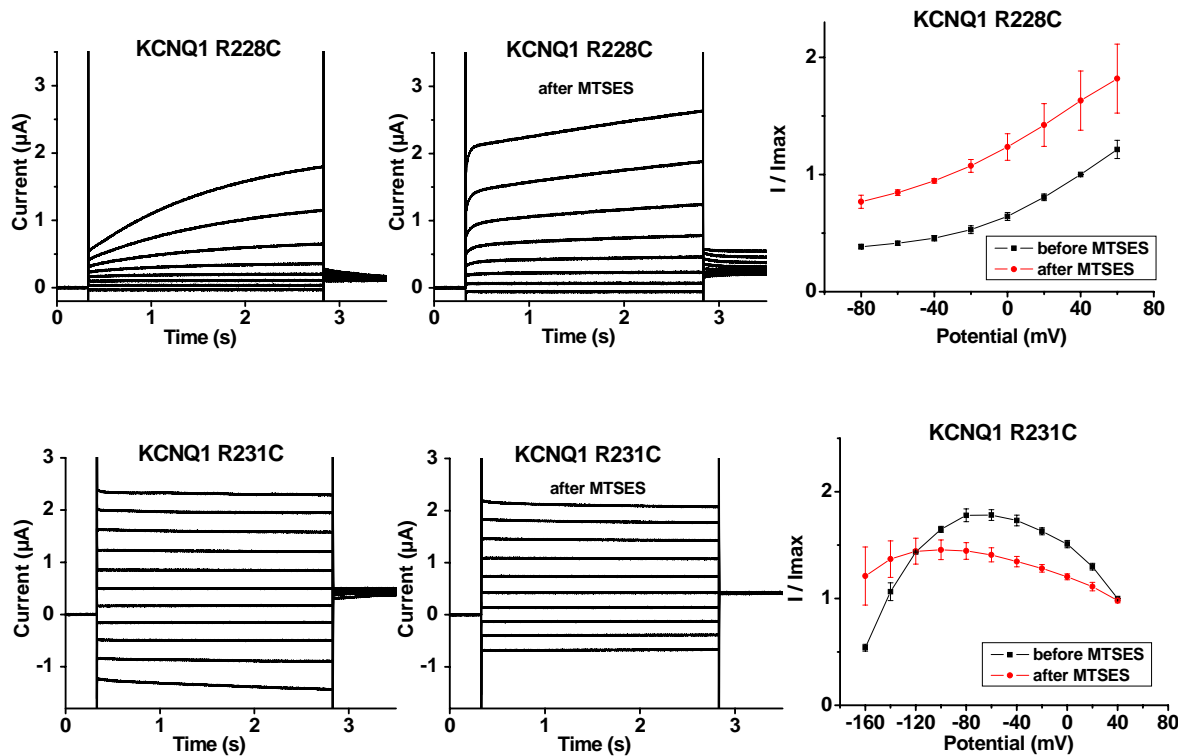
Figure C2.10: Typical current traces of oocytes expressing KCNQ1 mutants R228C (upper panels) and R231C (lower panels) before (left) and after (middle) 10 mM MTSES application. The voltage protocol used for these current traces is basically shown in the inset of Figure 2.4 but test pulse potentials from -160 to +60mV were applied. The corresponding I/I_{max} curves as obtained from tail current analysis are shown in the right panels. The activation parameters could not be determined from fits of a Boltzmann function to I/I_{max} curves (n=5).

In summary, from the 20 cysteine mutants investigated 7 showed clear indications for functional alterations upon MTSES treatment (A223C, T224C, S225C, A226C, I227C, R228C, I230C), thereby unambiguously showing accessibility from the extracellular side of the membrane and a critical role in structure-function relationship of the S4 segment. It is interesting to note, that these positions represent a rather continuous strech of amino acids, indicating that the whole region is solvent-accessible from outside the cell under our labeling conditions. In most cases, the introduction of the bulky MTS side chain led to a pronounced stabilization of the open state, thus preventing channels from closing at physiological potentials. In addition, G219C within the S3-S4 loop and Q234C, far downstream the S4 segment could be functionally affected by MTSES application. Therefore, these cystein accessibility studies yielded a number of candidate positions, which could potentially be used to probe helix proximity in the subsequent cross-linking experiments.

C 2.3   Testing proximity between S4 and other transmembrane segments of KCNQ1 based on model predictions

Based on the crystal structure of the mammalian voltage-gated Kv1.2 channel (Long et al., 2005) a molecular model of KCNQ1 was constructed, starting from sequence homology to *Shaker*-type channels (see **Figure C2.11**). This part of the work was carried out by PD Dr. Guiscard Seebohm (Tübingen University). Due to limited sequence homology, these molecular models may be inaccurate on the single amino acid level and deserve testing by experiment. Therefore, this model was used to propose potential amino acid positions within transmembrane domains of KCNQ1, which could be in close proximity of MTSES-accessible positions in S4. Accordingly, double mutants of certain pairs of amino acids were generated, which carried one cysteine on the S4 segment and one on another helix (S2 or S5). The strategy involved to use cross-linking by Cd^{2+} ions, which are coordinated by sulfhydryl groups within a relatively strict distance range of ~ 5 Å (Rulisek and Vondrasek, 1998), and due to their small size represent precise molecular "rulers". All these double cysteine mutants were constructed on the basis of single cysteine constructs, which could be functionally modified by MTSES, and showed effects consistent with a loss of flexibility of the S4 segment. Therefore, it can be assumed, that cross-linking by heavy metal cations also leads to effects which can be attributed to higher conformational rigidity. However, it has to be noted, that the Kv1.2-based model most likely represents the closed state of the channel. Thus, if cross-linking between positions proposed by the model would occur, the structural rigidity imposed by this treatment should lead to a channel behaviour, which would indicate a more or less pronounced stabilization of the closed state, because in the open state the residues might be required to move far away from each other. This is in contrast to the observations in MTSES modification experiments, in which predominantly open-state stabilization was observed, most likely because the attached bulky side chain prevents the S4 segment from returning into a "deactivated" position due to spatial constraints.
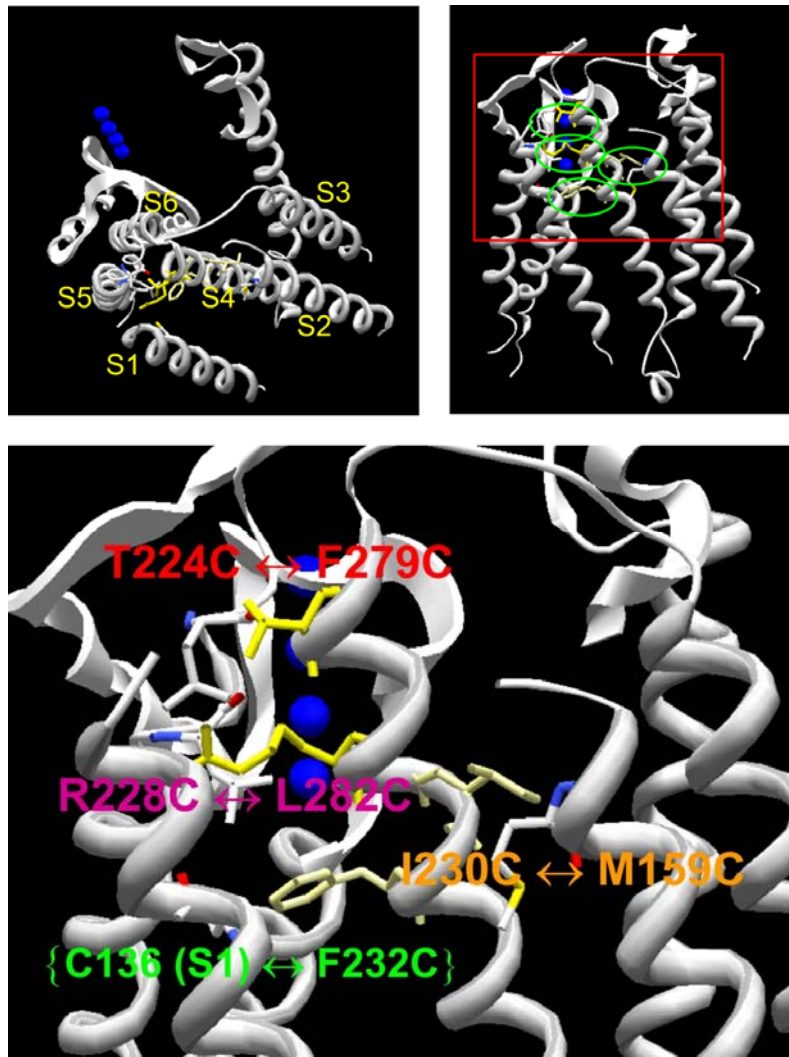
Figure C2.11: Structural model of the KCNQ1 channel, constructed according to the Kv1.2 crystal structure (Long et al., 2005). Left, overall arrangement of transmembrane helices of one subunit within the tetramer, viewed at some inclination angle from the extracellular side. The location and direction of the pore ist indicated by the series of blue balls. Right, overall location of putatively proximal amino acid side chains between the S4 and other transmembrane segments, viewed from inside the membrane plane. Proximal amio acid pairs are indicated by green ellipses. Bottom, detailed view of the region indicated by the red rectangle in the top right panel, the respective amino acid side chains are depicted together with labels.

The double mutants to be tested, as suggested by the molecular model of KCNQ1, were T224C / F279C (S4 - S5), R228C / L282C (S4 - S5), and I230C / M159C (S4 - S2). With a somewhat larger distance in between, it was proposed that F232C could also be in proximity to the endogenous C136 within the S1 segment. For probing the latter hypothesis, only the F232C single mutant had to be investigated for Cd^{2+} cross-linking effects.

The concentrations commonly used in heavy metal cation cross-bridging experiments are in the millimolar range. However, it had to be tested beforehand, whether adverse effects of Cd^{2+} addition could occur either in case of the wild-type channel (due to various endogenous cysteines, which might be coordinated) or in case of the single cystein mutants, in order to exclude unspecific effects. After confirming, that 1 mM Cd^{2+} did not alter function of KCNQ1 wild-type (**Figure C2.12**), and that the newly generated mutants M159C, F279C and L282C could be functionally expressed, all single cysteine mutants to be involved in this part of the study were tested with 100 µM and 1 mM Cd^{2+} (see **Figure C2.13, Figure C2.14**). The results in Figure 2.13 and Figure 2.14 show, that 1 mM Cd^{2+} ions produce unspecific effects in case of mutants M159C (current increase, hyperpolarizing shift of $V_{0.5}$), T224C (significant increase in current amplitudes), R228C (accelerated activation, large background conductance due to open state stabilization), and I230C (current and conductance increase, open state stabilization), whereas current characteristics of mutants F279C and L282C were not significantly affected. Since unspecific effects had to be avoided right from the beginning, also a 100 µM Cd^{2+} concentration was tested. Under these conditions no significant changes could be observed, and this was also valid for the constructs, which exhibited changes in presence of 1 mM Cd^{2+}. Therefore, a 100 µM Cd^{2+} concentration had to be used in subsequent experiments with paired cysteine mutants. This concentration is fairly low compared to values commonly reported in the literature. However, functional alterations observable at these low concentrations would indicate highly specific cross-linking events.
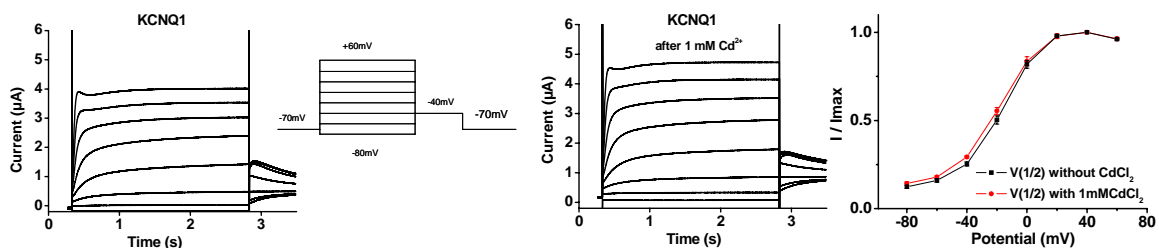
Figure C2.12: Current traces recorded from one oocyte expressing KCNQ1 wild-type before (left) and after (middle) the application of 1 mM Cd^{2+}. The right panel shows the corresponding I/I_{max} curves determined from tail current analysis. The voltage protocol is shown in the inset.

Also the double cysteine mutants yielded functional channels with KCNQ-like characteristics. For two of the tested paired cysteine constructs significant effects on

channel currents could be observed upon addition of 100 µM Cd^{2+}. Double mutant M159C/I230C displayed large, fast activating currents with pronounced overshoot characteristics at strongly depolarizing potentials. With 100 µM Cd^{2+} activation as well as deactivation of the channels was slowed down (see **Figure. C2.15**). In addition, the maximal values of the normalized I/I_{max} curves were significantly reduced, which argues for a decrease in the channel's maximal open probability. Such a marked decrease in the I/I_{max} curve was also observed for double mutant T224C/F279C upon addition of 100 µM Cd^{2+}, and in this case also the currents were largely reduced. These changes, especially the reduction of the I/I_{max} curves can be interpreted as a result of stabilization of the closed state of the channel, which is brought about by Cd^{2+} cross-linking. This is in line with the model predictions which originated from a closed channel conformation. No significant effects with 100 µM Cd^{2+} for the R228C/L282C double mutant and with 1 mM Cd^{2+} for the F232C/endogenous C136 could be observed. However, the results obtained with Cd^{2+} cross-linking of the cysteine pairs M159C/I230C and T224C/F279C demonstrate close proximity between the respective amino acid positions in the closed state of the channel, in accordance with a structural homology model based on the Kv1.2 crystal structure. These data can be of considerable value to define further constraints for model refinement.
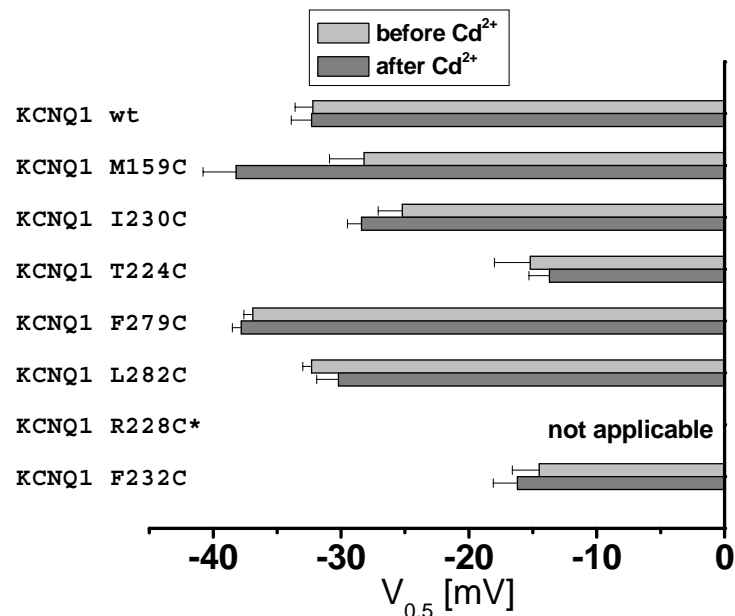
Figure C2.13: Values for the voltage of half-maximal activation for 7 cysteine mutants used for Cd2+ cross-linking studies, as inferred from tail current analysis (n = 3-6). From a holding potential of -70mV, oocytes were clamped for 2.5 s to potentials between -80mV and +60mV, followed by a constant tail pulse at -40mV. V0.5 values determined before addition of Cd2+ are indicated in light grey, after addition of 1 mM Cd2+ (in the case of F279C and L282C) and 100µM Cd2+ (in the case of M159C, I230C, R228C and F232C) in dark grey.
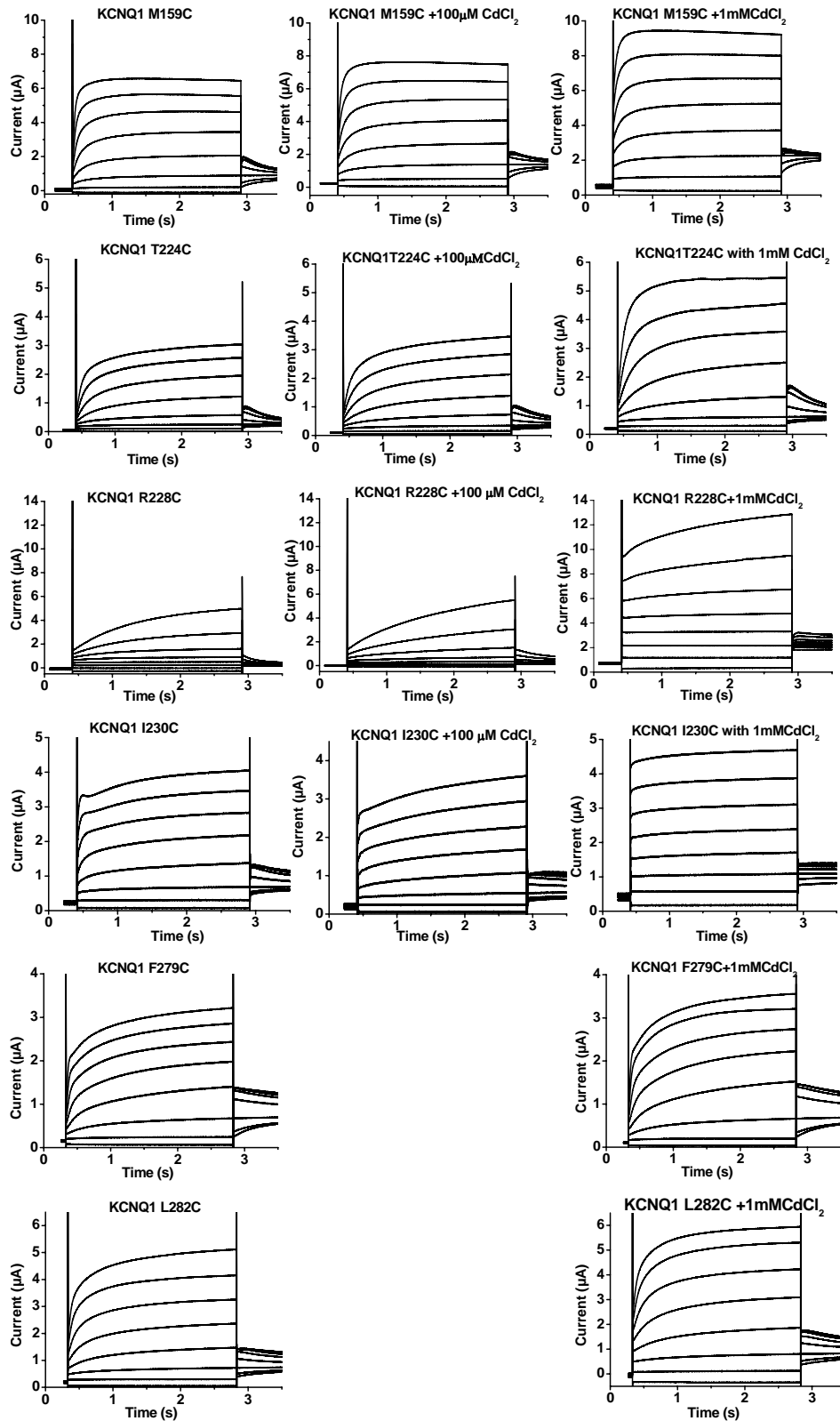
Figure C2.14: Typical current recordings from Xenopus oocytes expressing KCNQ1 cysteine mutants M159C, T224C, R228C, I230C, F279C, and L282C, without Cd^{2+} (left column panels), with 100 µM Cd^{2+} (middle column panels), and with 1 mM Cd^{2+}. Lower concentrations were not included for F279C and L282C since even at 1 mM Cd^{2+} no functional effects could be observed. The voltage protocol used for the experiments was the same as used in Figure 2.4.
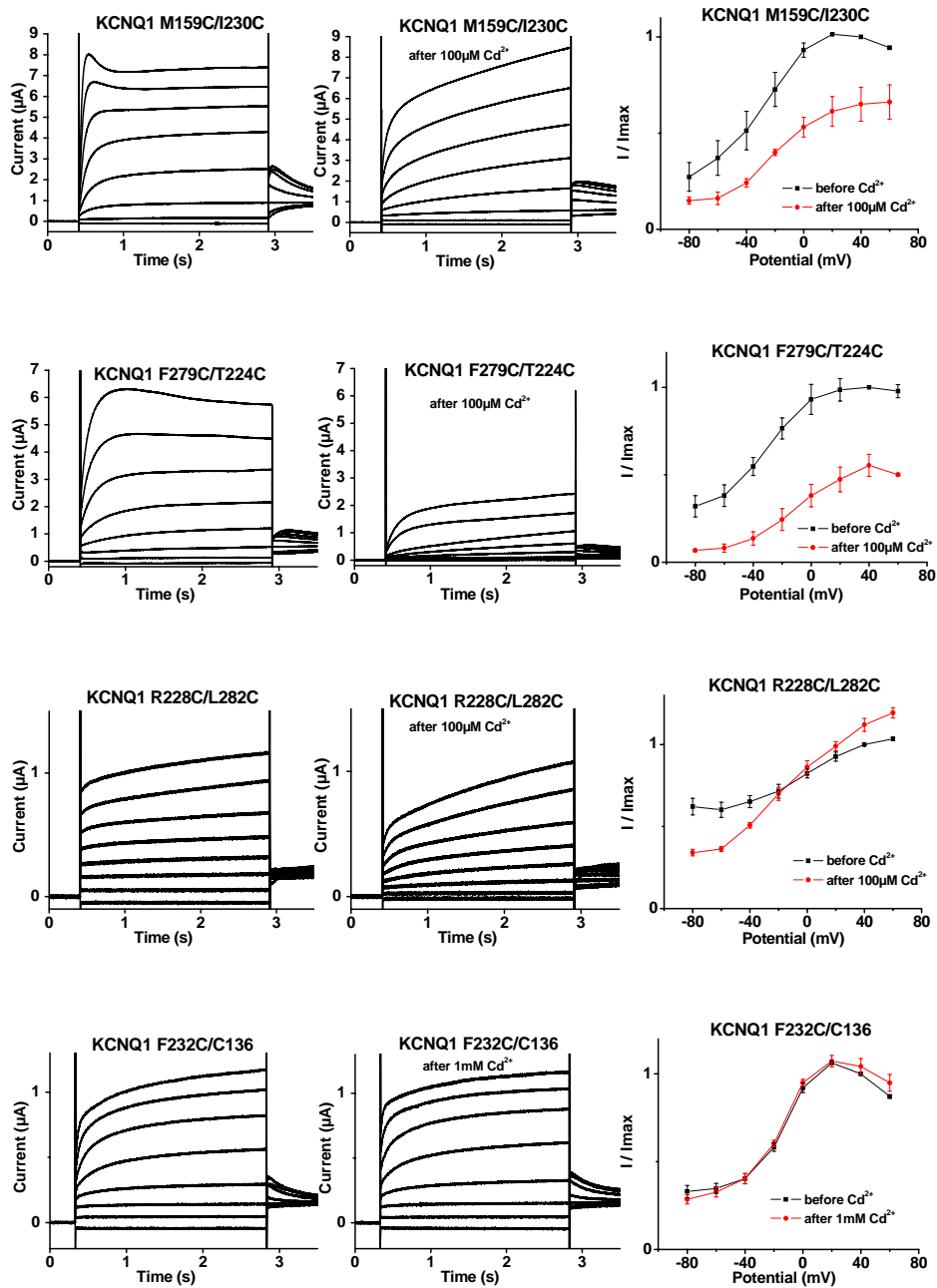
Figure C2.15: **A)** Characteristic current traces of the double cysteine mutants M159C-I230C, T224C/F279C, R228C/L282C and of construct F232C/C136 expressed in *Xenopus oocytes* before (left) Cd^{2+} and after (middle) Cd^{2+} application. From a holding potential of -70mV oocytes were depolarized to test potentials between -80mV and +60mV in 20mV steps for 2.5 s, followed by repolarisation to -70mV. **B)** The activation parameters as determined from fits of a Boltzmann function to I/I_{max} curves were for M159C/I230C $V_{0.5}$ = -28.6 ± 2.5 mV (without Cd^{2+}) and -19.3 ± 1.2 mV (with 100 µM Cd^{2+}), for F279C/T224C $V_{0.5}$= -30.5 ± 0.6 mV (without) and -8.0 ± 2.1 mV (with 100 µM Cd^{2+}), for R228C/L282C $V_{0.5}$= 1.1 ± 2.3 mV (without) and -12.3 ± 3.8 mV (with 100 µM Cd^{2+}) and for F232C/C136 $V_{0.5}$= -14.5 ± 2.1 mV (without) and -16.2 ± 1.9 mV (with 1 mM Cd^{2+}) (*n*=3-6).

D   DISCUSSION

D 1.1   The role of the TCC2 domain

KCNQ channels have the ability to form either homotetramers or heteromers composed of different α-subunits. It was already shown in previous work that the subunit-specific assembly of KCNQ subunits is mediated by the C-terminal *si* domain (Maljevic et al., 2003; Schwake et al., 2003). Jenke in 2003 pointed out that the KCNQ *si* domains contain putative coiled-coil structures that can drive the heteromerisation of channels using suitable coiled-coil prediction algorithms. These authors showed that coiled-coil sequences located within the C-termini of *eag* K^+ channels were able to form tetramers as isolated peptides. Therefore, Jenke et al. termed these sequences "tetramerizing coiled-coil" or TCC sequences. Coiled-coils are frequently found in protein-protein interaction domains and consist of an α-helical structural arrangement showing a heptad amino acid repeat pattern (*abcdefg*)$_n$ in which the positions *a* and *d* (**Figure D.1**) are preferably occupied by hydrophobic amino acids (Lupas, 1996).
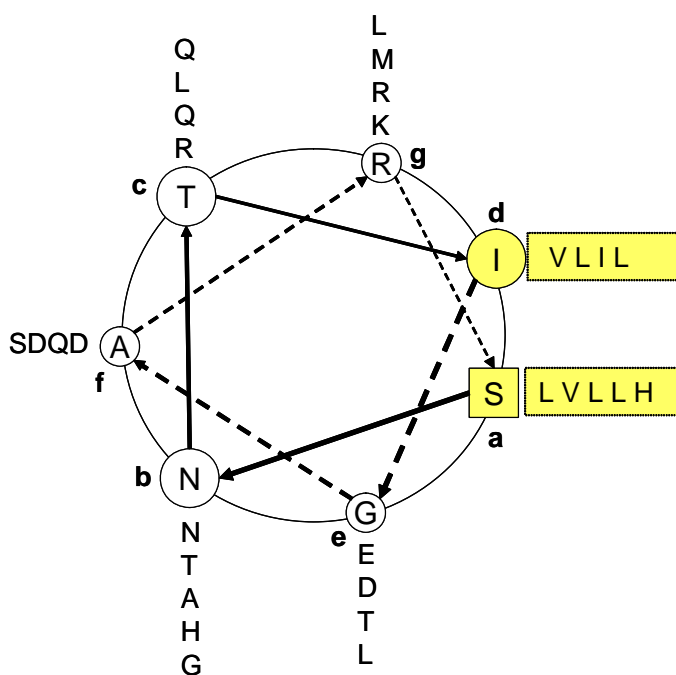
Figure D.1: Schematic helical wheel projection for coiled-coil helices of the KCNQ1 channel. Heptad positions are labelled a-g. Hydrophobic residues are boxed (positions *a* and *d*) and the rest are circled (positions b, c, e, f and g). Amino acids in position *a* and *d* are marked yellow.

TCC domains can be identified in diverse protein families such as cyclic nucleotide-gated cation channels, calcium-dependent potassium channels (SK channels), non-selective cation channels, calcium channels and voltage-gated potassium channels like Eag1, Eag2, Erg, Elk and, as already mentioned, in KCNQ channels. In most cases the TCC domain is a continuous stretch of periodically repeated hydrophobic residues, however, in the case of KCNQ channels the coiled-coil motifs are bipartite with a variable linker inbetween (**Figure D.2**) (Jenke et al., 2003).

Figure D.2: Alignment of the amino acids sequences of TCC domains from different ion channel families. Notably, the coiled-coil domain of the KCNQ channels is bipartite (blue boxes) (From Jenke et al.,2003).

The aim in the first part of this work was to study and analyse the role of the individual TCC domains of KCNQ channels in channel assembly, function and processing.

In the first part of the results it is demonstrated that the insertion of TCC2 from KCNQ3 instead of the homologous region within the KCNQ1 channel is sufficient to transfer the

assembly properties from KCNQ3 to the resultant KCNQ1(TCC2)Q3 chimera. This chimera was able to interact nearly as efficiently with KCNQ2 wild-type as KCNQ3, as judged from coexpression experiments with KCNQ2.

Evidence for this conclusion is drawn from several observations. First, a strong current enhancement after coexpression of KCNQ1(TCC2)Q3 with KCNQ2 is observed. The increase in current amplitudes compared to currents mediated by KCNQ2 expressed alone was about eight-fold, which is close to the factor of 10 reported from KCNQ2/KCNQ3 coexpression (Schroeder et al., 1998).

Second, the coexpression of the KCNQ1(TCC2)Q3-G314S pore mutant suppressed KCNQ2 currents in a dominant-negative fashion. The dominant-negative effect implies that the presence of one non-functional subunit in a tetramer is sufficient to completely abolish channel function. In such a situation the co-expression of wild-type and mutant subunits in a 1:1 fashion nearly completely suppresses functional K^+ channel currents.

Third, the KCNQ1(TCC2)Q3 chimera was able to dramatically stimulate the surface expression of KCNQ2 subunits, as probed by co-expression with epitope-tagged KCNQ2 in luminescence experiments on intact oocytes.

Fourth, in co-immunprecipitation experiments it was shown that the KCNQ1(TCC2)Q3 construct assembles with KCNQ2. Thus, the robust interaction of subunits can also be identified by biochemical techniques.

After confirming the role of the KCNQ3 TCC2 domain in channel assembly it was tested in a subsequent set of experiments, in which respect the TCC2 domain of KCNQ2 is required for heteromerisation with KCNQ3. For this purpose the TCC2 domain of KCNQ1 was inserted into the KCNQ2 backbone, and various deletion constructs of KCNQ2 were generated. It could be shown that the TCC2 domain of KCNQ2 is indispensable for efficient interaction with KCNQ3, since either the KCNQ2(TCC2)Q1 chimera or the KCNQ2-ΔTCC2 deletion construct did not induce an increase in current when co-

expressed with KCNQ3. Therefore, the TCC2 domains from KCNQ2 and KCNQ3 both are needed for an efficient transport of the heteromeric channels to the plasma membrane.

There are many possible ways to explain these results. It is known that for any protein which is synthesized and oligomerizes in the ER, the proper tertiary and quaternary structures must be achieved before release. Sorting mechanisms are in place to discriminate between the unassembled subunits and completed oligomers. These mechanisms include, for example, the exposure and masking of short discrete endoplasmic reticulum retention motifs (Pagano et al., 2001). So one possibility would be that either the coiled-coil interaction is responsible for masking an endoplasmatic reticulum retention motif or an efficient forward trafficking motif is formed by this interaction.

Several mechanisms which underlie the ER exit for ion channels are described in the paper of Carol Deutsch (Deutsch, 2003), in which several examples of sequence motifs are described. One of these ER motifs with a well-characterized function is present in the K_{ATP} class of K^+ channels. Proteins containing these sequences are retained in the ER or retrieved from Golgi compartment back to the ER. These ATP-dependent inward rectifier K^+ channels assemble as an octamer with a 1:1 stoichometry of four inward rectifier potassium channel subunits (KIR) and four auxiliary SUR (sulfonyl urea receptor) subunits. The SUR subunits modulate function and mediate drug sensitivity of the channel complex. Both KIR and SUR subunits have cytoplasmic RKR (for Arg-Lys-Arg) sequences, which must be masked by proper assembly of the octamer, before the channel can be transported to the cell surface. Similar motifs exist in the CFTR Cl^- channel, and within the C-terminus of $GABA_B$ receptor subunits. In the latter case heterodimeric coiled-coil interactions shield the motif, allowing the complex to be expressed in the cell surface.

Another ER motif has been identified in the first transmembrane domain of the nicotinic acetylcholine receptor channel (nAChR) α subunit, which govers trafficking of correctly assembled pentameric receptor channels. Due to its characteristic sequence it is called PL(Y/F) (F/Y) xxN.

An example for the role of masking a retention motif (YQFPQSIDPL) is present in cyclic nucleotide-gated (CNG) channels. A distal C-terminal domain in the A-subunit interacts with an N-terminal region of the B-subunit to mask a short sequence in the B-subunit, thereby allowing surface expression of the CNG channel.

Anterograde signals also play a role in exit from the ER, as exemplified in the case of KIR1.1 and 2.1 channels. Diacidic motifs can function as direct ER export signals(Deutsch, 2003). The flanking residues of diacidic motifs are also critical for ER export and vary among K^+-channels, thus providing a mechanism for differential distributions of K^+-channels on the cell surface.

A third determinant, phosphorylation, can also be involved in the regulation of ER exit. Dibasic motifs (one, two, or three sequential arginines or lysines) can lead to ER retention (Ma et al., 2001; Zerangue et al., 2001), and binding of a cytosolic protein allows forward movement. The unphosphorylated channel supports the retention mechanism, whereas phosphorylation of the channel channel favours forward transport (Deutsch, 2003).

ER exit can also be regulated by the association of channels with scaffold or anchoring proteins. Such proteins recruit other interaction partners to the channel to form macrocomplexes (**Figure D.6**) (more details in page 86 of the discussion).

Another possibility to explain the effects of certain protein domains on exit from the ER can be a newly identified mechanism, which occurs early in channel biogenesis. In this notion, the nascent TCC2 peptide could function as a barcode. It has been reported that amino acid motifs are decoded in the exit tunnel of the ribosome (composed of both protein and RNA) and influence elongation pausing and termination steps. The nascent peptide may not traverse the ribosome in a linear fashion but may circle back through the region of PTC (peptidyl transferase center). This would allow the nascent peptide to scan its own new domains immediately upon synthesis (Deutsch, 2003)

However, it has to be noted, that none of the ER retention or export motifs identified so far is present in the primary sequences of KCNQ channels. Therefore, the true structural nature of the proposed ER retention/export motif and the mechanism by which it acts during channel synthesis and/or processing still await clarification.

D 1.2   The role of the TCC1 domain

In contrast to TCC2 the sequence of the TCC1 domain is highly conserved in all KCNQ channels indicating that structural integrity of TCC1 is highly important. Interestingly, the KCNQ1(TCC1)Q3 chimera failed to stimulate currents when co-expressed with KCNQ2, although the TCC1 domains of KCNQ1 and KCNQ3 differ only in very few amino acids. In accordance with the lack of the stimulating effect on membrane currents, the

KCNQ1(TCC1)Q3 chimera did not increase surface expression when coexpressed with KCNQ2 and no dominant negative effect was observed upon co-expression of a chimeric channel carrying a mutation within the signature sequence of the selectivity filter.

However, this chimera was still different from KCNQ1 because it could be co-immunprecipitated with KCNQ2. This means that the TCC1 domain of KCNQ3 is able to mediate interaction with KCNQ2, most probably with the KCNQ2 TCC1 domain. Evidence for this conclusion is drawn from the fact that functional channels are obtained when the truncated construct KCNQ2-TCC1-X is coexpressed with KCNQ3 (Figure 3). The importance of the TCC1 domain is further underlined by the finding that the deletion construct KCNQ2ΔTCC1 did not yield functional K^+ currents and that no current enhancement could be observed upon coexpression of this deletion construct with KCNQ3.

Taken these results together it is apparent that the TCC1 domain is necessary for the formation and function of homomeric KCNQ2 channels and for heteromeric KCNQ2/KCNQ3 channels. However, is still needs to be clarified whether TCC1 is required during channel biosynthesis and processing or whether it is indispensable for proper channel function. It appears likely that the lack of the first TCC domain impairs the assembly of the channel subunits, but - in a much simpler sense - it could still be that in the absence of TCC1 domains channels are properly assembled, however they may be unable to gate open due to structural impairment. Surface expression luminescence experiments could help to discriminate between these possibilities.

D 1.3   Insertion of helix-breaking amino acids

Another way to probe the importance of the TCC structure for homo- and heteromer formation is the insertion of helix-breaking amino acids like proline into the TCC domains. The imido structure of proline leads to an exceptional conformational rigidity of the petide backbone compared to other amino acids. Proline acts as a structural disruptor in the middle of regular secondary structure elements such as alpha helices and beta sheets, and it is commonly found in turns of proteins.

Leu-to-Pro substitutions in the TCC1 domain of KCNQ2 and KCNQ3 already disrupted homomeric channel formation. This suggests that the structural integrity of the TCC1 domain is very important for channel assembly, as expected from the high degree of sequence conservation.

In contrast, experiments with Leu-to-Pro substitutions in the TCC2 domain yielded functional channels with properties similar to wild-type, implying that the structural integrity of the second TCC domain is less important for homomeric channel assembly.

Notably, the coexpression of KCNQ2 with a KCNQ3 channel, carrying a Leu-to-Pro mutation in the TCC2 domain, led to current augmentation as seen for KCNQ2/KCNQ3 coexpression. In contrast, coexpression of KCNQ3 with a KCNQ2 channel carrying a Leu-to-Pro mutation in the TCC2 domain did not lead to an increase in currents. These results imply that the structural integrity of TCC2 of KCNQ2 is necessary for KCNQ2/KCNQ3 heteromer formation, whereas the putative coiled-coil structure of TCC2 from KCNQ3 (for which the coiled-coil probability is already quite low as determined by prediction algorithms) is less important in this assembly.

D 1.4   Analysis of split channels

This strategy has successfully been used in case of voltage-gated chloride channels of the ClC-family (Scmidt-Rose und Jentsch). ClC channels contain two CBS domains (from homology to cystathionine-β-synthatase) within their C-termini, which were proposed to interact with each other within a functional channel. For probing this interaction and its functional significance two ClC channel fragments were generated, one consisting of the channel's N-terminal part including the transmembrane domains, which was truncated after CBS1 and a C-terminal fragment, which contained CBS2 and the rest of the channel's C-terminus. First, upon expression of the N-terminal fragment alone no characteristic ClC channel currents could be observed. However, functional channels were formed, when the N- and C-terminal fragments were coexpressed. These and further control experiments nicely demonstrated the interaction between the two CBS domains. The fact that CBS domains from other ClC channels could functionally be substituted for CBS1 or CBS2 in ClC-1 indicates that the overall conservation of the 3-D structure, despite the poorly

conserved primary sequence. Thus, conservation of the CBS domain's overall structure is sufficient for the interactions that are crucial for ClC channel function.

In order to clarify, whether such a functionally significant interaction also applies for the two TCC domains in KCNQ channels, we also generated KCNQ2 channel fragments, which were split between the two TCC domains. However, in our experiments reconstitution of functional KCNQ2 channels from the fragments termed KCNQ2-TCC1-X and CT-TCC2-KCNQ2 could not be observed. Even when the TCC2-CT-KCNQ2 cRNA was coinjected in large molecular excess no indication for functional channel formation could be found, suggesting that interaction between TCC domains of a KCNQ channel subunit does not occur.

However, unexpected results were obtained during our analysis of the channel fragments. Interestingly, coexpression of the C-terminal TCC2-CT-KCNQ2 fragment with KCNQ3 led to a strong current enhancement. To probe whether the presence of the TCC2 domain within the C-terminal fragment was the reason for this, fragment dCT-KCNQ2 was tested, which lacks TCC2 domain but includes the complete further C-terminus. No current enhancement could be observed in a KCNQ3/dCT-KCNQ2 coexpression scheme indicating that the presence of the TCC2 domain of KCNQ2 even in a soluble C-terminal fragment was sufficient to boost functional expression of KCNQ3, most probably by facilitating an efficient transfer channels to the cell surface, as in case of KCNQ2/KCNQ3 heteromeric channels.

Since the TCC2 domain of KCNQ2 apparently did not have to be linked in sequence after TCC1 to exert its effects on KCNQ3 currents, we also analysed a construct termed KCNQ2(NT-TCC2), which consisted of a KCNQ2 channel truncated after TCC1 with TCC2 fused in-frame to its N-terminus. Upon coexpression with KCNQ3 also an increase of currents was observed, which corroborated the assumption that the effect of the TCC2 domain is independent of its position within the primary sequence. These observations are also in agreement with the notion that the specific requirement for TCC2 from KCNQ2 may be either mask a retention motif or that it helps to expose a plasma membrane targeting motif present on KCNQ3.

D 1.5   Replacement of TCC domains by unrelated coiled-coil domains

Since the coiled-coil domains apparently play an important role in tetramerization of KCNQ channels we wanted to test the specificity by replacing the TCC domains with the unrelated artificial tetramerization domain GCN4-LI, which were shown to drive tetramerization of *Shaker*-type K^+ channels, as reported by (Zerangue et al., 2000). These authors inserted the GCN4-LI sequence instead of the cytoplasmic, N-terminal T1 domain, which is required for channel tetramerization. The GCN4-LI sequence restored formation of functional *Shaker* channels, suggesting that the ability of N-terminal domains to tetramerize in general promotes assembly ot the transmembrane parts of the channels, presumably by increasing the effective local subunit concentration for compatible subunits. In our experiments the substitution of the coiled-coil sequence GCN4-LI instead of the TCC1 and TCC2 domain of KCNQ1 did not produce any functional channels. This suggests that apart form the presumed ability to tetramerize the structural integrity of the TCC1 and TCC2 domain are highly important for KCNQ channel formation and function.

D 1.6   Effects of the TCC2-CT-KCNQ2 fragment on TEA sensitivity of KCNQ3 channels

In order to test the pore properties of the channels formed upon coexpression of KCNQ3 with the CT-TCC2-KCNQ2 the sensitivity for block by TEA was tested. Since KCNQ channels are differentially sensitive to this cation, this analysis might aid in identification of the channel pores formed by this coexpression scheme. Notably, in contrast to the expectation that the soluble fragment should not influence the properties of the pore-forming constituents, the CT-TCC2-KCNQ2 fragment modulated the TEA sensitivity of KCNQ3 in coexpression experiments. It is known from the literature that the high TEA sensitivity of KCNQ2 might result from the presence of a Tyrosine residue in the pore loop of the channel (Hadley et al., 2000). In contrast, KCNQ3 has a Threonine in homologous position, whereas KCNQ1 and KCNQ4 carry a Valin or a Threonine, respectively. Although KCNQ1 and KCNQ4 lack the Tyrosine, which seems to be required for high-affinity TEA block, both channels are even more sensitive to TEA than KCNQ3 indicating that the TEA block depends on additional structural elements. Our results favour this point

of view and suggest that even distant channel regions (the CT-TCC2-KCNQ2 certainly interacts with channels parts exposed to the cytoplasm) are able to modulate properties of the KCNQ3 channel pore. However, the reason for this effect is obscure and opens up interesting perspectives for future investigations. The molecular details for this long-range interaction may finally be clarified once high-resolution structural data of complete KCNQ channels are available.

It has to be noted, that similar findings have already been reported with the T1 domain of *Shaker* K^+ channels. Apart from the well-established role in driving and regulating the tetramerization of the *Shaker* α-subunits (Bixby et al., 1999), mutagenesis studies have shown that the T1 domain is able to alter the gating and conduction properties (Cushman et al., 2000; Minor et al., 2000; Kurata et al., 2002). Therefore, the observed effects are not singular in voltage-gated ion channel research.

Our findings about the KCNQ2/KCNQ3 heteromerisation agree with the well established results on KCNQ1 subunit assembly, as reported by Schmitt et al. (2000). These authors had identified a small domain between residues 589 and 620 in the KCNQ1 C-terminus (corresponding to our TCC2 domain) which may function as an assembly domain for KCNQ1 subunits. Without this domain KCNQ1 C-termini do not assemble and KCNQ1 subunits are not expressed as functional K^+-channels.

D 1.7   Correlation with recently published structural information concerning KCNQ TCC domains

Howard and coworkers were able to crystallize the A-domain tail (the second part of the *si*-domain including TCC2) of KCNQ4 channels and demonstrated that this domain, which is conserved among KCNQ subtypes, acts as a self-assembling four stranded, parallel coiled-coil (see **Figure D.4**).
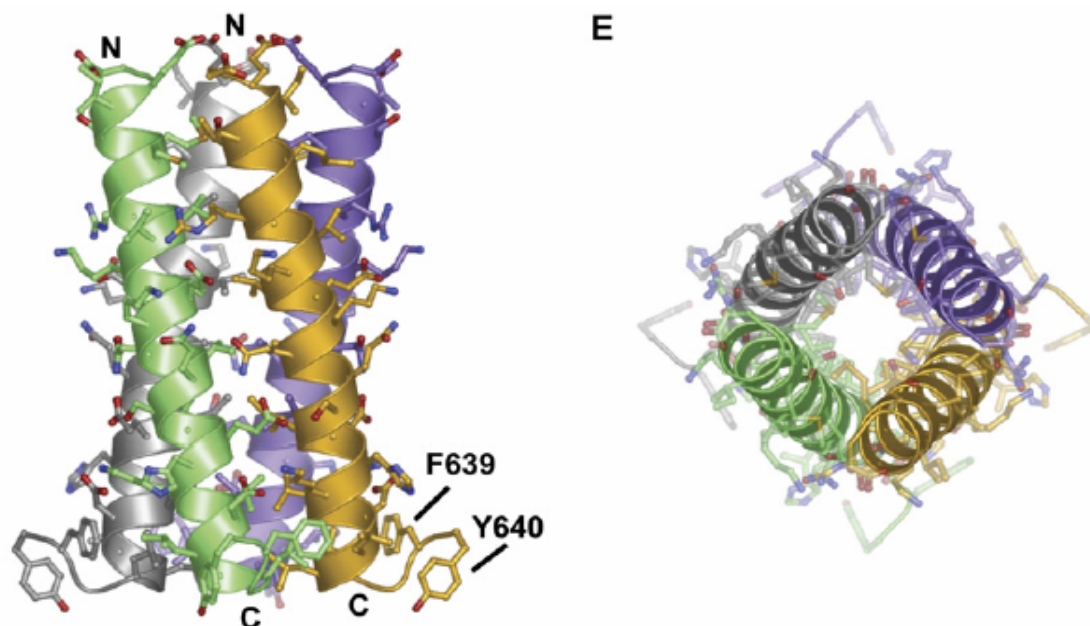
Figure D.4: A) Ribbon diagram of the Kv7.4 (KCNQ4) A-domain tail coiled-coil with side chains shown in ball-and-stick representation. Chains from individual subunits are coloured green, orange, purple, and grey. The N- and C-terminal ends of the green and orange subunits and the positions of F639 and Y640 of the orange subunit are also indicated. **B)** Ribbon diagram of the tetramer looking down the helical axis from the N terminus. Subunits are coloured as in (A). (From Howard et al., 2007)

From the crystal structure the helix interfaces involved in contact formation are clearly revealed. A critical core region and two types of networks are involved in mediating inter-helical contacts (Fig. 5). From this information the role of individual amino acids in favoring or destabilizing tetramer formation can be derived. Thus, the reason for the singular behavior of KCNQ1 (which does not co-assemble with any of the other subtypes) becomes apparent, since this channel has amino acid changes both at several core positions (M615I, V619L, I629L, and L636I) and in network 1 (K624D) as well as in network 2 (E360D and K632A) when compared to KCNQ4 (**Figure D.5A**). The networks are side chain salt bridges and hydrogen bonds that make interhelical contacts across helix interfaces (**Figure D.5B**). The K624 exchange for an Asp in network 1 of KCNQ1 alters the network surrounding E623. The KCNQ1 network 2 would be completely rearranged, since one of the central players in the ionic and hydrogen bond network, E630 (replaced by an Asp), is shortened by a methylene group, and the other (K632) is eliminated (replacement by Ala). It is striking that the remaining positions of the KCNQ1 network 2 are changed in a way that could still form a hydrogen bond and ionic network of side chain interactions around E630 (KCNQ1 carries an Asp in this position). These observations
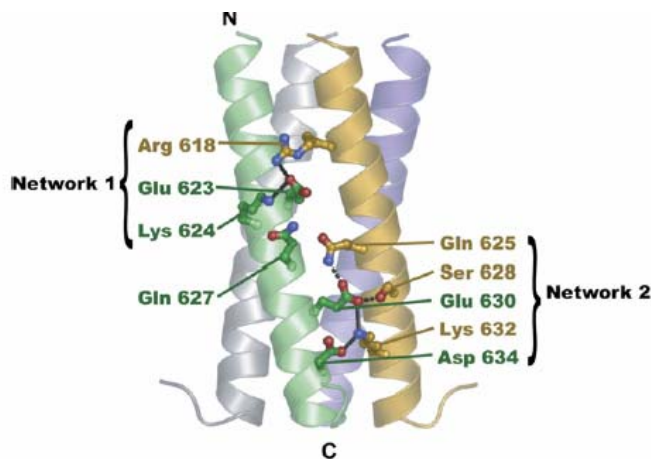
suggest the hypothesis that the differences in network 2 play a role in preventing the KCNQ1 A-domain tail from associating with other KCNQ subtypes.

A

B

Figure D.5: **A)** Comparative interaction mapping in all KCNQ subtypes. Column labels identify residue types involved in hydrophobic "a" (blue) and "d" (pink) layer contacts and electrostatic interactions (green) observed in the Kv7.4 (KCNQ4) coiled-coil structure. Filled boxes in the table indicate entirely conserved interactions; shaded boxes indicate non conserved residues that are still capable of interacting as predicted; white boxes indicate unfavourable contacts. Electrostatic interactions involved in networks 1 and 2 are indicated below the alignment. **B)** Intra- and intermolecular electrostatic interactions. Ribbon diagram of tetramer with helices coloured as in Figure 1D shows network 1 and network 2 interactions between the side chains (shown as sticks) of the green and orange subunits. Salt bridges (black lines) and hydrogen bonds (dotted lines) are indicated. Side chain labels are colour-coded to indicate the subunit of origin. (From Howard et al., 2007)

From these structural data also a reason can be derived for the usually poor plasma membrane expression of KCNQ3, which is dramatically boosted upon co-assembly with KCNQ2 and KCNQ5. Howard and coworkers showed that the KCNQ3 A-domain tails are

divergent at a number of critical positions (**Figure D.5A**). There are changes at two coiled-coil core positions compared to KCNQ4: V619 is replaced by a Phe in an "*a*" position, and I629 is replaced by a Met in a "*d*" position. The changes in the interhelical interface networks include a reversal in the relative positions of the basic residues that surround E623 in network 1, R618 (which is a Lys in KCNQ3) and K624 (an Arg in KCNQ3), and a relocation of the carboxylate of one of the central side chains in network 2, E630 (a Gly in KCNQ3), to a position at a similar altitude on the adjacent subunit by the S628 change for an Asp (**Figure D.5B**).

These alterations in the core and the interface networks appear to be critical for the unique assembly properties of the KCNQ3 A-domain tail. The KCNQ3 A-domain is prevented from making stable tetramers by both the incompatability of placing four phenylalanines within the core of the tetramer at the "*a*" position of the coiled-coil and by the disruption of the interhelical hydrogen bond and salt bridge interactions made by network 2. Although the combination of both factors is important for impairing homotetramerization, neither factor alone is incompatible with homotetramer formation. Thus, it appears that the KCNQ3 A-domain tail is poised to form tetramers provided that the destabilizing factors can be overcome.

These findings may have interesting implications for therapy. It is possible that drugs that disrupt the coiled-coil interaction may influence the number KCNQ channels expressed in the surface. Possibly the coiled-coil domains also serve functions other than surface trafficking and support interactions with additional proteins. Such proteins are calmodulin, and the A-kinase anchorin protein (AKAP) Yotiao (**see Figure D.6**). Yotiao binds to a Leucin zipper (LZ) motif in the KCNQ1 C-terminus and in turn then recruits PKA and protein phosphatase 1 to form a regulatory complex with the channel, thus controlling the phosphorylation state of the channel (Marx et al., 2001). Calmodulin (CaM) also interacts with the intracellular C-terminal region of several members of the KCNQ family and acts as a mediator in the Ca^{2+}-dependent modulation of KCNQ channels, but may also be important in other processes such as assembly or trafficking (Yus-Najera et al., 2002).
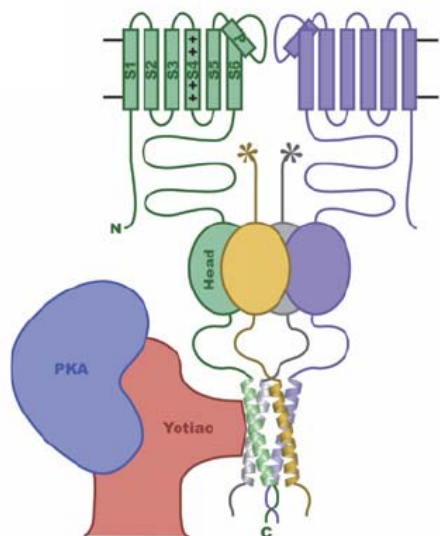
Figure D.6: Cartoon of a Kv7 channel regulatory complex. Two complete Kv7 pore-forming subunits are shown (green and purple). S1-S6 transmembrane segments and the pore helix (P) are indicated for the green subunit. ''+''s indicate the S4 voltage sensor segment. All four subunits of the Kv7 A-domain are shown. The Head domain is shown as an oval. The Tail domain helices are shown. The Linker domain connects the Head and Tail. An interaction between a portion of the scaffolding protein Yotiao (red) and the channel is shown bringing protein kinase A ''PKA'' (blue) near the channel. The stoichiometry of the Yotiao/channel complex is not known. (From Howard et al., 2007)

Recently, Schwake and coworkers (Wehling et al., 2007) succeeded to express the isolated complete *si* domain of KCNQ2 in *E. coli* cells and carried out size exclusion chromatography experiments to determine the oligomeric state and analysed secondary structure by CD spectroscopy of the fragments in solution. These experiments showed, that the isolated *si* domain of KCNQ2 autonomously folds to a regular structure with high α-helical content (~30 %), in line with the predicted formation of coiled-coils. The formation of higher oligomeric complexes including tetrameric arrangements could also be demonstrated. Insertion of a helix-breaking proline into TCC1 of the *si* domain fragment drastically reduced the α-helical content (~16 %), although no effect on the oligomerization properties was observed. This implies that an intact α-helical structure of TCC1 might not be a prerequisite for tetramerization. In addition, a Leu-to-Pro mutation in TCC2 changed secondary structure to random-coil characteristics (~10 % α-helical content), however, only dimeric complexes could be observed. The formation of dimers also occured in a double mutant which carried Leu-to-Pro substitutions in both TCC domains, although this polypeptide also showed random-coil characteristics. Thus, at least homodimer formation does not seem to depend on an ordered α-helical structure of the *si*

domain. However, intact coiled-coil structural elements of at least some of the subunits apparently are required for efficient heteromeric interactions. It will be interesting to see in future experiments, how the specificity of interaction and the oligomerization pattern is affected in case of mixtures of isolated *si* domains from different KCNQ channels.

D 2.1   Cysteine-scanning mutagenesis and structure-function studies of the KCNQ1 channel

Whereas e.g. *Shaker* K^+ channels have been heavily studied for decades by a large variety of techniques including exhaustive mutageneses, detailed systematic investigations regarding structure-function relationships of KCNQ potassium channels are still sparse. Owing to the great physiological importance of KCNQ channels for human physiology a deeper understanding of the structural determinants for these channel's unique functional and regulatory properties is highly desirable. KCNQ channels differ from *Shaker* in many respects, including their disparate activation/inactivation behaviour, voltage dependence, and determinants of assembly or regulation.

Our motivation for carrying out a cysteine scanning mutagenesis within the S3-S4 loop and the S4 segment of KCNQ1 was three-fold: (1) We wanted to obtain data concerning solvent accessibility of individual amino acids to elucidate environmental parameters for the S4 voltage sensor, (2) the functional importance of individual amino acids and the influence of the introduction of bulky side chains on the distribution of channel states should be addressed, and (3) the validity of structural homology models should be challenged by testing model predictions concerning the proximity of individual amino acids, which belong to different transmembrane segments.

It has to be noted that despite the availability of high-resolution Kv channel structures, the precise orientation of the S1-S4 voltage sensor with respect to the channel pore or the membrane plane is still under discussion, and open questions still remain. Thus, biochemical and electrophysiological experiments are still helpful in validating or disproving molecular models. After all, a correct molecular description of the voltage-sensing and gating mechanisms may emerge from a combination of all these structural and functional data.

In order to address these issues, single cystein mutants of KCNQ1 were generated and probed for functional properties. Then, the effects of side chain modifications using the thiol-reactive compound MTSES were monitored, and, after an iterative loop into structural modeling, cross-linking of suitable candidate cysteines in S4 with additionally introduced cysteines in other TM segments was attempted, as suggested from these model predictions.

From the 20 cysteine mutants, which were initially constructed within the S3-S4 loop and the extracellular portion of the S4 voltage sensor, all besides mutant L233C could be functionally expressed in oocytes, mediating characteristic Kv channel-like currents. As expected from the critical role of this stretch of amino acids on channel activation many mutants exhibited a significantly shifted $V_{0.5}$ values for half-maximal activation compared to KCNQ1 wild-type. Interestingly, mutants with hyperpolarizing $V_{0.5}$ shifts clustered between G219C and F222C (but also included Q234C and G216), whereas those with positive $V_{0.5}$ shifts were (besides S217C) located more C-terminally: S217C, A223C, T224C, S225C, A226C, G229, I230C, F232C and I235C. A negative shift in $V_{0.5}$ can be considered as stabilisation of the open state/destabilization of the closed state of the mutant channel, since smaller depolarizations are needed to activate the channel. The reverse argument applies for positive $V_{0.5}$ shifts. Therefore, mutations in the N-terminal portion of the S4 segment (which are also solvent accessible from extracellular, as judged from subsequent MTSES studies) tend to destabilize the closed state, whereas cysteine replacements further downstream the S4 segment (which are also solvent accessible under the chosen conditions) preferably lead to a closed-state stabilization.

Of particular importance for the activation process are the positively charged arginines in position 228 and 231. Therefore, mutations which remove the gating charge are expected to change channel characteristics dramatically. Indeed, mutant R228C exhibited a very slow activation and deactivation, and currents resembled those, which can be measured for a coexpression of KCNQ1 with KCNE1. In contrast, mutant R231C behaved like an open channel, mediating a large, virtually voltage-independent K^+-selective conductance upon expression in oocytes and only a weak residual gating could be observed at strongly hyperpolarizing potentials. Such behaviour indicates that the voltage sensor of this mutant channel is locked in a position which stabilizes the open state. Since the Cys side chain is

much shorter than that of an arginine it is likely that the destabilisation of the closed state is due to disfavorable electrostatic interactions.

Larson (Larsson et al., 1996; Vemana et al., 2004) used a similar strategy to study accessibility of S4 residues in *Shaker* K^+ channels, applying the MTSET reagent as a probe, which is a small positively charged reagent, which on reaction with a cysteine converts it to an arginin-like moiety. Reaction of an exposed cysteine with MTSET resulted in a shift of the *I/V* curve of some of the mutants studied. The nature and extend of the shift were dependent on the residue that was changed to cysteine. He also attempted to test the accessibility of arginines of the mammalian HCN channels. The cysteine accessibility results suggest that the four most NH_2-terminal S4 charges in HCN1 (K238, R241, R244 and R247) are not part of the voltage sensor.

Stuhmer (Stuhmer et al., 1989) also observed that neutralization of the positively charged residues in the S4 segment was found to reduce the steepness of voltage dependent gating, as expected for a reduction in gating charge, and to shift the voltage dependence of channel activation.

A behaviour resembling an at least partially open phenotype was also displayed by mutants V221C and Q234C. These channels had a comparatively large background conductance, but still showed some additional KCNQ1-like activation behaviour, with hyperpolarizing $V_{0.5}$ shifts in both cases, again indicating destabilisation of the closed/stabilization of the open state.

From the 19 cysteine mutants, which could be functionally expressed, seven showed clear functional alterations upon treatment with the MTSES reagent (from A223C to I227C and I230C), weaker effects were observed for G219C, R231C, and Q234C. These results demonstrate, that these residues are solvent-accessible from the extracellular side of the membrane. From the lack of functional effects for the mutants in S3-S4 loop positions it can not be concluded that these residues are not exposed to the extracellular space, since attachment of the MTS side chain might not lead to functional alterations. It is interesting to note, that the mutants, which could be modified by MTSES in general showed an

activation behaviour comparable to KCNQ1 wild-type before treatment, but consistently resembled constitutively open channels after MTSES modification. It is not likely that the apparently "ohmic" currents after MTSES modification represent MTSES-induced unspecific leakage of the oocytes, because the oocyte reversal potentials were generally very hyperpolarized (< -60 mV) compared to uninjected control oocytes, which is an indication for a K^+-selective conductance in the membrane of the oocytes. For some mutants (T224C and S225C) residual activation behaviour could be observed upon depolarizing voltage pulses, whereas currents measured for mutants A223C, A226C and I230C showed, that these MTSES-modified channels could be driven into deactivation at strongly hyperpolarizing potentials. The observed changes in current characteristics were correlated with a hyperpolarizing shift of the activation curves indicating that the attachment of the bulky side chain prevents the voltage-sensing S4 segment from returning to a conformational position which promotes channel closure. If channel closure could be observed, this would occur only at very negative membrane potentials. Another possibility to explain the observed effects is that MTSES modification could disrupt the coupling between the movement of the voltage sensor and the opening and closing of the activation gate.

It has to be noted, that we can not draw conclusions about state-dependence of residue accessibility, which was beyond the scope of this work. Since MTSES incubation was carried out for several minutes at -70 mV holding potential, whereas much larger hyperpolarizing potentials would have been required to keep the mutant channels in the completely deactivated state during MTSES incubation, it was assumed that we achieved steady-state labelling, regardless of the channel state. However, our data could serve as a good starting point to study the state dependence of residue modification and accessibility, which eventually could yield information about the possible extent of S4 movements during the activation process.

After having established which residues within the S3-S4 loop and the N-terminal half of the S4 segment were solvent-accessible due to their functional sensitivity for MTSES modification, structural homology modelling of KCNQ1 was carried out, based on the Kv1.2 high-resolution crystal structure. Since sequence identity between KCNQ1 and Kv1.2 (despite structural homology) is rather poor, the validity of such models can be

checked by testing model predictions e. g. based upon amino acid proximity. From these modeling studies, four amino acid pairs could be proposed, which could be in close proximity in the closed state of the channel (since the Kv1.2 structure presumably resembles this state). These were T224(C) - F279(C) (S4 - S5), R228(C) / L282(C) (S4 - S5), I230(C) / M159(C) (S4 - S2), and F232(C) which could be proximal to the endogenous C136 within the S1 segment, although at a somewhat larger distance. Therefore, additional cysteine mutations were introduced to generate double cysteine constructs in the respective positions. Cysteine cross-linking reagents are frequently used to probe for proximity of protein subdomains or assembly of subunits within protein complexes.

Cadmium ions are particularly sensitive in this respect, since due to their small size cross-bridging of cysteine pairs can be tested on a very short distance scale. However, (membrane) proteins may carry endogenous cysteines, which could blur observations, and unspecific effects have to be avoided, which might occur at high concentrations of Cd^{2+} ions. Therefore, KCNQ1 wild-type and all single cysteine mutants to be included in this part of the study were tested for Cd^{2+} effects. A concentration of 100 μM was found optimal, since no functional alterations could be observed under these conditions. This value is rather low compared to concentrations used in the literature indicating that functional effects can be considered as highly specific if they could be observed at these low concentrations.

The propensity of the two cysteines to readily form a Cd^{2+} crossbridge suggests that the distance between the β-carbons in the disulfide-bonded cysteines may be close to 4.6 Å (Aziz et al., 2002). However, distance estimates tend to be less accurate because a number of factors can influence the rate of disulfide crossbridge formation. For example, motions in a protein can bring cysteines as far apart as 15 Å close enough to result in a disulfide bridge (Careaga and Falke, 1992).

All three cysteine double mutants yielded functional channels. Upon addition of 100 μM Cd^{2+} two constructs, M159C/I230C and T224C/F279C, exhibited clear functional alterations. Notably, in both cases a reduction of steady-state current amplitudes was observed, which was paralleled by a significant decrease in the saturation values of the normalized I/I_{max} curves. Both observations imply, that the respective cysteine pairs could

be cross-bridged by heavy metal ions and that this induces structural constraints, which disfavour channel activation/opening. This is in accordance with the fact, that residue proximity was proposed based on a closed channel conformation. Thus, the respective residues are proximal to each other and can be cross-linked only in the closed state, but they presumably have to move away from each other during the voltage sensing/activation process of the channel, which is sterically prevented after Cd^{2+} treatment. Thus, these data corroborate the validity of the derived KCNQ1 structure model regarding amino acid positions in various transmembrane segments. In addition, these data can be the starting point for future studies on residue proximity in the open state by carrying out state-dependent Cd^{2+} cross-linking in order to reveal information about the arrangement of the voltage sensor upon channel activation. Since the precise arrangement of the voltage-sensing S1-S4 block either in the closed or in the open state is still not entirely clear, such data could be valuable for researchers involved in K^+ channel structural biology.

It is still not known how and to what extent S4 moves .Many different labarotories tried in the past to investigate the above question.Gating-dependent reactivity of sulfhydryl reagents with cysteine residues led to an initial hypothesis of large (~15 Å)) translations of S4 in some models (Larsson et al., 1996; Yusaf et al., 1996) On the other hand very small distance changes measured in fluorescence resonance energy transfer(FRET)experiments suggested much smaller movements of S4 across the membrane (Cha et al., 1999). Crevices surrounding S4 were invoked to account for the sulfhydryl reactivity in the setting of these smaller movements, with translations and/or rotations of S4 occurring across a narrow neck inside a hourglassshaped canaliculus.

The data in this thesis concerning the helix proximity between the S4 and S5 segment are in line with those of Neale (Neale et al., 2003), who demonstrated that residues situated just outside the membrane border of S4 (357) and S5 (418) of the *Shaker* channel lie in close proximity. They indicate that the N-terminal end of S4 lies close to the C-terminal end of S5 of the neighbouring subunit, suggesting that S4 might lie at a steep angle to the pore domain.

The model in Figure D7 demonstrates the proximity between the voltage sensor S4 and the other transmemrane segments.
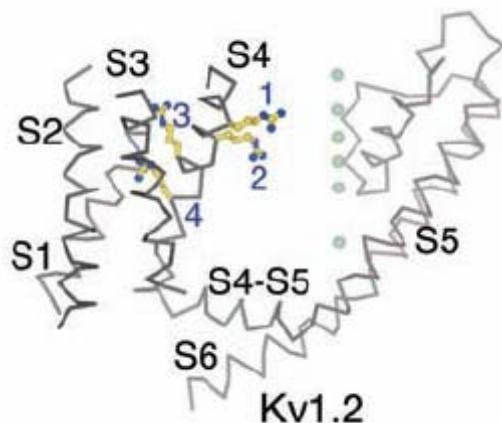
Figure D.7: A single subunit of the integral membrane pore and partial model of the voltage sensor of Kv1.2 viewed from the side as a gray Ca trace. Arg residues 1 to 4 on the S4 helix (blue labels) are depicted as yellow and blue sticks. The side chain for Arg 4, although not included in the final coordinates, is modeled in a chemically reasonable conformation for the purpose of illustration. (From Long et al., 2005)

The crystals of the Kv1.2 K$^+$ channel provide information of of Kv channels with its voltage sensors. First the voltage sensors are self-contained domains, quite independent of the pore except for their specific localized attachments through the S4-S5 linker that enable them to perform mechanical work on the pore. Second the Kv1.2 structure shows that motion of the S4 helices are transmitted to the inner helix bundle (activation gate) via the S4-S5 linker helices. Third in the open conformations Arg residues 1 and 2 are on the lipid-exposed surface of the voltage sensor and Arg residues 3 and 4 are in a position to interact with acidic amino acids between the voltage sensor paddle (S3and S4) and the voltage sensor helices S1 and S2 (Long et al., 2005).

Another interesting aspect could be to test the effects of the "channel opener" retigabine on the conformation of e.g. the KCNQ3 voltage sensor. Since critical amino acids involved in retigabine binding are located in the pore domain of the channel (mostly S5 and the pore loop), it could be interesting to test whether cysteine crosslinking of S4 residues, which is possible in the closed state, would also occur in a channel activated by retigabine. From such data one could conclude whether retigabine would only act on the conformation of the channel pore (without an effect on the conformation of the S1-S4 block) or whether binding of the compound would also involve movement of the voltage sensor into an

"activated" position. It will also be interesting in future investigations to look for either MTSES or Cd^{2+} effects in KCNQ1/KCNE1 or KCNQ1/KCNE3 heteromeric channels, since the incorporation of the KCNE protein transmembrane domain into the channel complex might have severe consequences regarding the arrangement of the KCNQ transmembrane helices.

ZUSAMMENFASSUNG

Die Fähigkeit von KCNQ-(K_v7)-Kanälen Hetero-Oligomere aus verschiedenen KCNQ-Untereinheiten zu bilden, ist von hoher physiologischer Bedeutung, da Heteromere von KCNQ3 mit KCNQ2 oder KCNQ5 dem neuronalen M-Strom zugrunde liegen, welcher die neuronale Erregbarkeit moduliert.

Die fünf Mitglieder dieser Familie (KCNQ1-KCNQ5) sind homolog zu *Shaker* Kanälen jedoch unterscheiden sie sich in ihrer Struktur dadurch, daß die KCNQ-Kanäle längere Carboxytermini haben, die intrazellulär lokalisiert sind. Außerdem führen Mutationen bei vier von den fünf Mitgliedern dieser Familie (KCNQ1-KCNQ4) zu genetischen Störungen.

KCNQ1-Mutationen verursachen das Romano-Ward-Syndrom (RWS), eine Sonderform (Typ1) des Long-QT-Syndroms (LQT). Dieser Name leitet sich von der charakteristischen Verlängerung des QT–Intervalls im Elektrokardiogramm ab. Dabei handelt sich um eine dominant vererbliche Repolarisations-Störung des Herzmuskels. Diese kann Ursache für Herzrhythmusstörungen sein, die häufig zu plötzlichen Herztod führen.

Bestimmte rezessive KCNQ1- und KCNE1-Mutationen sind zudem für das Jervell-und-Lange-Nielsen-Syndrom verantwortlich. Bei dieser Mutation leiden die Patienten zusätzlich zu kardialen Abnormalitäten auch noch unter progressiver Taubheit.

KCNQ2- und KCNQ3-Mutationen verursachen die dominant vererbliche Form der Neugeborenenepilepsie „benign famillial neonatal convulsions" (BFNC). Die molekulargenetische Ursache dieser Erkrankung ist ein KCNQ2/KCNQ3-Heteromer. Diese K^+-Kanal-Untereinheiten werden hauptsächlich im Gehirn exprimiert und repräsentieren das molekulare Korrelat des sogenannten M-Stroms, welcher über muskarinerge Stimulation (M1-Rezeptoren) reguliert wird.

KCNQ4-Mutationen können eine dominant vererbliche Taubheitsform, DFNA2 genannt, verursachen.

Der KCNQ5-Kanal weist ein breites Expressionsmuster auf, für den aber noch keine Beteiligung an menschlichen Erbkrankheiten nachgewiesen werden konnte.

Innerhalb dieser Familie unterscheiden sich KCNQ1 und KCNQ3 am meisten hinsichtlich ihrer Eigenschaft, Heteromere mit anderen KCNQ-Untereinheiten zu bilden.

Im C-Terminus von KCNQ-Kanälen wurde vor kurzem eine ca. 100 Aminosäuren umfassende Domäne identifiziert, welche die Spezifität des Untereinheiten-Zusammenbaus bestimmt. Innerhalb dieser sog. *si*-Domäne gibt es zwei Abschnitte, die jeweils aus ~30 Aminosäuren bestehen und eine hohe Wahrscheinlichkeit zur Ausbildung einer coiled-coil-Struktur aufweisen.

Durch Übertragung der ersten oder der zweiten coiled-coil- bzw. TCC-Domäne von KCNQ3 auf KCNQ1 wurden KCNQ1(TCC1)Q3- und KCNQ1(TCC2)Q3-Chimären generiert, die sich beide mit KCNQ2 koimmupräzipitieren ließen. Allerdings konnte nur mit KCNQ1(TCC2)Q3 eine Erhöhung der Ströme und der Oberflächenexpression in Koexpression mit KCNQ2 beobachtet werden, wie sie für die KCNQ2/KCNQ3-Interaktion charakteristisch ist. Die Deletion von TCC2 innerhalb von KCNQ2 resultierte zwar in funktionalen homomeren Kanälen, es entfiel jedoch die Zunahme des Stromes nach der Koexpression des Deletionskonstrukts mit KCNQ3.

Im Gegensatz dazu konnten nach Deletion von TCC1 innerhalb von KCNQ2 keine funktionalen homomeren KCNQ2- bzw. heteromere KCNQ2/KCNQ3-Kanäle beobachtet werden. Auch hoben Mutationen, die die vorhergesagte coiled-coil-Struktur von TCC1 in KCNQ2 oder KCNQ3 unterbrachen, die funktionelle Expression dieser Konstrukte einzeln oder in Kombination mit der jeweils intakten anderen Untereinheit auf. Demgegenüber waren homomere KCNQ2-Kanäle mit helix-brechenden Mutationen in TCC2 zwar funktionell, es unterblieb jedoch die Heteromerisation mit KCNQ3. Im Gegensatz dazu hetero-oligomerisierte ein KCNQ3-Konstrukt mit einer coiled-coil-brechende Mutation in TCC2 weiterhin mit KCNQ2.

Die Daten in dieser Arbeit unterstreichen, dass die TCC1-Domänen von KCNQ2 und KCNQ3 notwendig sind, funktionale homomere als auch heteromere Kanäle zu bilden, während beide TCC2-Domänen für einen effizienten Transport heteromerer KCNQ2/KCNQ3-Kanälen zur Plasmamembran verantwortlich sind.

Die funktionellen Eingenschaften von KCNQ-Kanälen unterscheiden sich in vielerlei Hinsicht deutlich von z. B. denen von *Shaker* K$^+$-Kanälen aus *Drosophila* , welche als am besten untersuchte K$_v$-Kanäle betrachtet werden können. Um einen systematischen Beitrag zu Struktur-Funktions-Beziehungen an KCNQ-Kanälen zu erbringen, wurde im zweiten Teils dieser Arbeit der Versuch unternommen, den Einfluss verschiedener Aminosäuren-Seitenketten durch eine Cystein-Scanning-Mutagenese im Bereich des S4-Segments und der vorangehenden S3-S4-Schleife von KCNQ1 zu analysieren. Um die extrazelluläre Zugänglichkeit der eingeführten Cysteine zu detektieren, wurde nach Effekten extrazellulärer Applikation der thiol-spezifisch reagierenden Substanz MTSES auf die funktionellen Eigenschaften der Kanäle gesucht.

Alle 20 untersuchten Cystein-Mutanten konnten in *Xenopous* Oozyten funktionsgemäß exprimiert werden, mit Ausnahme der Mutanten L233C. Die exprimierten Mutanten erzeugten charakteristische Kv-Kanal-ähnliche Ströme. Wie zu erwarten war, führten die untersuchten Mutanten zu signifikanten Verschiebungen des $V_{0.5}$-Wertes, verglichen mit denen des KCNQ1 Wildtyps.

Interessant zu beobachten war, daß Mutanten, die eine Verschiebung des $V_{0.5}$-Wertes in Richtung negativen Potentials zeigten, sich zwischen G219C und F222C (miteinbezogen auch Positionen G216C und Q234C) befanden. Mutanten die eine positive Verschiebung aufwiesen, waren mehr C-terminal lokalisiert: A223C, T224C, S225C, A226C, G229C, I230C, F232C und I235C. Eine Ausnahme hierzu bildet die Mutante S217C.
Eine negative Verschiebung des $V_{0.5}$-Wertes kann als Stabilisierung des offenen Kanalzustandes beziehungsweise als Destabilisierung des geschlossenen Kanalzustands betrachtet werden, da kleinere Depolarisationen schon ausreichen, um den mutierten Kanal zu aktivieren. Das genaue Gegenteil der obig beschriebenen Situation gilt bei positiven Verschiebungen des $V_{0.5}$-Wertes, d.h. Stabilisierung des geschlossenen bzw. Destabilisierung des offenen Kanalzustands. Deswegen tendieren Mutationen im N-terminalen Bereich des S4 Segments dazu, den geschlossenen Zustand des Kanals zu destabilisieren. Wohingegen Cystein-Substitutionen weiter abwärts des S4 Segments gelegen vorzugsweise zur Stabilisierung den geschlossenen Kanalzustands führen.

Von den 20 untersuchten Mutanten wiesen die Konstrukte A223C bis I227C, I230C, G219C sowie Q234C z.T. drastische Veränderungen nach Inkubation mit MTSES auf, wodurch die extrazelluläre Zugänglichkeit der betreffenden Positionen eindeutig belegt wird.

Von den untersuchten Konstrukten, wiesen die Mutanten T224C und S225C in ihrem Verhalten bei depolarisierenden Spannungssprüngen nach MTSES-Inkubation eine Restaktivierung auf. Dagegen zeigten die Ströme, die bei den Mutanten A223C, A226C und I230C aufgenommen wurden, daß diese mit MTSES modifizierten Kanäle bei stark hyperpolarisierenden Potentialen zu einem Deaktivierungszustand getrieben werden können.

Die beobachteten Veränderungen in der Stromcharakteristik konnten mit der hyperpolarisierenden Verschiebung des $V_{0.5}$-Wertes korreliert werden. Dies bedeutet, daß die kovalente Anknüpfung der MTSES-Seitengruppe, das spannungssensitive S4 Segment verhindert, wieder zurück zu einer Kanal-Konformation zu gelangen, welche die Schließung des Kanals ermöglicht.

In den meisten Fällen führte die kovalente Anknüpfung der MTS-Seitengruppe zu einem Erscheinungsbild, wie es für konstitutiv offene Kanäle charakteristisch ist. Auch im Falle der Cystein-Insertion an der Spannungssensor-Position R228 waren charakteristische Veränderungen nach MTSES-Zugabe zu beobachten. Die R231C-Mutante (ebenfalls eine der Schaltladungen betreffend), zeigte bereits vor der MTSES-Applikation einen Offenkanal-Phänotyp, infolge MTSES-Zugabe trat keine weitere Veränderung auf.

Basierend auf der Kristallstruktur des spannungsgesteuerten $K_v1.2$-Kanals wurde ein Strukturmodell von KCNQ1 konstruiert, welches dazu diente, potentielle Aminosäure-Positionen innerhalb anderer Transmembrandomänen von KCNQ1 vorzuschlagen, die in unmittelbarer Umgebung der MTSES-zugänglichen S4-Positionen liegen könnten. Dementsprechend wurden Doppelmutanten mit je einem Cystein auf dem S4-Segment und einem auf einer anderen Helix untersucht.

Zuvor wurde der KCNQ1-Wildtyp und die einzelnen Cystein-Mutanten auf Cd^{2+} Sensitivität getestet. Eine Konzentration von 100µM wurde als optimal bestimmt, da keine funktionellen Veränderungen der Kanäle bei dieser Konzentration beobachtet werden konnten.

Von den vier vorgeschlagenen Cystein-Paaren konnte für die Kombinationen I230C/M159C und T224C/F279C mittels Cd^{2+}-Quervernetzungsversuchen eine enge Nachbarschaft zwischen den entsprechenden Aminosäure-Positionen gezeigt werden.

In beiden Fällen konnte eine Reduktion der steady-state Stromamplituden beobachtet werden, die parallel einherging mit einer entsprechend signifikanten Erniedrigung der Sättigungskurve I/Imax.

Beide Beobachtungen sind ein Indiz dafür, daß die obig genannten Doppelcystein-Mutanten sich mit Cd^{2+} quervernetzen. Diese Quervernetzung führt zu strukturellen Einschränkungen, welche das Öffnen des Kanals verhindern.

Die beobachteten funktionellen Konsequenzen der Cd^{2+}-Quervernetzung lassen sich im Sinne einer Stabilisation des Geschlossen-Zustands des Kanals interpretieren. Diese Befunde belegen die Gültigkeit des erstellten Struktur-Modells, welches auf der Kristallstruktur eines geschlossenen Kv-Kanals beruhte.

LIST OF ABBREVIATIONS

AKAP	A-kinase anchorin protein
BFNC	benign familial neonatal convulsions
CaM	Calmodulin
CBS	cystathionine-b-synthase
CFTR	Cystic fibrosis transmembrane conductance regulator
CHO	Chinese hamster ovary
CLC	chloride channels
CNG	cyclic nucleotide-gated
COS	Cercopithecus aethiops
cRNA	coding RNA sequence
DIDS	4,4′-diisothiocyanatostilbene-2,2′-disulfonic acid
DNA	desoxyribonucleic acid
Eag	ether-á-gogo
ECG	Electro-cardiogramm
EGTA	ethylene glycol-bis(β-aminoethyl ether)
ELISA	enzyme-linked immunosorbent assay
Elk	Electro-cardiogramm
ER	endoplasmic reticulum
GABA	γ-Aminobuttersäure
HA	Hemagglutinin
HEK	human embryonic kidney
HEPES	N-(2-hydroxyethyl) piperazine-N´-(2-ethanesulphonic acid)
HERG	human ether-á-gogo-related gene
HRP	horse radish peroxidase
IC_{50}	drug concentration giving 50% block of current
JLNS	Jervell-and-Lange-Nielsen syndrome
KIR	inward rectifier K^+-channels
MthK	Methanobacterium thermoautrophicum
MTS	methane thiosulphonate
MTSEA	2-aminoethylmethane thiosulphonate
MTSES	2-sufonatoethylmethane thiosulphonate
MTSET	2-trimethylammoniumethylmethane thiosulphonate
nAChR	nicotinic acetylcholine receptors
OHC	Outer hair cells
PAGE	polyacrylamide gel electrophoresis
PCMBS	Parachloromercuribenzenesulphonate
PKA	cyclic AMP-dependent protein kinase
PTC	Peptidyl transferase center
RGB	retigabine
RNA	ribonucleic acid
SCAM	substituted-cystein accessibility method
SCG	superior cervical ganglion
SDS	sodium dodecyl sulphate

si-domain	subunit interaction domain
SUR	sulfonyl urea receptors
TCC	tetramerized coiled-coil
TEA	tetraethylammonium
TEVC	two-electrode voltage clamp
TMD	transmembrane domain

Symbols of amino acids

A	Ala	Alanine
C	Cys	Cysteine
D	Asp	Asparagic acid
E	Glu	Glutamic acid
F	Phe	Phenylalanine
G	Gly	Glycine
H	His	Histidine
I	Ile	Isoleucine
K	Lys	Lysine
L	Leu	Leucine
M	Met	Methionine
N	Asn	Asparagine
P	Pro	Proline
Q	Gln	Glutamine
R	Arg	Arginine
S	Ser	Serine
T	Thr	Threonine
V	Val	Valine
Y	Tyr	Tyrosine

BIBLIOGRAPHY

Abbott, G.W., F. Sesti, I. Splawski, M.E. Buck, M.H. Lehmann, K.W. Timothy, M.T. Keating, and S.A. Goldstein. 1999. MiRP1 forms IKr potassium channels with HERG and is associated with cardiac arrhythmia. *Cell*. 97:175-187.

Abitbol, I., A. Peretz, C. Lerche, A.E. Busch, and B. Attali. 1999. Stilbenes and fenamates rescue the loss of I(KS) channel function induced by an LQT5 mutation and other IsK mutants. *Embo J*. 18:4137-4148.

Ackerman, M.J., D.J. Tester, C.J. Porter, and W.D. Edwards. 1999. Molecular diagnosis of the inherited long-QT syndrome in a woman who died after near-drowning. *N Engl J Med*. 341:1121-1125.

Aziz, Q.H., C.J. Partridge, T.S. Munsey, and A. Sivaprasadarao. 2002. Depolarization induces intersubunit cross-linking in a S4 cysteine mutant of the Shaker potassium channel. *J Biol Chem*. 277:42719-42725.

Barhanin, J., F. Lesage, E. Guillemare, M. Fink, M. Lazdunski, and G. Romey. 1996. K(V)LQT1 and lsK (minK) proteins associate to form the I(Ks) cardiac potassium current. *Nature*. 384:78-80.

Biervert, C., B.C. Schroeder, C. Kubisch, S.F. Berkovic, P. Propping, T.J. Jentsch, and O.K. Steinlein. 1998. A potassium channel mutation in neonatal human epilepsy. *Science*. 279:403-406.

Bixby, K.A., M.H. Nanao, N.V. Shen, A. Kreusch, H. Bellamy, P.J. Pfaffinger, and S. Choe. 1999. Zn2+-binding and molecular determinants of tetramerization in voltage-gated K+ channels. *Nat Struct Biol*. 6:38-43.

Brown, D.A., and P.R. Adams. 1980. Muscarinic suppression of a novel voltage-sensitive K+ current in a vertebrate neurone. *Nature*. 283:673-676.

Busch, A.E., T. Herzer, C.A. Wagner, F. Schmidt, G. Raber, S. Waldegger, and F. Lang. 1994. Positive regulation by chloride channel blockers of IsK channels expressed in Xenopus oocytes. *Mol Pharmacol*. 46:750-753.

Careaga, C.L., and J.J. Falke. 1992. Structure and dynamics of Escherichia coli chemosensory receptors. Engineered sulfhydryl studies. *Biophys J*. 62:209-216; discussion 217-209.

Cha, A., G.E. Snyder, P.R. Selvin, and F. Bezanilla. 1999. Atomic scale movement of the voltage-sensing region in a potassium channel measured via spectroscopy. *Nature*. 402:809-813.

Chen, J.W., and R.A. Eatock. 2000. Major potassium conductance in type I hair cells from rat semicircular canals: characterization and modulation by nitric oxide. *J Neurophysiol*. 84:139-151.

Constanti, A., and D.A. Brown. 1981. M-Currents in voltage-clamped mammalian sympathetic neurones. *Neurosci Lett*. 24:289-294.

Cooper, E.C., K.D. Aldape, A. Abosch, N.M. Barbaro, M.S. Berger, W.S. Peacock, Y.N. Jan, and L.Y. Jan. 2000. Colocalization and coassembly of two human brain M-type potassium channel subunits that are mutated in epilepsy. *Proc Natl Acad Sci U S A*. 97:4914-4919.

Costa, A.M., and B.S. Brown. 1997. Inhibition of M-current in cultured rat superior cervical ganglia by linopirdine: mechanism of action studies. *Neuropharmacology*. 36:1747-1753.

Cushman, S.J., M.H. Nanao, A.W. Jahng, D. DeRubeis, S. Choe, and P.J. Pfaffinger. 2000. Voltage dependent activation of potassium channels is coupled to T1 domain structure. *Nat Struct Biol*. 7:403-407.

Delmas, P., and D.A. Brown. 2005. Pathways modulating neural KCNQ/M (Kv7) potassium channels. *Nat Rev Neurosci*. 6:850-862.

Deutsch, C. 2003. The birth of a channel. *Neuron*. 40:265-276.

Doyle, D.A., J. Morais Cabral, R.A. Pfuetzner, A. Kuo, J.M. Gulbis, S.L. Cohen, B.T. Chait, and R. MacKinnon. 1998. The structure of the potassium channel: molecular basis of K+ conduction and selectivity. *Science*. 280:69-77.

Gandhi, C.S., and E.Y. Isacoff. 2002. Molecular models of voltage sensing. *J Gen Physiol*. 120:455-463.

Gulbis, J.M., M. Zhou, S. Mann, and R. MacKinnon. 2000. Structure of the cytoplasmic beta subunit-T1 assembly of voltage-dependent K+ channels. *Science*. 289:123-127.

Hackos, D.H., T.H. Chang, and K.J. Swartz. 2002. Scanning the intracellular S6 activation gate in the shaker K+ channel. *J Gen Physiol*. 119:521-532.

Hadley, J.K., M. Noda, A.A. Selyanko, I.C. Wood, F.C. Abogadie, and D.A. Brown. 2000. Differential tetraethylammonium sensitivity of KCNQ1-4 potassium channels. *Br J Pharmacol*. 129:413-415.

Hille, B. 2001. Ion Channels of Excitable Membranes. Third Edition.

Housley, G.D., and J.F. Ashmore. 1992. Ionic currents of outer hair cells isolated from the guinea-pig cochlea. *J Physiol*. 448:73-98.

Howard, R.J., K.A. Clark, J.M. Holton, and D.L. Minor, Jr. 2007. Structural insight into KCNQ (Kv7) channel assembly and channelopathy. *Neuron*. 53:663-675.

Jenke, M., A. Sanchez, F. Monje, W. Stuhmer, R.M. Weseloh, and L.A. Pardo. 2003. C-terminal domains implicated in the functional surface expression of potassium channels. *Embo J*. 22:395-403.

Jentsch, T.J. 2000. Neuronal KCNQ potassium channels: physiology and role in disease. *Nat Rev Neurosci*. 1:21-30.

Kharkovets, T., J.P. Hardelin, S. Safieddine, M. Schweizer, A. El-Amraoui, C. Petit, and T.J. Jentsch. 2000. KCNQ4, a K+ channel mutated in a form of dominant deafness, is expressed in the inner ear and the central auditory pathway. *Proc Natl Acad Sci U S A*. 97:4333-4338.

Kristufek, D., G. Koth, A. Motejlek, K. Schwarz, S. Huck, and S. Boehm. 1999. Modulation of spontaneous and stimulation-evoked transmitter release from rat sympathetic neurons by the cognition enhancer linopirdine: insights into its mechanisms of action. *J Neurochem*. 72:2083-2091.

Kubisch, C., B.C. Schroeder, T. Friedrich, B. Lutjohann, A. El-Amraoui, S. Marlin, C. Petit, and T.J. Jentsch. 1999. KCNQ4, a novel potassium channel expressed in sensory outer hair cells, is mutated in dominant deafness. *Cell*. 96:437-446.

Kurata, H.T., G.S. Soon, J.R. Eldstrom, G.W. Lu, D.F. Steele, and D. Fedida. 2002. Amino-terminal determinants of U-type inactivation of voltage-gated K+ channels. *J Biol Chem*. 277:29045-29053.

Larsson, H.P., O.S. Baker, D.S. Dhillon, and E.Y. Isacoff. 1996. Transmembrane movement of the shaker K+ channel S4. *Neuron*. 16:387-397.

Lee, M.P., M.R. DeBaun, K. Mitsuya, H.L. Galonek, S. Brandenburg, M. Oshimura, and A.P. Feinberg. 1999. Loss of imprinting of a paternally expressed transcript, with antisense orientation to KVLQT1, occurs frequently in Beckwith-Wiedemann syndrome and is independent of insulin-like growth factor II imprinting. *Proc Natl Acad Sci U S A*. 96:5203-5208.

Leppert, M., V.E. Anderson, T. Quattlebaum, D. Stauffer, P. O'Connell, Y. Nakamura, J.M. Lalouel, and R. White. 1989. Benign familial neonatal convulsions linked to genetic markers on chromosome 20. *Nature*. 337:647-648.

Lerche, C., C.R. Scherer, G. Seebohm, C. Derst, A.D. Wei, A.E. Busch, and K. Steinmeyer. 2000. Molecular cloning and functional expression of KCNQ5, a potassium channel subunit that may contribute to neuronal M-current diversity. *J Biol Chem*. 275:22395-22400.

Lohrmann, E., I. Burhoff, R.B. Nitschke, H.J. Lang, D. Mania, H.C. Englert, M. Hropot, R. Warth, W. Rohm, M. Bleich, and et al. 1995. A new class of inhibitors of cAMP-mediated Cl- secretion in rabbit colon, acting by the reduction of cAMP-activated K+ conductance. *Pflugers Arch*. 429:517-530.

Long, S.B., E.B. Campbell, and R. Mackinnon. 2005. Crystal structure of a mammalian voltage-dependent Shaker family K+ channel. *Science*. 309:897-903.

Loots, E., and E.Y. Isacoff. 2000. Molecular coupling of S4 to a K(+) channel's slow inactivation gate. *J Gen Physiol*. 116:623-636.

Lupas, A. 1996. Coiled coils: new structures and new functions. *Trends Biochem Sci*. 21:375-382.

Ma, D., N. Zerangue, Y.F. Lin, A. Collins, M. Yu, Y.N. Jan, and L.Y. Jan. 2001. Role of ER export signals in controlling surface potassium channel numbers. *Science*. 291:316-319.

MacKinnon, R. 1991. Determination of the subunit stoichiometry of a voltage-activated potassium channel. *Nature*. 350:232-235.

Maljevic, S., C. Lerche, G. Seebohm, A.K. Alekov, A.E. Busch, and H. Lerche. 2003. C-terminal interaction of KCNQ2 and KCNQ3 K+ channels. *J Physiol*. 548:353-360.

Marx, S.O., S. Reiken, Y. Hisamatsu, M. Gaburjakova, J. Gaburjakova, Y.M. Yang, N. Rosemblit, and A.R. Marks. 2001. Phosphorylation-dependent regulation of ryanodine receptors: a novel role for leucine/isoleucine zippers. *J Cell Biol*. 153:699-708.

Minor, D.L., Y.F. Lin, B.C. Mobley, A. Avelar, Y.N. Jan, L.Y. Jan, and J.M. Berger. 2000. The polar T1 interface is linked to conformational changes that open the voltage-gated potassium channel. *Cell*. 102:657-670.

Neale, E.J., D.J. Elliott, M. Hunter, and A. Sivaprasadarao. 2003. Evidence for intersubunit interactions between S4 and S5 transmembrane segments of the Shaker potassium channel. *J Biol Chem*. 278:29079-29085.

Nerbonne, J.M. 2000. Molecular basis of functional voltage-gated K+ channel diversity in the mammalian myocardium. *J Physiol*. 525 Pt 2:285-298.

Neyroud, N., P. Richard, N. Vignier, C. Donger, I. Denjoy, L. Demay, M. Shkolnikova, R. Pesce, P. Chevalier, B. Hainque, P. Coumel, K. Schwartz, and P. Guicheney. 1999. Genomic organization of the KCNQ1 K+ channel gene and identification of C-terminal mutations in the long-QT syndrome. *Circ Res*. 84:290-297.

Pagano, A., G. Rovelli, J. Mosbacher, T. Lohmann, B. Duthey, D. Stauffer, D. Ristig, V. Schuler, I. Meigel, C. Lampert, T. Stein, L. Prezeau, J. Blahos, J. Pin, W. Froestl, R. Kuhn, J. Heid, K. Kaupmann, and B. Bettler. 2001. C-terminal interaction is essential for surface trafficking but not for heteromeric assembly of GABA(b) receptors. *J Neurosci*. 21:1189-1202.

Papazian, D.M. 1999. Potassium channels: some assembly required. *Neuron*. 23:7-10.

Ramanathan, K., T.H. Michael, G.J. Jiang, H. Hiel, and P.A. Fuchs. 1999. A molecular mechanism for electrical tuning of cochlear hair cells. *Science*. 283:215-217.

Robbins, J. 2001. KCNQ potassium channels: physiology, pathophysiology, and pharmacology. *Pharmacol Ther*. 90:1-19.

Rogawski, M.A. 2000. KCNQ2/KCNQ3 K+ channels and the molecular pathogenesis of epilepsy: implications for therapy. *Trends Neurosci*. 23:393-398.

Rulisek, L., and J. Vondrasek. 1998. Coordination geometries of selected transition metal ions (Co2+, Ni2+, Cu2+, Zn2+, Cd2+, and Hg2+) in metalloproteins. *J Inorg Biochem*. 71:115-127.

Rundfeldt, C., and R. Netzer. 2000. The novel anticonvulsant retigabine activates M-currents in Chinese hamster ovary-cells tranfected with human KCNQ2/3 subunits. *Neurosci Lett*. 282:73-76.

Sanguinetti, M.C., M.E. Curran, A. Zou, J. Shen, P.S. Spector, D.L. Atkinson, and M.T. Keating. 1996. Coassembly of K(V)LQT1 and minK (IsK) proteins to form cardiac I(Ks) potassium channel. *Nature*. 384:80-83.

Schmidt-Rose, T., and T.J. Jentsch. 1997. Reconstitution of functional voltage-gated chloride channels from complementary fragments of CLC-1. *J Biol Chem*. 272:20515-20521.

Schmitt, N., M. Schwarz, A. Peretz, I. Abitbol, B. Attali, and O. Pongs. 2000. A recessive C-terminal Jervell and Lange-Nielsen mutation of the KCNQ1 channel impairs subunit assembly. *Embo J*. 19:332-340.

Schoppa, N.E., K. McCormack, M.A. Tanouye, and F.J. Sigworth. 1992. The size of gating charge in wild-type and mutant Shaker potassium channels. *Science*. 255:1712-1715.

Schroeder, B.C., M. Hechenberger, F. Weinreich, C. Kubisch, and T.J. Jentsch. 2000. KCNQ5, a novel potassium channel broadly expressed in brain, mediates M-type currents. *J Biol Chem*. 275:24089-24095.

Schroeder, B.C., C. Kubisch, V. Stein, and T.J. Jentsch. 1998. Moderate loss of function of cyclic-AMP-modulated KCNQ2/KCNQ3 K+ channels causes epilepsy. *Nature*. 396:687-690.

Schwake, M., T.J. Jentsch, and T. Friedrich. 2003. A carboxy-terminal domain determines the subunit specificity of KCNQ K+ channel assembly. *EMBO Rep*. 4:76-81.

Schwake, M., M. Pusch, T. Kharkovets, and T.J. Jentsch. 2000. Surface expression and single channel properties of KCNQ2/KCNQ3, M-type K+ channels involved in epilepsy. *J Biol Chem*. 275:13343-13348.

Selyanko, A.A., J.K. Hadley, I.C. Wood, F.C. Abogadie, T.J. Jentsch, and D.A. Brown. 2000. Inhibition of KCNQ1-4 potassium channels expressed in mammalian cells via M1 muscarinic acetylcholine receptors. *J Physiol*. 522 Pt 3:349-355.

Shapiro, M.S., J.P. Roche, E.J. Kaftan, H. Cruzblanca, K. Mackie, and B. Hille. 2000. Reconstitution of muscarinic modulation of the KCNQ2/KCNQ3 K(+) channels that underlie the neuronal M current. *J Neurosci*. 20:1710-1721.

Stauffer, D.A., and A. Karlin. 1994. Electrostatic potential of the acetylcholine binding sites in the nicotinic receptor probed by reactions of binding-site cysteines with charged methanethiosulfonates. *Biochemistry*. 33:6840-6849.

Stuhmer, W., F. Conti, H. Suzuki, X.D. Wang, M. Noda, N. Yahagi, H. Kubo, and S. Numa. 1989. Structural parts involved in activation and inactivation of the sodium channel. *Nature*. 339:597-603.

Tinel, N., S. Diochot, I. Lauritzen, J. Barhanin, M. Lazdunski, and M. Borsotto. 2000. M-type KCNQ2-KCNQ3 potassium channels are modulated by the KCNE2 subunit. *FEBS Lett*. 480:137-141.

Tinel, N., I. Lauritzen, C. Chouabe, M. Lazdunski, and M. Borsotto. 1998. The KCNQ2 potassium channel: splice variants, functional and developmental expression. Brain localization and comparison with KCNQ3. *FEBS Lett*. 438:171-176.

Tristani-Firouzi, M., and M.C. Sanguinetti. 1998. Voltage-dependent inactivation of the human K+ channel KvLQT1 is eliminated by association with minimal K+ channel (minK) subunits. *J Physiol*. 510 (Pt 1):37-45.

Vemana, S., S. Pandey, and H.P. Larsson. 2004. S4 movement in a mammalian HCN channel. *J Gen Physiol*. 123:21-32.

Viskin, S. 1999. Long QT syndromes and torsade de pointes. *Lancet*. 354:1625-1633.

Wang, H.S., Z. Pan, W. Shi, B.S. Brown, R.S. Wymore, I.S. Cohen, J.E. Dixon, and D. McKinnon. 1998. KCNQ2 and KCNQ3 potassium channel subunits: molecular correlates of the M-channel. *Science*. 282:1890-1893.

Wang, Q., M.E. Curran, I. Splawski, T.C. Burn, J.M. Millholland, T.J. VanRaay, J. Shen, K.W. Timothy, G.M. Vincent, T. de Jager, P.J. Schwartz, J.A. Toubin, A.J. Moss, D.L. Atkinson, G.M. Landes, T.D. Connors, and M.T. Keating. 1996. Positional cloning of a novel potassium channel gene: KVLQT1 mutations cause cardiac arrhythmias. *Nat Genet*. 12:17-23.

Wehling, C., C. Beimgraben, C. Gelhaus, T. Friedrich, P. Saftig, J. Grotzinger, and M. Schwake. 2007. Self-assembly of the isolated KCNQ2 subunit interaction domain. *FEBS Lett*. 581:1594-1598.

Wollnik, B., B.C. Schroeder, C. Kubisch, H.D. Esperer, P. Wieacker, and T.J. Jentsch. 1997. Pathophysiological mechanisms of dominant and recessive KVLQT1 K+ channel mutations found in inherited cardiac arrhythmias. *Hum Mol Genet*. 6:1943-1949.

Yang, W.P., P.C. Levesque, W.A. Little, M.L. Conder, F.Y. Shalaby, and M.A. Blanar. 1997. KvLQT1, a voltage-gated potassium channel responsible for human cardiac arrhythmias. *Proc Natl Acad Sci U S A*. 94:4017-4021.

Yellen, G. 1998. The moving parts of voltage-gated ion channels. *Q Rev Biophys*. 31:239-295.

Yifrach, O., and R. MacKinnon. 2002. Energetics of pore opening in a voltage-gated K(+) channel. *Cell*. 111:231-239.

Yusaf, S.P., D. Wray, and A. Sivaprasadarao. 1996. Measurement of the movement of the S4 segment during the activation of a voltage-gated potassium channel. *Pflugers Arch*. 433:91-97.

Yus-Najera, E., I. Santana-Castro, and A. Villarroel. 2002. The identification and characterization of a noncontinuous calmodulin-binding site in noninactivating voltage-dependent KCNQ potassium channels. *J Biol Chem*. 277:28545-28553.

Zerangue, N., Y.N. Jan, and L.Y. Jan. 2000. An artificial tetramerization domain restores efficient assembly of functional Shaker channels lacking T1. *Proc Natl Acad Sci U S A*. 97:3591-3595.

Zerangue, N., M.J. Malan, S.R. Fried, P.F. Dazin, Y.N. Jan, L.Y. Jan, and B. Schwappach. 2001. Analysis of endoplasmic reticulum trafficking signals by combinatorial screening in mammalian cells. *Proc Natl Acad Sci U S A*. 98:2431-2436.

Zhu, G., M. Okada, T. Murakami, A. Kamata, Y. Kawata, K. Wada, and S. Kaneko. 2000. Dysfunction of M-channel enhances propagation of neuronal excitability in rat hippocampus monitored by multielectrode dish and microdialysis systems. *Neurosci Lett*. 294:53-57.

Acknowledgements

Curriculum Vitae

Name	Despina Athanasiadu
Date of birth	05.02.1976
Place of birth	Mannheim

Education

1994	Graduation from the „Polykladiko Lyceum", Drama (Greece)
1995-2001	Diploma in Biology from the Johannes Gutenberg-Universität Mainz
2001-2003	Motherhood
2004-2007	PhD student at the Max-Planck-Institute of Biophysics Frankfurt am Main under supervision of Prof. Thomas Friedrich

Publications

2003	D. Athanasiadou, B. Stradmann-Bellinghausen, C. Rittner and P.M. Schneider: „Development of a quadruplex-PCR-system for the genetic analysis of X-chromosomal short tandem repeat loci" International Congress Series 1239 (2003) 311-314
2005	K. A. Tabbada, M. Corazon, A. De Ungria, L. P. Faustino, D. Athanasiadu, B. Stradmann-Bellinghausen and P.M.Schneider: „Development of a pentaplex X-chromosomal short tandem repeat typing system and population genetic studies" Forensic Science International 154 (2) (2005) 173-180
2006	M. Schwake, D. Athanasiadu, C. Beimgraben, J. Blanz, C. Beck, T. J. Jentsch, P. Saftig and Th. Friedrich: „Structural determinants of M-type KCNQ channel assembly" The Journal of Neuroscience 26 (14) (2006) 3757-3766
2007	D. Athanasiadu, G. Seebohm, J. Enderich and Th. Friedrich: „Structure-function studies of the voltage sensor in KCNQ1 potassium channels" (in preparation)